Spectroscopic and Electrical Investigations into Chemical Interactions with Carbon Nanotubes

by

Douglas R. Kauffman

B.S. in Chemistry, University of Pittsburgh, 2004

Submitted to the Graduate Faculty of

Chemistry in partial fulfillment

of the requirements for the degree of

Doctor of Philosophy

University of Pittsburgh

2010

UNIVERSITY OF PITTSBURGH

Graduate School of Arts and Sciences

This dissertation was presented

by

Douglas R. Kauffman

It was defended on

March 24, 2010

and approved by

Dr. David W. Pratt, Professor, Department of Chemistry

Dr. Shigeru Amemiya, Associate Professor, Department of Chemistry

Dr. Minhee Yun, Assistant Professor, Department of Electrical and Computer Engineering

Dissertation Advisor: Dr. Alexander Star, Assistant Professor, Department of Chemistry

Spectroscopic and Electrical Investigations into Chemical Interactions with Carbon Nanotubes

Douglas R. Kauffman, PhD

University of Pittsburgh, 2010

Decorating single-walled carbon nanotubes (SWNTs) with appropriate nanoparticle species or polymeric layers can induce unique chemical sensitivities and/or catalytic activities. The approach of decorating SWNTs with various chemically sensitive materials is advantageous because undecorated SWNTs are only inherently sensitive towards a limited range of molecules. Because they are electrically conductive and optically active, the enhanced chemical sensitivity of decorated SWNTs can be exploited for the development of chemical sensors or catalytic platforms. Of particular interest are the transduction mechanisms between the decoration layer and underlying SWNTs, which serves to signal the adsorption and/or reaction of particular molecular species at the SWNT surface.

A variety of techniques have been employed to characterize the properties of decorated SWNTs towards the development of chemical sensors and catalytic platforms. In particular, a combination of optical spectroscopy, electrochemistry and solid-state electrical transport measurements provide real-time information about the charge transfer occurring at the decorated SWNT surface. This information provides valuable mechanistic insight into the electronic processes that dictate sensor response or catalyst efficiency.

Using the above-mentioned techniques, we have demonstrated that charge transfer between SWNTs and adsorbing gaseous species creates simultaneous and complementary changes in the optical spectroscopy and electrical transport properties of SWNTs. Moreover, our

approach has allowed us to develop mechanistic descriptions of the interaction between adsorbing gas molecules and the decorated SWNT networks. The decorated SWNT system has potential applications in the field of chemical sensors and heterogeneous catalysis, and a fundamental understanding of the chemical processes may lead to better chemical sensors and/or catalysts.

TABLE OF CONTENTS

LIST OF TABLES

LIST OF FIGURES

DISSERTATION PREFACE

I would like to thank all of my laboratory coworkers and colleagues who have participated in research projects, discussed results and ideas, or provided me with advice over the years. I would also like to express my gratitude towards my research advisor, Professor Alexander Star, for helping me grow as a scientist and navigate through the graduate school process. Sincere appreciation goes to my parents, who in addition to their love and support, rarely questioned why I wanted to spend almost 10 years in college, and to my friends, who have provided me with many entertaining distractions. Last, but certainly not least, I thank my fiancée, Dr. Kristi L. O'Neal (soon to be Dr. Kristi L. Kauffman!), for her unwavering support, kindness and seemingly endless desire to spoil me. Kristi, your shared love of stray animals, lazy weekends and tasty food has made me indescribably happy, and without you, I may have lost sight of what is truly important in life.

1.0 INTRODUCTION

Carbon nanotubes (CNTs) are an elongated member of the fullerene family with a cylindrical structure composed of carbon atoms.[1] CNTs have diameters between one and several nanometers and their lengths can exceed several micrometers. The very high aspect ratio (length to width) and nano-scale diameter of CNTs creates some unique properties that allow for exciting applications. For example, CNTs can be electrically conductive, and their micrometer-scale length allows them to function as one-dimensional wires in electronic devices. Additionally, CNTs have an extraordinarily large percentage of surface atoms, which makes them extremely sensitive to their local chemical environment. Subsequently, if placed between two electrodes they can function as a chemically sensitive resistor or transistor for sensor applications. Additionally, their nano-scale diameter can produce quantum mechanical phenomena, such electron confinement around the tube circumference. Electron orbital overlap in some forms of CNTs can induce molecule-like electronic structures with rich optical properties. The small size, ability to function in electrical circuitry, and molecule-like characteristics of CNTs create a unique platform for studying chemical systems.

1.1 THE PHYSICAL AND ELECTRONIC STRUCTURE OF CNTS

The discovery of CNTs was first reported in 1991,[2] and they are best conceptualized as a sheet of graphene (an atomically thin layer of perfectly sp^2 hybridized carbon) "rolled-up" into a cylinder, as depicted in Figure 1-1A. CNTs composed of many concentrically nestled tubes are called

multi-walled carbon nanotubes (MWNTs), as shown in Figure 1-1B. CNTs containing only one wall are termed single-walled carbon nanotubes (SWNTs).[3]

Many properties of a particular SWNT stem directly from its chirality, or more conceptually, how the SWNT is "rolled-up" from a sheet of graphene. For example, the sheet of graphene can be rolled in such a way that the ends directly overlap, or that they meet at a particular angle. This geometry of the rolled-up cylinder of graphene can be described by two vectors, termed roll-up vectors which are denoted as (n,m),[4] as shown in Figure 1-1C. In graphene, each carbon atom has three sp^2 electrons that bond to the nearest carbon neighbors and one 2p electron that projects orthogonally from the SWNT surface that creates a delocalized π-electron structure.[5] The roll-up vectors describe the relative overlapping of the orthogonal p electron orbitals and dictate whether a SWNT is metallic or semiconducting. Metallic SWNTs have n–m values equal to 3k or zero (n–m = 3k,0), where k is any integer value; all other n–m values produce semiconducting SWNT varieties.

To give physical meaning to this distinction, metallic SWNTs have a finite density of allowed electronic states at their Fermi level—the position between the valence (VB) and conduction bands (CB), and they have electrical characteristics analogous to metals. On the other hand, semiconducting SWNTs have regions of forbidden electronic states between the VB and CB, and this electronic band gap gives them the electrical and optical characteristics of a semiconductor. Based on this convention, the VB and CB can loosely be considered the CNT highest occupied molecular orbital (HOMO) and lowest unoccupied molecular orbital (LUMO), respectively. Current synthetic techniques result in a mixture of semiconducting and metallic varieties with a composition of one-third metallic to two-thirds semiconducting.[6a]

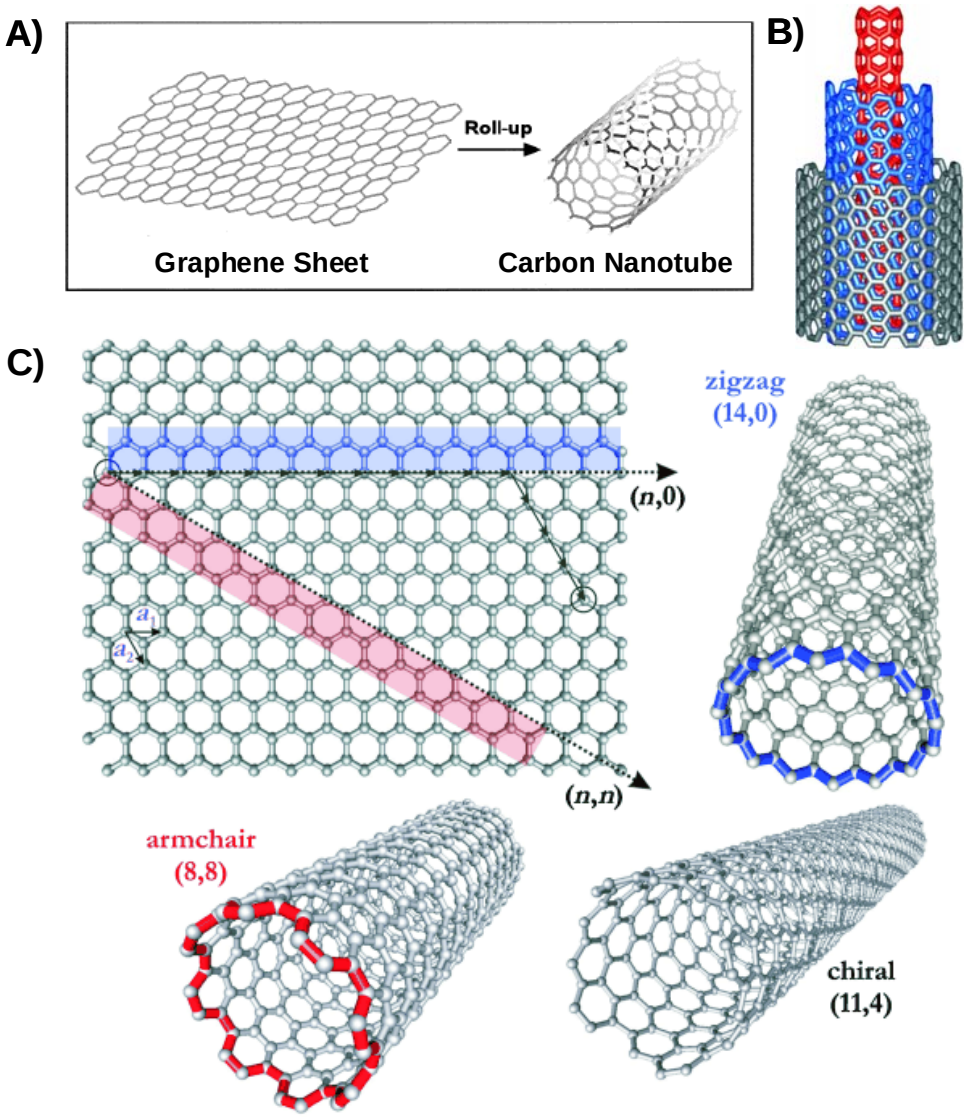

Figure 1-1. Carbon nanotube (CNT) structure. A) Depiction of carbon nanotube (CNT) formation by "rolling up" a sheet of graphene. Reproduced with permission from Reference 4a; copyright 2000 American Chemical Society. B) Representation of the concentric walls of a multi-walled carbon nanotube (MWNT) where the innermost red CNT is considered a single-walled carbon nanotube (SWNT). C) Schematic of a graphene sheet depicting the roll up vectors (n, m) of a CNT, showing armchair (n = m), chiral (n ≠ m) and zigzag (n, 0) SWNTs. Panels B and C have been reproduced with permission from Reference 4b; copyright 2007 Wiley-VCH Verlag GmbH & Co. KGaA.

1.2 OPTICAL SPECTROSCOPY OF SWNTS

SWNTs possess well-defined electronic transitions in the ultraviolet (UV), visible (Vis) and near infrared (NIR) wavelength ranges. Since the circumference of the SWNT is on the nano-scale, the delocalized π-electrons experience quantum confinement and their energy levels become quantized. A density of states (DOS) diagram is a way to describe the allowed energy states of particular material, and a partial DOS diagram for a metallic and a semiconducting SWNT is presented in Figure 1-2A. Here, regions of constructive interference between the delocalized π–electrons produce sharp spikes called van Hove singularities[7] that lead to characteristic electronic transitions. The top of the semiconducting SWNT VB is depicted as being partially depleted of electrons, which is a property of all semiconducting SWNTs under ambient conditions due to the adsorption of oxygen.

The optical absorption spectrum of SWNT samples is a superposition of individual peaks from a mixture of semiconducting and metallic SWNTs of varying chirality and diameter.[6] The electronic transitions of SWNTs are governed by selection rules that state allowed transitions must occur between symmetric van Hove singularities (Figure 1-2A).[8] More conceptually, this rule means that only electronic transitions between van Hove singularities of equal energy from the Fermi level can occur. This leads to semiconducting SWNTs having three prominent absorption peaks in the UV, visible, and NIR regions called the S_{11}, S_{22}, and S_{33} transitions, respectively. Even though metallic SWNTs are technically zero-band gap materials, they do possess a single absorption peak in the visible region that results from the curvature of SWNT wall; the metallic transition is called the M_{11}. Current synthetic methods produce a mixture of semiconducting and metallic varieties of SWNTs, which has two implications for the optical

spectrum of bulk SWNT samples. First, each characteristic absorption band will be a superposition of the individual transitions of many SWNTs of differing diameter and chirality. Secondly, the absorption spectrum of a SWNT sample will be composed of both semiconducting and metallic absorption bands.

Figure 1-2B shows the absorption spectra of a thin film of commercial SWNTs obtained from *Carbon Solutions Inc.* that were produced using the electric arc discharge method.[3,9] *Carbon Solutions Inc.* reports that their SWNT samples contain an average tube diameter of ~1.4 nm in bundles of 2-10 nm.[10] In this spectrum three of the four prominent absorption bands (S_{11}, S_{22}, M_{11}) are clearly observed; however, strong absorbance towards the UV region that stems from the so-called π-electron plasmon has a tendency to mask the SWNT S_{33} band,[6] making it appear as a series of small ripples between 450-550 nm.

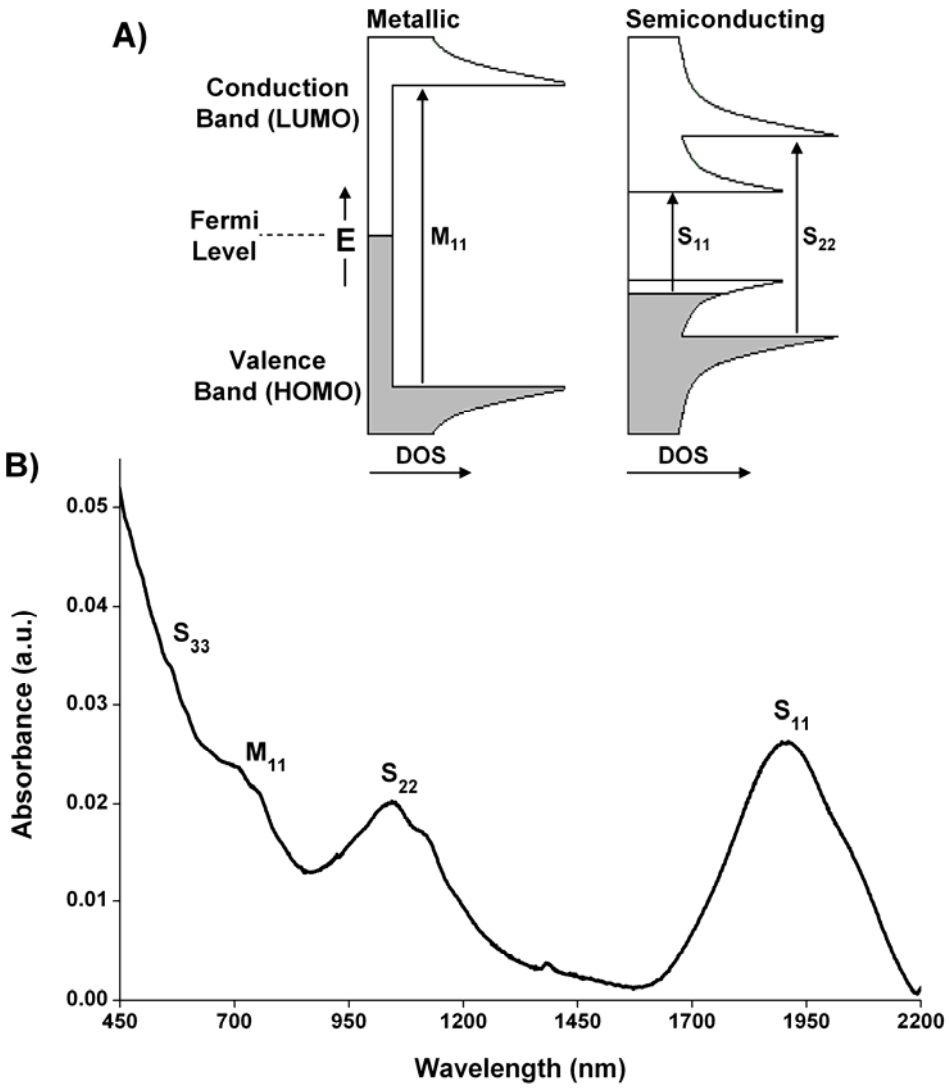

Figure 1-2. Single-walled carbon nanotube (SWNT) electronic structure and absorption spectrum. A) Partial density of states (DOS) diagram displaying the number density of states at each energy level. The spikes in the DOS diagram are called van Hove singularities and result from electron confinement around the SWNT circumference. The transitions between these spikes are labeled as S_{11} and S_{22} for the semiconducting SWNTs, and M_{11} for the metallic SWNTs. Notice that the metallic SWNT has finite electronic density at the Fermi level, while the semiconducting SWNT does not. Furthermore, the S_{11} band of the semiconducting SWNT is partially depleted of electrons, making it a p-type semiconductor. B) The UV-Vis-NIR optical absorption spectra of a film of SWNTs on quartz. Each broad absorption band (S_{11}, S_{22}, S_{33}, M_{11}) is actually a superposition of many individual absorption peaks from SWNTs of varying diameters and chiralities.

1.3 INTEGRATING SWNTS INTO ELECTRONIC DEVICES

The relatively long length scale of SWNTs (μm or longer) allows them to be incorporated into electronic devices by serving as the conduction channel between two metallic electrodes. An interesting phenomenon occurs when a metal comes into contact with a semiconductor. Due to the mismatch in work function (Φ) between a metal and a semiconductor, the Fermi levels of the two materials will equilibrate, bending the p-type semiconductor valence band towards higher energy. Under ambient conditions, the valence band of semiconducting SWNTs is partially depleted of electronic density, making them p-type semiconductors and meaning that they will conduct holes instead of electrons. As a result, when a semiconducting SWNT comes into contact with a metal, some electronic density is donated into the valence band, pushing it to higher energy. At the SWNT-metal interface a region of increased electronic density forms in the SWNT valence band, called a depletion region (DR). This depletion region forms a potential barrier, called a Schottky Barrier (SB), which inhibits the transmission of holes from the metal into the SWNT valence band. The formation of a SB at the metal-SWNT interface is shown in Figure 1-3.

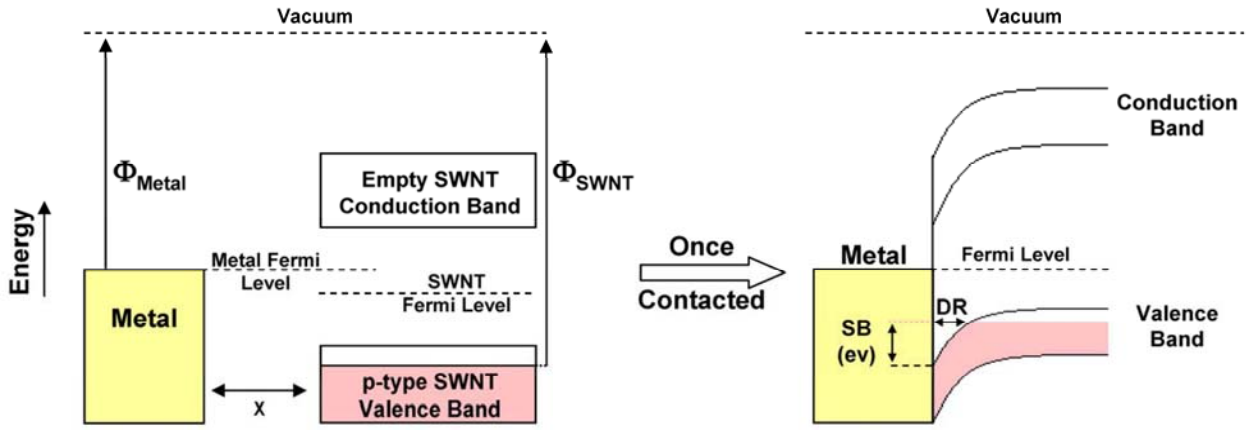

Figure 1-3. P-type semiconductor and metal band diagram describing the effects of bringing a metal and p-type semiconductor of dissimilar work function into contact. When separated by some distance x, the metal and p-type semiconducting SWNT have unequal work functions (Φ) and Fermi level energies. When they are brought into contact Fermi level equilibration occurs; this results in a donation of electronic density into the SWNT and an upward bending of valence band—even though the conduction band is empty it will experience a similar bending. The donation of electronic density creates a depletion region (DR) at the p-type SWNT-metal interface that may extend several nm into the SWNT. The existence of a region of increased electronic density produces a potential barrier for the transmission of holes between the SWNT valence band and the metal contact; this potential barrier is called a Schottky Barrier (SB) and is measured in units of eV.

1.4 SWNT DEVICE DESIGN AND OPERATION

Two common SWNT-based electronic devices both employ the SWNT as a conductive channel between two metal electrodes. Au has typically been used for device electrodes; however, Pd has also been found to create excellent electrical connections with SWNTs.[11] This trait is believed to be a function of the close match in work function of the metals (Au ~ 5.0 and Pd ~ 5.1 eV) and the SWNT (~5 eV),[12] and should result in small SBs. Furthermore, Pd can efficiently stick to (wet) the SWNT surface.[13] The first, and more simple design consists of a SWNT (or network of SWNTs) placed between two metal electrodes on an insulating substrate. In this configuration the SWNT acts as a chemically sensitive resistor (chemiresistor), and the device resistance (R; ohms, Ω) or conductance (G; Siemens, S) is measured as a function of time. If chemical species engage in charge transfer with the SWNT and modify the electronic density of the SWNT VB, then a change in the device resistance (or conductance) will be measured. For example, if a molecule donates electronic density into the SWNT, then the relative concentration of current carrying holes will decrease and the SWNT resistance will increase (conductance decrease). This picture is a slight oversimplification, because molecular adsorption can introduce charge scattering sites along the SWNT length, and molecular interaction with the metal electrode can modify the device SB by changing the metal work function; both of these events will alter the measured SWNT resistance (or conductance) and present a challenge when studying chemical systems.

A more sophisticated device design was first reported in 1998 and is called a nanotube field-effect transistor (NTFET).[14] A typical NTFET device is shown in Figure 1-4A.[15] Here, the schematic describes a NTFET composed of a randomly oriented SWNT network deposited onto

a Si substrate with a thin (~100 nm) SiO_2 insulating layer and two electrodes (typically Au) labeled source (S) and drain (D) that are deposited *via* electron beam evaporation. A bias voltage is applied across the SWNT through the S-D electrodes (V_{SD}) and a gate voltage (V_G) is applied to the Si substrate that acts as a back gate electrode to modulate the device conductance. NTFET devices composed of randomly oriented SWNT networks are advantageous because they allow higher electrical conductance and their multiple conduction channels make them more defect tolerant;[16] however, they will contain a finite concentration of metallic SWNTs in the conduction network due to the nature of SWNT synthesis.[6a]

Typical NTFET experiments monitor the device conductance as a function of the applied V_G at a particular V_{SD}, and the device output is called a transistor transfer characteristic, or G-V_G curve. The behavior of NTFET devices relies on the formation of SBs at the SWNT-metal contact interface,[17] as presented in Figure 1-3. In NTFET devices, the height of the SB at the SWNT-contact interface depends on the work function of the metal,[18] where a larger work function mismatch between the SWNT and metal electrode will result in a larger SB. Under a constant V_{SD} the conductance of semiconducting SWNTs can be modulated by varying the V_G. Specifically, sweeping the V_G towards more negative voltages will push the SWNT VB towards higher energy. This narrows the depletion region at the SWNT-metal interface and decreases the tunneling barrier for hole transport into and out of the SWNT, increasing the measured device conductance.[19] A representative G-V_G curve of a NTFET composed of a network of SWNTs between interdigitated Au electrodes is shown in Figure 1-4B; a constant V_{SD} of 0.05 V was used. Under ambient conditions the return sweep may be slightly offset (as shown), creating what is called "hysteresis"; this is caused by adsorbed H_2O molecules or other ionic

contaminants on the SWNT or SiO_2 surface,[20] and it is a characteristic of most NTFET measurements conducted under ambient conditions.

The transfer characteristics of a NTFET will change if it is exposed to certain chemical species. For example, an electron-donating molecule will shift the G-V_G curve towards more negative gate voltages and produce decreased device conductance at any arbitrary gate voltage when measured in a conductance versus time configuration. This phenomenon can be rationalized in the following way.Tthe donation of electronic density into the SWNT valence band results in charge carrier (electron-hole) recombination, and effectively decreases the number of current carrying holes. A similar way to describe this phenomenon is that the added electronic density serves to fill the partially depleted valence band, and by increasing the SB height and depletion barrier width at the SWNT-metal interface, decreases the transmission of holes into the SWNT. Alternatively, an electron withdrawing molecule can cause an increase in the device conductance and shift the G-V_G curve towards more positive gate voltages for reasons opposite to those given above. An example of this is given in Figure 1-5, where exposure to NH_3 or NO_2 gases (both in N_2), which are respective e^- donating or withdrawing molecules,[21] creates opposite shifts in the NTFET transfer characteristic; the NTFET device was composed of a network of SWNTs between interdigitated Ti/Au S-D electrodes and was operated at V_{SD} = 0.05 V.

Operation of a SWNT-based device in a chemiresistor configuration, *i.e.* when the device conductance is monitored versus time at V_G = 0, can be inferred from Figure 1-5. Specifically, exposure to either NH_3 or NO_2 would cause a respective decrease or increase in conductance during the gas exposure period. This mode of operation is advantageous because it allows one to easily monitor the kinetics of device response during analyte exposure.

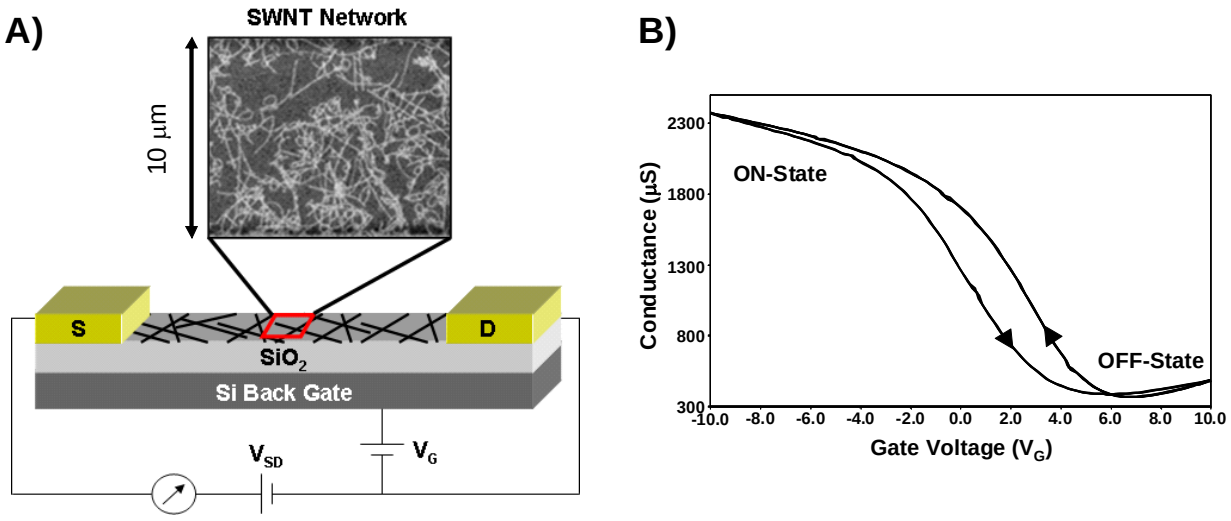

Figure 1-4. SWNT field effect transistor (NTFET) diagram and operation. A) Schematic diagram of an random network NTFET. A Si substrate is thermally annealed to produce a thin SiO_2 insulating layer, the underlying Si is used as a back gate electrode. Source (S) and drain (D) electrodes (typically Au) are deposited onto the substrate and SWNT *via* electron beam evaporation. A bias voltage (V_{SD}) is applied across the SWNT through the S-D electrodes and the device conductance is modulated through application of a gate voltage (V_G) with the Si back gate electrode. The enlarged view is a scanning electron microscope (SEM) image of a NTFET surface containing a network or randomly oriented SWNTs. B) Typical NTFET transfer characteristic monitoring the device conductance between gate voltages of 10 to -10 V; the V_G sweep directions are indicated with arrows. This particular NTFET device was composed of a network of SWNTs between interdigitated Au S-D electrodes and was operated at V_{SD} = 0.05 V. Reproduced with permission from Reference 15; copyright 2007 Wiley-VCH Verlag GmbH & Co. KGaA.

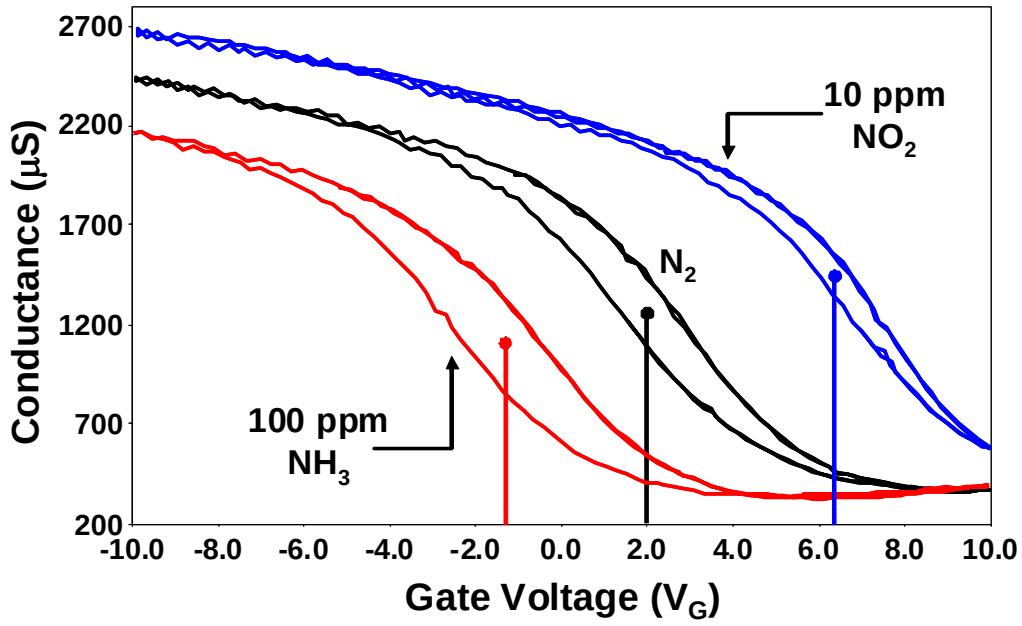

Figure 1-5. NTFET transfer characteristics. NTFET conductance versus gate voltage G-V_G transfer characteristics under N2 (black curve), 100 ppm NH_3 in N_2 (red curve) and 10 ppm NO_2 in N_2 (blue curve). Because the devices were initially exposed to ambient conditions, all G-V_G curves demonstrated hysteresis; VSD = 0.05 V for all three curves. Here NH_3, considered to be an electron donating molecule, creates a decrease in the device maximum conductance and a negative shift in the G-V_G curve as measured from the center of the hysteresis. Exposure to NO_2, considered an electron-withdrawing molecule, creates an increase in the device maximum conductance and positive shift in the device gate voltage as measured from the center of the hysteresis.

Based on the change of the SWNT electrical properties that result from molecular adsorption / charge transfer, it is possible to develop chemically sensitive platforms that can monitor the adsorption and / or reaction of molecular species. This ability provides a means to develop highly sensitive chemical sensors, and study catalyzed reactions at the SWNT surface. The following chapters serve to highlight the ability of SWNT-based devices to function not only as chemical sensors, but also as a general platform for studying the mechanistic aspects of molecular interactions with SWNTs.

2.0 CHEMICALLY INDUCED POTENTIAL BARRIERS AT THE CARBON NANOTUBE—METAL NANOPARTICLE INTERFACE

2.1 CHAPTER PREFACE

The aim of this work was to investigate the transduction mechanism between metal nanoparticle decorated SWNTs and adsorbing nitric oxide gas molecules. Specifically, we used NTFET devices that contained SWNTs electrochemically decorated with Ag, Au, Pd and Pt nanoparticles to explore the electronic interactions that occur between the SWNTs, nanoparticles, and adsorbing nitric oxide gas molecules. The material contained in this chapter was published as a research paper in the journal *Nano Letters*; the figures and table in this chapter have been reproduced with permission from *Nano Lett.* **2007**, *7*, 1863. Copyright 2007 American Chemical Society; the full citation is listed as Reference 22 in the bibliography section.

List of Authors: Douglas R. Kauffman and Alexander Star.

Author contributions: DRK and AS designed the experiments, interpreted the data and wrote the manuscript, DRK performed all experimental work.

2.2 ABSTRACT

Single-walled carbon nanotube (SWNT) field effect transistors (FETs) were electrochemically decorated with Pt, Pd, Au, and Ag nanoparticles. After exposure to 10 ppm NO gas in N_2 we found a trend wherein the magnitude of electron transfer into the SWNT valence band scaled with the work function of the individual metal. This trend gives experimental support for the formation of a metal work function dependent potential barrier at the SWNT-nanoparticle interface, and provides a means to mechanistically describe the transduction mechanism between the adsorbing gas molecules, metal nanoparticles and SWNTs.

2.3 INTRODUCTION

Considerable interest surrounds the fabrication and application of carbon nanotubes (CNTs) decorated with metal nanoparticles (NPs).[23] While the use of such nano-hybrids is becoming more popular, the intimate electronic relationship between the CNT and deposited NP is still poorly understood. On the other hand, the electronic interactions between CNTs and bulk metal contacts is well described in the literature.[18,24] For example, Dai and coworkers have reported that nanotube field-effect transistors (NTFETs) experience sensitivity towards H_2 as a result of modification of the Schottky barrier at the CNT-metal junction.[11] Similarly, H_2 sensitivity was seen in Pd decorated NTFETs, and has been explained in terms of electron donation through H_2 lowering the Pd work function.[25] This explanation relies upon the ability of hydrogen to dissolve into bulk Pd metal, and it was first suggested in the report of a hydrogen sensitive Metal-Oxide-Semiconductor FET (MOSFET).[26] However, this explanation may not be complete because it

does not give any special consideration to the electronic interaction at the NP-SWNT interface. Recently we reported a gas sensor array based on metal decorated NTFETs that showed unique electronic response for various metal-analyte combinations,[27] but the fundamental mechanism behind the signal transduction remained unclear.

By exposing NTFET devices decorated with different metals to a single gas one could monitor the electronic response as a function of metal work function. NO has an unpaired electron in the $2\pi^*$ orbital, and the literature abounds with reports of NO-metal interactions because it is an ideal candidate for probing metal surfaces.[28] In this chapter we compare the behavior of NTFETs decorated with Pt, Pd, Au, and Ag NPs upon exposure to nitric oxide (NO) gas. We have found that devices decorated with different species of NPs demonstrated unique electronic behavior upon exposure to NO gas in N_2. Based on our experimental findings we show a correlation between the metal work function of the NP and the magnitude of electron transfer into the SWNT network of the NTFET device, which points towards a work function dependent potential barrier at the NP-SWNT interface.

2.4 EXPERIMENTAL SECTION

NTFETs were fabricated by chemical vapor deposition (CVD) growth of SWNTs onto Si/SiO_2 wafers, and interdigitated Au electrodes were photolithographically patterned onto the SWNT network.[27] The chips were wire-bonded and packaged in a 40-pin ceramic dual-inline package (CERDIP). The fabrication process creates multiple devices per chip allowing the simultaneous measurement of several individual devices.

Aqueous solutions of 1mM H_2PtCl_6, $HAuCl_4$, $AgNO_3$ and 0.5 mM K_2PdCl_6 (Sigma Aldrich) were prepared with a supporting electrolyte of 0.1 M HCl or KNO_3 (for $AgNO_3$) and used to electrochemically deposit metal NP onto the SWNT network of the NTFET device. The experimental setup for the metal decoration is given in Figure 2-1. Each NTFET chip contained several individual NTFET devices that were connected to bulk Au contact pads with thin (30 μm) Au wires. To ensure that electrochemical deposition did not occur on the thin Au wires we carefully paced an epoxy layer (Epoxy Technologies) around the perimeter of the device face such that the individual NTFET devices were exposed, but the gold wires were encased in the hardened epoxy. This effectively passivated, or chemically insulated, the gold wires from the exterior environment; the epoxy can be seen as an amber color in the small gold square in the center of the NTFET chip (Figure 2-1A and inset). To carry out the electrochemical deposition a pair of stainless steel tweezers was used to bridge the source and drain bulk contacts of one particular device; this was then connected to a CH Instruments Model 600 electrochemical analyzer and used as the working electrode. Connecting the device in this manner allowed for the entire SWNT network between the device S-D electrodes to function as a working electrode. A small drop (~100 μL) of metal salt solution was placed on top of the epoxy passivated devices and a Ag/AgCl reference and a Pt wire counter electrode were brought into contact with the surface of the solution, as shown in the inset of the Figure 2-1A. This configuration allowed the drop to act as a miniaturized 3-electrode electrochemical cell, which is further illustrated in the experimental schematic in Figure 2-1B. Due to the experimental setup it was not possible to deaerate the solution, and the deposition was conducted under ambient conditions. After electrochemical decoration the devices were rinsed with deionized water to remove any remaining metal salt solution and dried in a vacuum oven at 75 ^{o}C overnight.

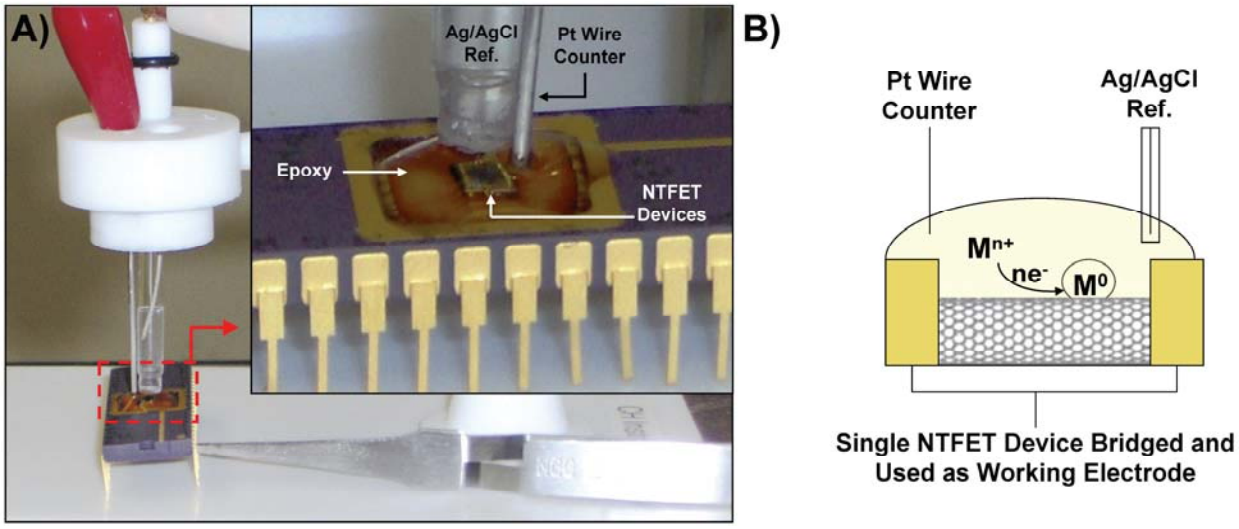

Figure 2-1. Metal nanoparticle (NP) deposition on NTFET devices. A) A digital photograph of the experimental setup for electrochemical decoration of NTFET devices with metal nanoparticles. Here a drop of metal salt solution is placed onto the surface of an epoxy passivated NTFET chip and a Ag/AgCl reference electrode and Pt wire counter electrode are placed just in contact with the surface of the solution. A pair of stainless steel tweezers was used to bridge two device pins (S-D electrodes) which functioned as the working electrode to complete the electrochemical cell. The inset shows a magnified view of the solution drop on the NTFET device surface where the Ag/AgCl reference and Pt counter electrodes are contacting the solution surface. B) Schematic of the experimental setup that illustrates each component of the electrochemical cell. Here, the application of a cathodic potential reduces the metal ions at the SWNT surface, which serves to nucleate and grow the metal NPs.

Scanning electron microscopy (SEM) was performed with a *Phillips XL30 FEG* microscope equipped with an energy dispersive x-ray (EDX) spectroscopy accessory to confirm the species of the NPs on the SWNT surface. Conductance versus gate voltage ($G\text{-}V_G$) transfer characteristics or conductance versus time measurements were performed on the NTFET devices under research grade N_2 or 10 parts per million (ppm) NO (in N_2) in a gas delivery system consisting of mass-flow controllers and a custom built gas delivery chamber; all gases were introduced at a flow rate of 300 standard cubic cm per minute (SCCM). The flow system was purged with dry N_2 for 1 hour before introduction of 10 ppm NO in N_2; this was done to remove any latent humidity and/or oxygen remaining in the flow system from exposure to ambient conditions. After the initial 1 hr N_2 exposure the devices were exposed to NO for 1 hr to ensure a homogenous environment and create at steady state concentration of NO at the NP-SWNT surface.

2.5 RESULTS AND DISCUSSION

The NTFET chips used in this study contained multiple devices on the surface, as shown in the center of Figure 2-2, where the epoxy coating (black) is seen surrounding the wire-bonded contacts. Three sets of degenerate devices, each with identical geometry and electrode separation (pitch), were present on each chip; degenerate devices are denoted with subscripts (a_1, a_2, etc.). Through the selective electrochemical deposition of metal NPs it was possible to decorate particular devices while leaving their degenerate devices bare. To demonstrate the device selective decoration a deposition time of 60 seconds was used to deposit ~150-300 nm Au

nanoparticles on device a_1, 90 seconds was used to deposit ~150 nm Pd nanoparticles on device b_1, and 30 seconds was used to deposit ~120 nm Pt nanoparticles on device c_2 while their degenerate devices were left bare. These long NP deposition times resulted in a nearly complete loss of NTFET transfer characteristics due to large nanoparticles screening the gate voltage;[27] to reduce this effect, smaller deposition times between 10 and 20 seconds were used to decorate chips for gas exposure experiments.

Figure 2-3 shows the G-V_G transfer characteristics of degenerate devices a_1 and a_2 from Chip 1. During deposition both devices were in the $HAuCl_4$/HCl solution; however, Figure 2-3A shows that after device a_1 was held at potential for 20 seconds it experienced modest G-V_G modification, whereas Figure 2-3B shows the G-V_G transfer characteristic of device a_2 (not held at potential) remained essentially unchanged. This indicates Au NPs were selectively deposited on device a_1, while a_2 remained pristine. Figure 2-3C shows the modifcation of Chip 1 devices c_1 and c_2 transfer characteristics resulting from different Pt deposition times. Both devices were independently held in the H_2PtCl_6 / HCl solution at -1.0 V for different amounts of time; device c_2 was held at potential for 20 seconds, while device c_1 was only held at potential for 10 seconds to obtain a smaller Pt coverage on the SWNT surface. It can be seen that while device c_1 experienced modest G-V_G modification, device c_2 experienced an almost complete loss of gate voltage dependency due to increased Pt deposition time. Subsequent SEM images show small Pt nanoparticles around 20 nm in diameter in device c_1 (Figure 2-3D) and comparatively large 50-100 nm diameter particles in device c_2 (Figure 2-3E). These results are representative of the G-V_G modifications seen in NTFET devices after the electrochemical deposition of NPs, and they are consistent with previous reports of metal deposition on NTFET devices.[27]

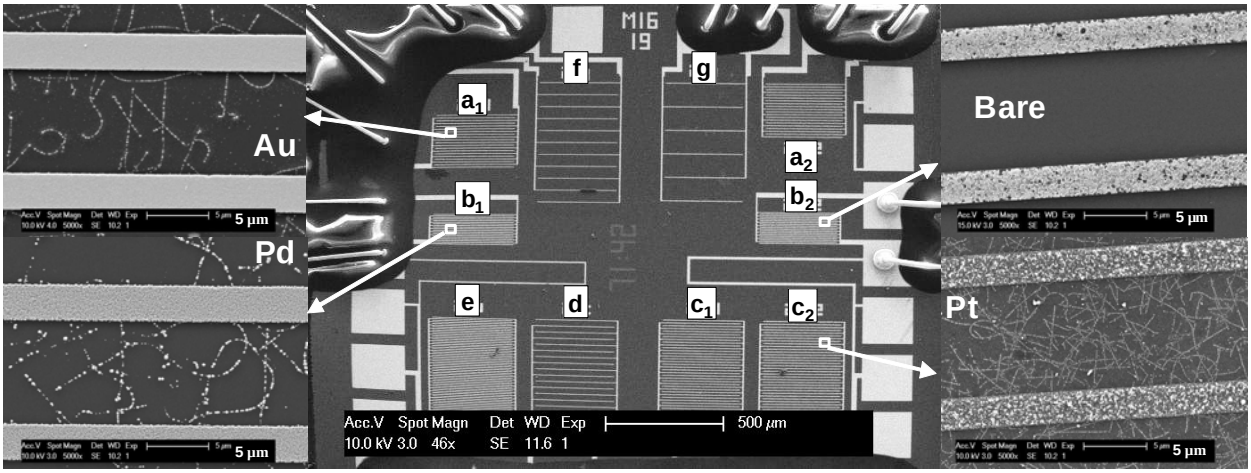

Figure 2-2. NP decorated NTFETs. Scanning electron microscope (SEM) images showing multiple interdigitated device geometries present on the NTFET chips (center) and selective Au deposition on device a_1, Pd deposition on device b_1, and Pt deposition on device c_2 while the complimentary degenerate devices remained bare, as shown with device b_2.

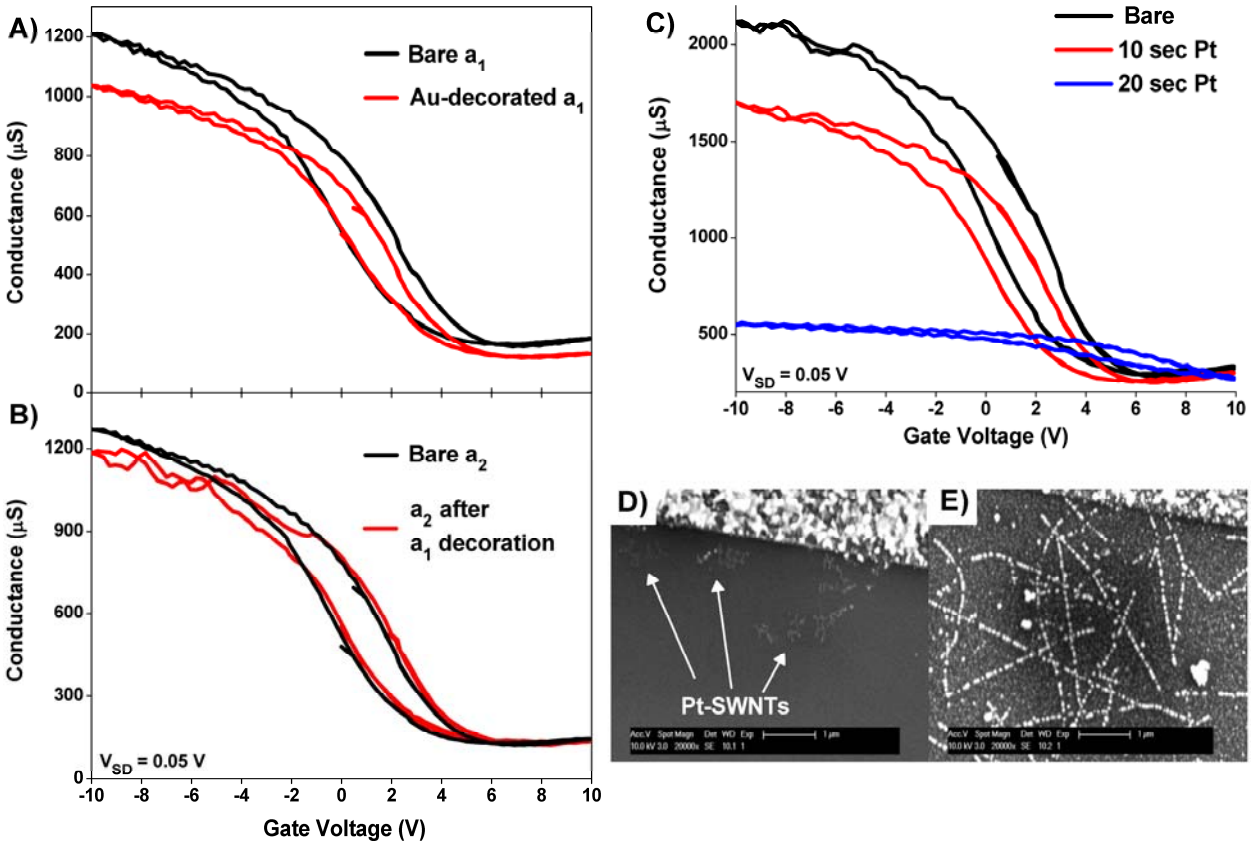

Figure 2-3. NP decorated NTFET transfer characteristics. G-V_G transfer characteristics of A) device a_1 and B) device a_2 before and after selective Au nanoparticle (NP) deposition on device a_1. Au NP deposition caused a slight tilt in G-V_G curve of device a_1 while the undecorated device a_2 G-V_G curve does not significantly change, indicating selective Au deposition only on device a_1. C) G-V_G modification of Pt-decorated devices c_1 and c_2 due to different deposition times where devices c_1 and c_2 were held at -1.0 V for 10 and 20 s, respectively; before deposition the G-V_G curves of c_1 and c_2 were equivalent. SEM images of devices after (D) 10 seconds of Pt deposition showing small (~20 nm) Pt nanoparticles and (E) 20 seconds of Pt deposition showing larger (50-100 nm) Pt nanoparticles, illustrating how larger MNPs distort the device G-V_G curve. V_{SD} = 0.05 V for all G-V_G curves.

G-V_G transfer characteristics of all devices on a particular NTFET chip were simultaneously monitored under a 300 SCCM flow of dry N_2 and 10 ppm NO in N_2. The flow system was flushed with dry N_2 for 1 hour prior to NO exposure to remove any O_2 or humidity present from atmospheric exposure during insertion of the NTFET chip. Removal of O_2 and trace H_2O from the flow system was necessary to ensure that NO did not undergo any Red/Ox reactions in transit to the chip. Initially NO exposure caused a positive shift in device gate voltage which reversed and stabilized upon further exposure. We hypothesize that NO consumed surface-bound oxygen species on the NPs, and by producing electron-withdrawing NO_2 caused the positive shift in device gate voltage.[21b,27] Further NO exposure depleted the surface bound oxygen, and eventually resulted in a NO-saturated equilibrium on the nanoparticle surface. NO_2 production time varied depending on the metal species, but an exposure time of 1 hour was used for all experiments to ensure measurement in a homogeneous atmosphere and equilibrium state NO coverage on the nanoparticle. As NO has an unpaired electron, it is expected to be a weak electron donor, and after the device transfer characteristics stabilized it was found that exposure to 10 ppm NO resulted in a small decrease in conductance and negative shift in gate voltage for all devices on the same chip, with metal-decorated devices showing consistently larger gate voltage shifts.

Figure 2-4 shows the representative response of Chip 1 devices a_2 (bare) and a_1 (Au decorated) upon exposure to dry 10 ppm NO in N_2. It can be seen that NO exposure caused a smaller gate voltage shift in the bare device a_2 (Figure 2-4A) compared to the Au decorated device a_1 (Figure 2-4B), indicating increased electronic donation into the SWNT network of device a_1. Without extensive passivation techniques[29] to isolate the device contacts, it is difficult to determine if the small response of the bare a_1 device originate from NO interaction with the

SWNT network or the contacts; however, the increased gate voltage shift in the Au-decorated NTFET suggests that the NPs enhanced the electron donation effects of the adsorbed NO molecules. The G-V_G transfer characteristics of six bare devices and three metal decorated devices were monitored on two NTFET chips during gas exposure. For a particular chip it was found that bare devices with different geometries and electrode separations (pitch) showed consistent gate voltage shifts, and NP decorated devices all demonstrated unique gate voltage shifts larger than the bare devices. Additionally, the gate voltage shifts in NP decorated devices showed a dependence on the metal work function, where larger shifts were seen in devices decorated with smaller work function metals.

We noticed that while the two NTFET chips demonstrated different magnitude responses to NO gas, the trend between smaller work function and increased device gate voltage shift was consistent. After comparing degenerate bare and decorated devices on separate chips and finding the trend was independent of the particular device geometry, owing to an average nanoparticle density on the nanotube network, all four metals were used to decorate devices on a single chip (Chip 3). Two devices on Chip 3 were decorated with each metal for either 10 or 20 seconds (see Table 2-1 for specific details). Depositing the metals in this manner allowed a direct comparison between metal decorated NTFET devices on one chip, removing the inconsistency in response magnitude between individual chips. Additionally, this allowed the comparison between the NP size and device response to be made for each metal. It was found that devices decorated with a particular metal nanoparticle showed equivalent gate voltage shifts upon NO exposure despite the difference in particle size, which indicates that metal work function, and not particle size, influenced electronic donation into the SWNT network.

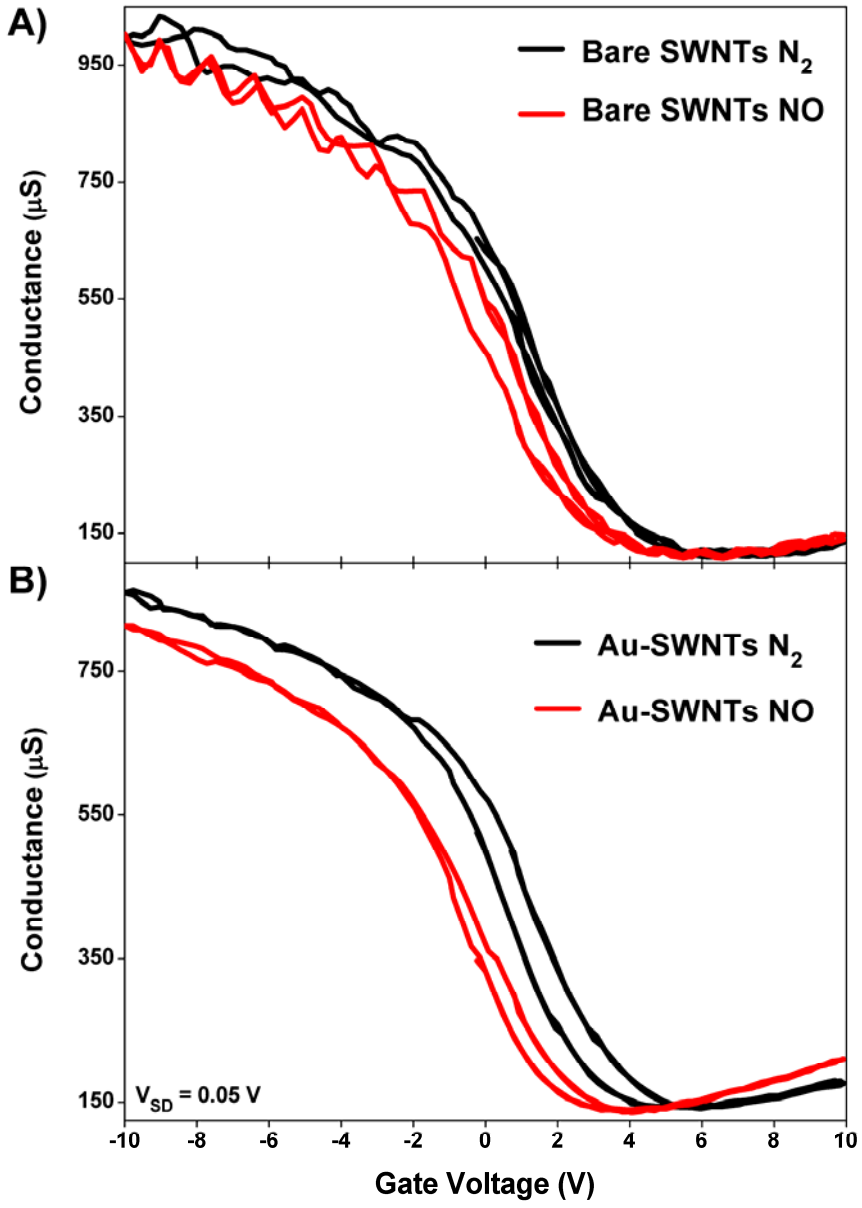

Figure 2-4. NP-decorated NTFET response to NO gas. G-V_G transfer characteristics of NTFETs composed of (A) bare SWNTs and (B) Au-SWNTs in the presence of pure N_2 (black curves) and 10 ppm NO gas (red curves). The response can be taken as the magnitude of the gate voltage shift from N_2 to NO, and a larger gate voltage shift indicates increased electron transfer into the Au-SWNT network.

Table 2-1. Summary of NTFET device gate voltage shifts (ΔV_G) after NO gas exposure. All devices were measured before and after decoration with a particular NP species; the particle size and work function (Φ) of each metal is listed.

Device	**Pitch (μm)**	**Metal**	**Deposition Time (s)**	**Particle Size (nm)**	**Φ (eV)**	**Δ V_G (V)**
All (n = 8)	5-100	Bare	0	N/A	N/A	-0.30 ± 0.02
a_1	10	Ag	10	70-140	4.26	–0.84
a_2	10	Ag	20	80-200	4.26	–0.83
b_1	5	Au	10	40-80	~ 5.0	–0.75
b_2	5	Au	20	110-150	~ 5.0	–0.73
e	5	Pd	10	45-80	5.12	–0.66
d	25	Pd	20	100-190	5.12	–0.69
c_1	10	Pt	10	40-80	5.65	–0.57
c_2	10	Pt	20	80-200	5.65	–0.55

Each metal decorated NTFET device had a unique gate voltage shift upon exposure to NO gas, and when the absolute value of the shift was plotted against the metal work function (Φ) a clear trend was found where smaller work function lead to a larger gate voltage shift. Figure 2-5 shows the relationship between metal work function and absolute value of the voltage shifts in response to NO for metal decorated devices on Chip 3, where hollow and solid labels represent the response of devices held at a deposition time of 10 (solid labels) or 20 (hollow labels) seconds. Mention should be made concerning the discrepancy found in literature values for Φ_{Au}.[30] Common values for Φ_{Pd}, Φ_{Pt} and Φ_{Ag}[30d] were used, and in the absence of a consistent value for Φ_{Au}, an appropriate value was picked (~5.0 eV); in light of this discrepancy we contend any reasonable literature value for Φ_{Au} will still show trend similar to that presented in Figure 2-5.

Schottky barriers at bulk metal-semiconductor interfaces are known to depend on work function and gas exposure;[17,18,31] however, the description of the potential barrier at NP interfaces is still incomplete. Difficulty in applying traditional Schottky junction behavior has lead some to suggest that metal NPs create interfacial "Schottky-type" potential barriers on semiconducting substrates,[32] and it has been shown experimentally that Au NPs form a size dependent "nano-Schottky" potential barriers on semiconducting substrates that asymptotically approach the macroscopic Schottky barrier.[33] Regardless of the controversy over the nature of the potential barrier existing at a NP-semiconductor interface, several important observations can be made regarding the electronic interaction at the SWNT-nanoparticle interface.

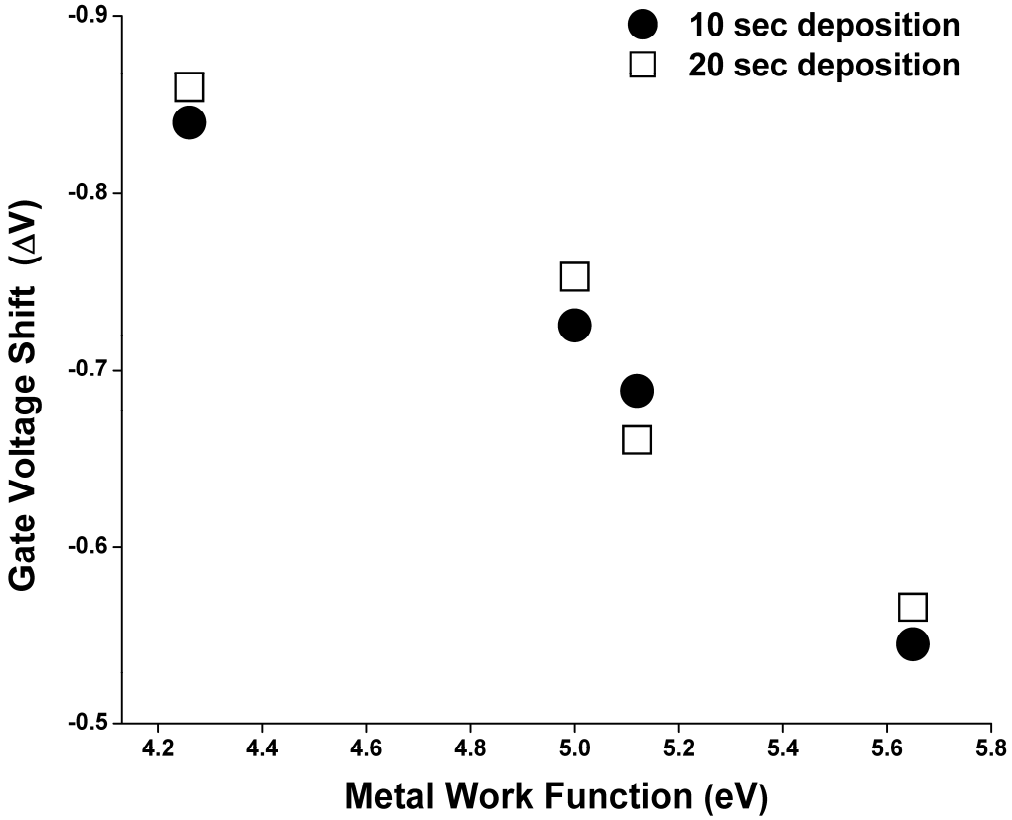

Figure 2-5. Summary of NP-decorated NTFET response to NO gas. Relationship between metal work function and absolute value of observed gate voltage shift in metal decorated NTFET. Each metal was used to decorate two devices with either a 10 second (solid labels) or 20 second (hollow labels) deposition time.

First, NP deposition creates a characteristic "tilt" in the device transfer characteristic. This has been previously described as a screening effect on the gate voltage,[27] but deformation of the G-V_G curve geometry can also be attributed to changes in carrier mobility.[34] It is known that Fermi level alignment occurs whenever a metal and semiconductor are placed in contact, resulting in charge redistribution and the formation of a depletion layer surrounding the metal.[31] The SWNT supported NP will experience this effect and create localized depletion regions on the SWNT wall.[35] These charge depletion regions should act as charge scattering sites that would create deviation in the hole trajectory, as shown in Figure 2-6A. The result would be a reduction in charge mobility through the SWNT network, causing the observed tilt in the decorated device transfer characteristic. Because larger (≥20 nm) nanoparticles were used, the thickness of the depletion region at the SWNT-nanoparticle interface should not be size dependent;[33,35] therefore, decreased charge mobility should be a proportional to SWNT surface coverage. Secondly, it appears the potential barrier at the NP-SWNT interface only affects the number of charge carriers upon exposure to NO gas. This can be rationalized by the addition of electronic density into the NP during NO adsorption and subsequent electron-hole recombination in the SWNT. As shown in Figure 2-6B, the added electronic density must overcome a small potential barrier to enter the SWNT, whereupon charge recombination occurs. This reduction of hole density in the SWNT is seen as a negative shift in device gate voltage. It was mentioned that the gate voltage shifts of devices decorated with different sized NPs were equivalent, this observation is important because it gives experimental evidence that the small potential barrier at the SWNT-nanoparticle interface is not dependent upon nanoparticle size, but rather metal work function.

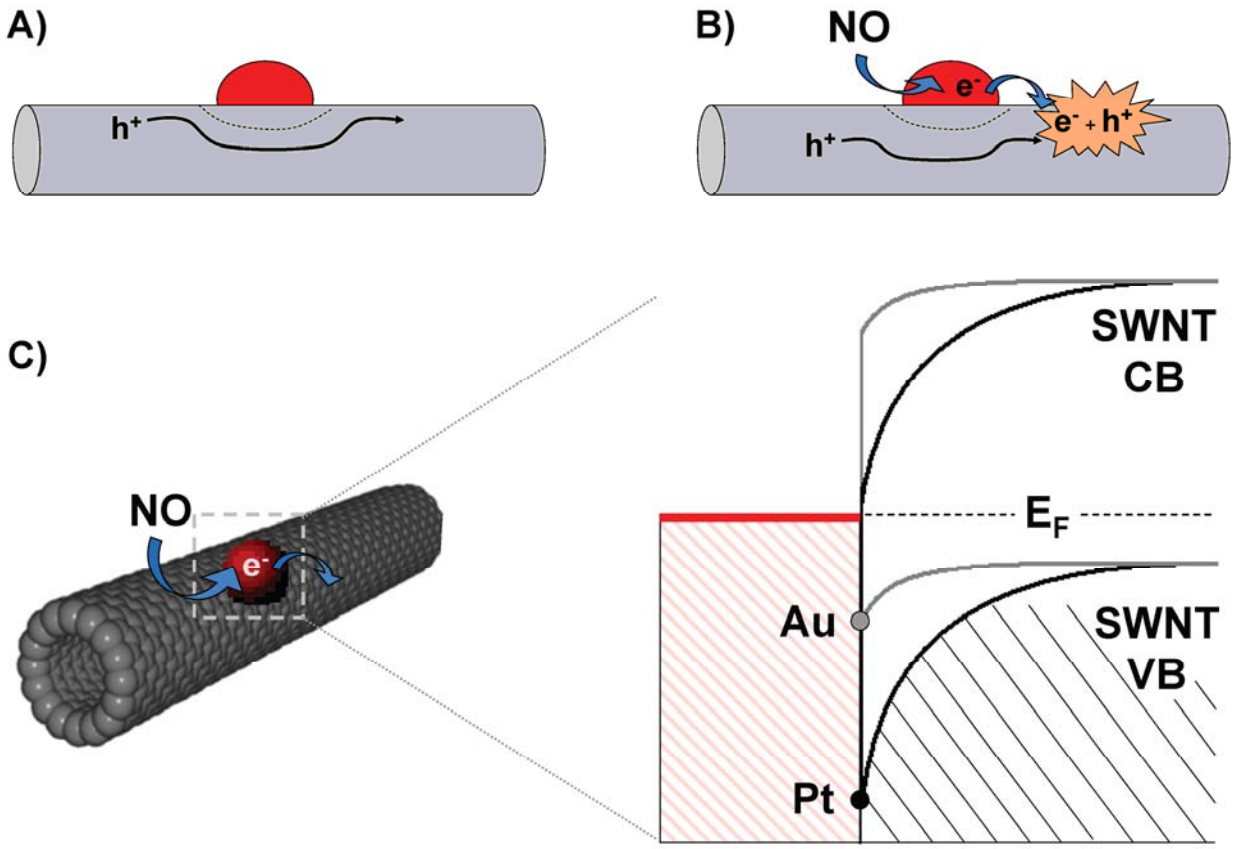

Figure 2-6. NP-decorated NTFET response mechanism. A) Deposition of NPs on the SWNT results in a localized depletion regions (dashed line) surrounding the NPs; this depletion layer creates an obstacle for hole transport and reduces carrier mobility. B) Adsorption of NO at the NP surface increases the electron density of the NP, which after crossing a small potential barrier recombines with holes in the SWNT and creates a negative shift in the device gate voltage. C) Expanded view of the electronic interaction occurring at the NP-SWNT. The potential barrier for electron travel into the SWNT valence band is dependent upon the work function of the metal nanoparticle with lower work functions resulting in lower potential barriers for charge recombination.

Lastly, the electronic donation into the SWNT network (negative gate voltage shift) scaled inversely with the work function of the NP, indicating the existence of a metal work function dependent potential barrier between the SWNT and NP. Figure 2-6C depicts the potential barrier at the NP-SWNT interface. Due to the much smaller size of the metal nanoparticle, we rationalize that the NP Fermi level was most affected, and we contend that the SWNT Fermi level remained relatively constant. By holding the SWNT Fermi level constant, the relative scale of the interfacial potential barrier can be correlated with the work function of the metal. Here, Au and Pt are used as an example, and it can be seen that lower work function results in a lower potential barrier; this allows a larger amount of electronic density to transfer into the SWNT, and creates a larger negative shift in the device gate voltage. Interestingly, similar results were seen in SWNTs end-contacted to bulk metals of similar work function; it was found that SWNTs contacted with lower work function metals resulted in negative shifts in the device threshold voltage.[18,36] The main difference between the SWNT supported NPs and bulk metal contacts is that until electronic density is introduced, *via* molecular interaction, the NP acts as an inert hole scattering site. Only upon electronic interaction do the SWNT-supported NPs show behavior similar to bulk metal contacts. Based on these observations we contend that the potential barrier at the SWNT-metal nanoparticle interface is not a traditional Schottky barrier, and the effect of the potential barrier on the device gate voltage is only felt when a molecular bias (electronic interaction) is applied.

2.6 CONCLUSION

Through device selective electro-deposition of Ag, Au, Pd and Pt NPs, we have shown experimentally that electronic donation into the SWNT network of a NTFET upon exposure to NO gas in N_2 depends upon the work function of the metal. Furthermore, we have given evidence that a potential barrier exists at the NP-SWNT interface that is intimately related to the work function of the metal. While the potential barrier at the NP-SWNT interface does resemble traditional Schottky barriers in some regards, there are several differences that make it stand apart and necessitate a unique description. Additionally, we have shown that the NP-SWNT potential barrier is not size dependent, as devices decorated with NPs of different sizes gave equivalent gate voltage shifts upon exposure to NO gas. It is now possible to rationalize metal decorated SWNT sensor array response as a combination of analyte electronic transfer and the potential barrier at the particular NP-SWNT, where a work function dependent response should be expected for each metal-analyte interaction. It is that hoped further investigation into the intimate electronic relationship between CNTs and NPs will lead to the design of higher sensitivity chemical sensor platforms and more efficient catalytic reaction pathways.

Acknowledgement. We thank Nanomix Inc. for supplying the NTFET devices used in this study. The authors thank the Department of Materials Science and Engineering for the provision of access to the electron microscopy instrumentation and Dr. P. D. Kichambare and A. Stewart for assistance with the execution of this part of our research.

3.0 SINGLE-WALLED CARBON NANOTUBE SPECTROSCOPIC AND ELECTRONIC FIELD-EFFECT TRANSISTOR MEASUREMENTS: A COMBINED APPROACH

3.1 CHAPTER PREFACE

The aim of this work was to propose the use of both optical spectroscopy and electrical measurements to understand the mechanistic aspects of SWNT sensor response. Here we intended to highlight how optical spectroscopy and electrical transport measurements could be complementary, and a combination of both techniques to investigate SWNT response to a particular analyte was superior approach to using either method exclusively. Specifically, we suggested that this combination of optical spectroscopy and electrical transport measurements could shed light onto the controversy of charge transfer *versus* Schottky barrier modification-based mechanisms for SWNT-based sensor response. The material contained in this chapter was published as a research paper in the journal *Small*, and the figures have been reproduced with permission; The full citation of this paper is listed as Reference 37 in the bibliography section.

List of Authors: Douglas R. Kauffman and Alexander Star.

Author contributions: DRK and AS wrote this paper.

3.2 ABSTRACT

Spectroscopic and electronic field-effect transistor measurements reveal complementary information about molecular interactions with single walled carbon nanotubes (SWNTs). Here we demonstrate how these two techniques can be combined to further understand electronic modification of the SWNT. The complementary nature of these techniques stems from the perturbation of the SWNT electronic structure upon electronic interaction with an electron donating, or accepting species.

3.3 INTRODUCTION

The study and application of carbon nanotubes (CNTs) has gained much interest in recent years.[38,39] The rapid progress and seemingly limitless application of CNTs is quickly bridging the field between traditional chemistry and device physics. Two predominant techniques have been used to monitor the electronic structure of CNTs in the presence of molecular species, namely optical spectroscopy and electronic field effect transistor (FET) measurements. While these methods have independently revealed vast amounts of information about the electronic structure and nature of molecular interactions, they are seldom used in tandem. The scheme outlined in this chapter serves to illustrate the intimate relationship between optical spectroscopy and electrical transport measurements. The relation between the two techniques stems from the outcome of molecular interactions with the SWNT; perturbation of the SWNT electronic structure.

3.4 PRINCIPLES OF SINGLE-WALLED CARBON NANOTUBE OPTICAL SPECTROSCOPY MEASUREMENTS

Conceptualization of SWNT electronic structure has often been aided through the analogy of a perfect sheet of graphene rolled into a cylinder.[2,4] Depending on how the cylinder is "rolled-up" the SWNT will have a particular chirality that depends upon two so-called "roll up" vectors *n* and *m*,[40] as shown in Figure 3-1A. The roll-up vectors describe the orbital overlap of the SWNT creating metallic (*n-m=3k)*, and semiconducting (*n-m≠3k,0*) varieties. The chirality of semiconducting SWNT dictates π-orbital overlap such that three discrete electronic transitions are present called the S_{11}, S_{22} and S_{33}, as show in Figure 3-1B. The chirality of metallic SWNT creates non-zero electronic density at the Fermi level, and results in one metallic transition called the M_{11} positioned in energy between the semiconducting S_{22} and S_{33}. In addition to chirality the nanotube diameter also affects absorption energy,[6] with smaller diameter SWNT absorbing at higher energy wavelengths.

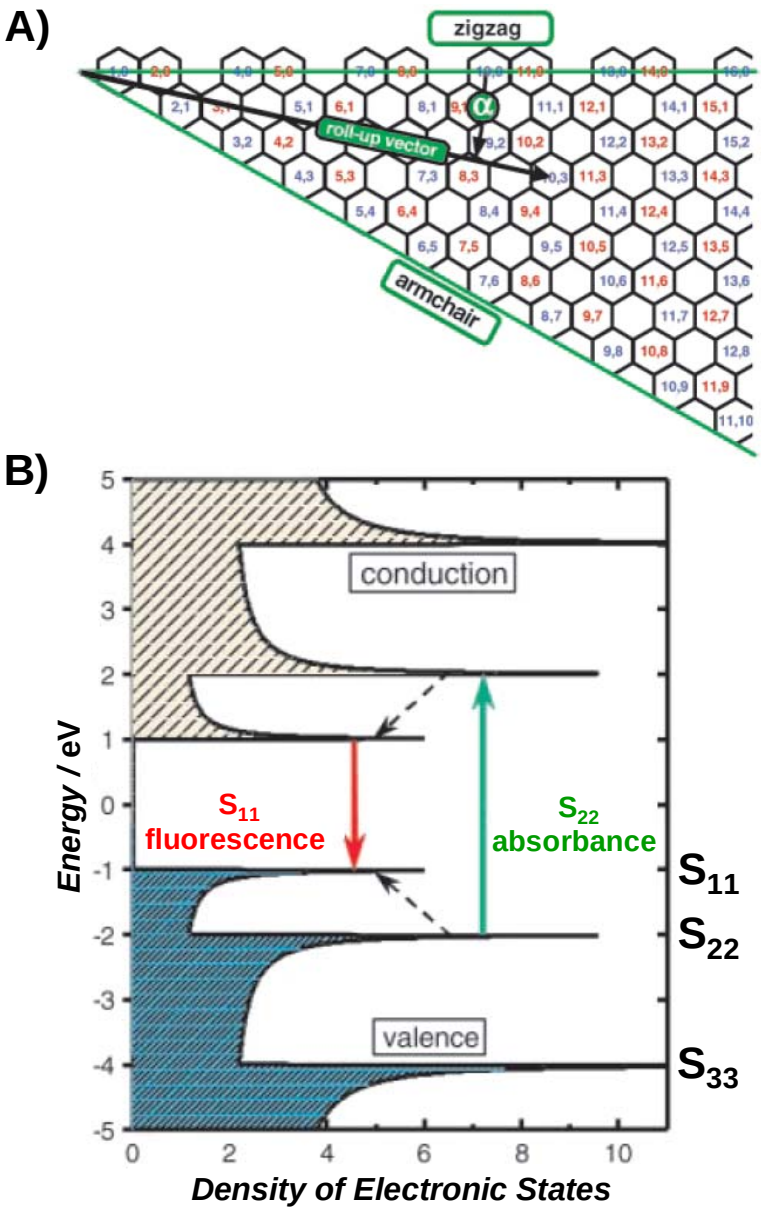

Figure 3-1. SWNT roll-up vectors and band structure. A) Depiction of SWNT roll-up vector with different chiral indices. B) Density of states diagram showing the semiconducting SWNT and the S_{11}, S_{22}, and S_{33} electronic transitions. Reproduced with permission from Ref. 6b; Copyright AAAS, 2002.

Previous reports have shown that some molecules will preferentially interact with either semiconducting or metallic SWNTs,[41] and as a result only certain electronic transitions will be modified by charge transfer. In metallic SWNT selective interactions, the M_{11} band will be modified, whereas in semiconducting selective interactions the S_{11} and S_{22} bands will experience some type of spectral alteration. For example, Strano *et al.*[42] reported diazonium reagents show covalent attachment exclusive to metallic SWNT that leads to a degradation of the M_{11} absorption band while leaving the semiconducting bands essentially unaffected. Similar results were realized by Yang *et al.*[43] with the preferential attack of metallic SWNT by fluorine gas. Exposure to fluorine gas, and subsequent heating resulted in a near complete loss of the metallic M_{11} optical absorption band, while the semiconducting SWNT absorption bands remained intact. In both cases, the selectivity towards metallic SWNT was attributed to finite electronic density at the Fermi level. Semiconducting SWNTs can also experience modification of the characteristic absorption bands. For example, by using a sample of SWNTs enriched with semiconducting chiralities Zheng and Diner[44] reported that strong oxidants, such as $KMnO_4$ and K_2IrCl_6 will decrease the S_{11} absorption band, and it was found that sidewall protonation in acidic conditions will produce similar S_{11} degradation.[45] While the previous two examples are not strictly semiconducting specific interactions, they do serve to illustrate the effective of modifying the SWNT absorption spectra *via* chemical interactions.

3.5 PRINCIPLES OF SINGLE-WALLED CARBON NANOTUBE FIELD-EFFECT TRANSISTOR MEASUREMENTS

A typical nanotube field-effect transistor (NTFET) is comprised of an individual or random network of SWNTs between source and drain electrodes with a Si back gate separated by SiO_2 insulating layer, as depicted in Figure 1-4. Applying a variable voltage through a gate electrode creates a so-called transfer characteristic, where the source-drain conductance is measured as a function of the gate voltage that is swept between negative and positive values. Molecular interactions will lead to charge transfer with the SWNT, which will change the number of charge carriers in the SWNT and subsequently shift the device gate voltage and modify the conductance. Under ambient conditions NTFETs behave as p-type semiconductors;[14] therefore, electron donation results in electron-hole recombination which is seen electronically as a decrease in the device conductance and a negative shift in the gate voltage. Conversely, electron withdrawal will serve to increase the hole concentration in the SWNT valence band and create a positive gate voltage shift and increased conductance. NTFET response to electronic withdrawal and donation has been shown experimentally with molecules such as NO_2 causing positive shifts in gate voltage and NH_3 causing negative shifts in gate voltage (Figure 1-5).[21] The interactions between SWNT and aromatic organic molecules have been investigated with NTFETs, and it was found that a linear relationship exists between the device gate voltage shifts and the electronegativity of the substituents on the aromatic ring, *i.e.* the Hammett constant.[46] Additionally, it is possible to quantify electron transfer based on the area of the NTFET device and the magnitude of the gate voltage shift through evaluation of the SWNT capacitance.[34] The SWNT specificity of the interaction can also be deduced from the transfer characteristic because semiconducting and metallic SWNTs demonstrate different electronic behavior in a NTFET.

Semiconducting SWNTs show a conductance dependency on the device gate voltage which resides in the upper portion of the curve, whereas metallic SWNT conductance is independent of the gate voltage and resides in the lower portion of the curve. Lastly, changes in the shape of the transfer characteristic yields information about the nature of the interaction. Changes in the carrier mobility modifies the tilt of the device G-V_G curve, called the transconductance (dG/dV),[14] and can be rationalized as the addition of charge scattering sites through molecular adsorption.[34] However, NTFET behavior is known to depend on the Schottky barrier existing at the SWNT-metal contact.[17] This has raised some controversy over the actual signal transduction mechanism because some have argued that molecular interactions modify the work function of the NTFET contact.[29,47] This argument suggests that device gate voltage shifts actually arise from changes in the contact work function and not electronic interaction with the SWNT.[18] This topic remains a subject of controversy, and it will be discussed in more detail later in the chapter.

3.6 A COMBINED APPROACH OF OPTICAL SPECTROSCOPY AND ELECTRICAL MEASUREMENTS

The spectroscopic and electronic behavior of SWNT undergoing non-covalent electronic interactions with an electron donation or electron accepting molecule can be further developed using frontier orbital theory.[41a] As SWNTs are p-doped in ambient atmosphere, the valence band will be partially depleted,[14] and charge transfer interactions with adsorbing molecular species will occur at the top of the valence band.[48] As a result, molecular interactions necessitate correct molecular orbital (MO) energy, and SWNT response can be thought of in terms of how the interaction shifts the top of the SWNT valence band with respect to the Fermi level. While it is

known that covalent bonds destroy the aromaticity of the SWNTs and ultimately result in the loss of spectral features,[49] non-covalent interactions allow electronic interaction with the SWNT valence band (Figure 3-2) while maintaining the π-electron system. This non-destructive electronic exchange is ideal for applying a tandem approach.

An electron withdrawing molecule will have an unfilled MO positioned below the top of the SWNT valence band, whereas an electron donating species will have a full MO positioned above the SWNT valence band. As a result, electron transfer into or out of the SWNT valence band will have several consequences: (1) electron transfer will render the nanotube either less (electron donation) or more (electron withdrawal) p-type. This can be monitored electronically through shifts in the NTFET transfer characteristics. Electronic donation will result in electron-hole recombination and create a negative shift in the NTFET transfer characteristic, whereas electronic withdrawal will result in positive shifts in the NTFET transfer characteristics. (2) Electronic transfer with the SWNT valence band will serve to modify the electronic density and optical band gap. A decrease in electronic density will result in a decreased S_{11} band absorbance (bleaching) and should correspond to a shift towards smaller wavelengths as a result of increased band gap. Alternatively, electronic donation will add electronic density into the SWNT valence band and increase S_{11} band absorbance. Moreover the decreased band gap should also serve to shift to S_{11} absorption band towards longer wavelengths. Interestingly this approach has been illustrated in the creation of an optical NTFET, where the valence band of a SWNT film was modified by applying varied gate voltages.[50]

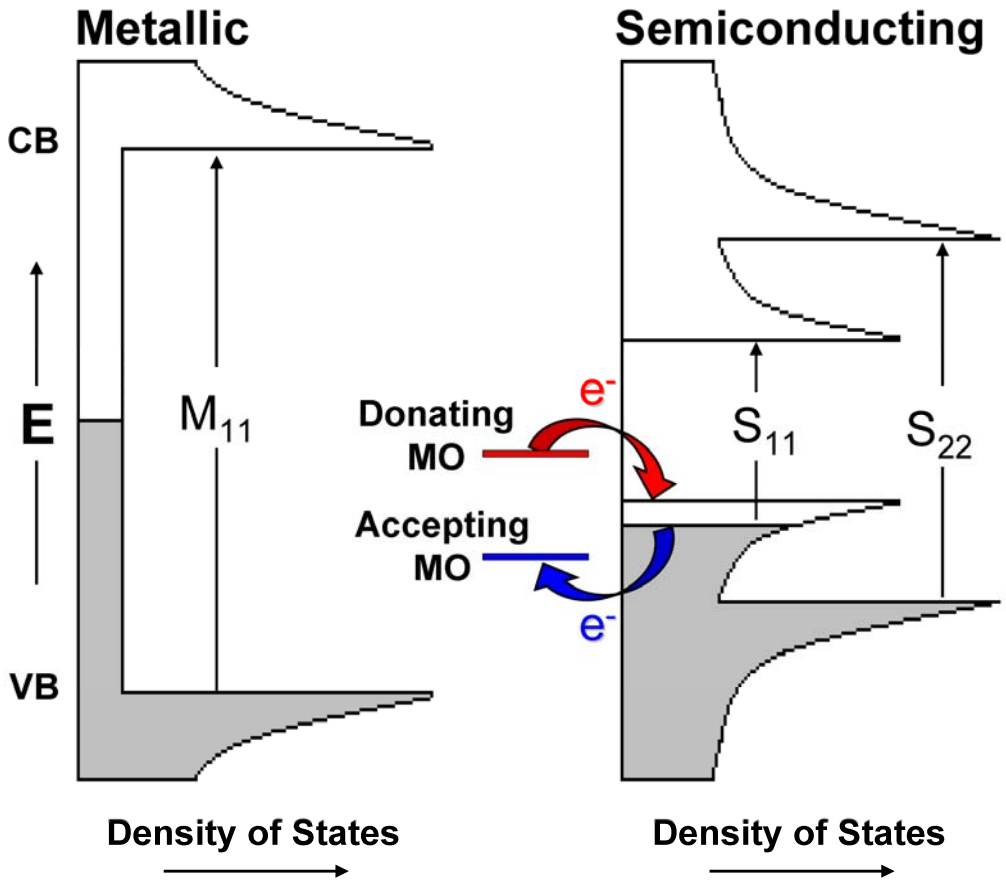

Figure 3-2. Molecular interactions with SWNTs. Partial density of states diagram representing the relative energy levels of the semiconducting SWNT valence band (VB) with interacting molecular orbitals (MOs) in two different scenarios: (1) interaction with an electron donating MO, and (2) interaction with an electron accepting MO. In order for a MO to donate electronic density it must reside higher in energy than the partially vacant SWNT valence band. Alternatively, to accept electronic density the MO must be partially vacant and reside lower in energy than the SWNT valence band.

Lastly, this combined approach can shed some new light on the controversy over the true mechanism of signal transduction in NTFET devices. Specifically, it can indicate whether the signal is a result of electronic interaction with the SWNT or Schottky barrier modification. This debate arises because supposed electron donating molecules will lower the work function of the device contact, and produce results similar to that of electron donation. For this reason it has been difficult to determine the true transduction pathway during NTFET sensing events. However, thinfilm optical absorption spectroscopy, when combined with NTFET measurements, can differentiate between the electronic interactions with the SWNT, and modification of the device Schottky Barrier. For example, the interaction with an electron donating species will cause a negative shift in the gate voltage of NTFET devices. If electronic donation into the SWNT is indeed occurring, then spectral modification in the S_{11} absorption band should result. Conversely, if Schottky barrier modification is the dominant mechanism behind the NTFET behavior then no spectral changes should occur. Accordingly, this approach can not only be used to track electronic transfer in the SWNT system, but it can be used to determine to what extent Schottky barrier modification plays in the response of the NTFET device, and should help to alleviate some of the controversy surrounding molecular sensing using NTFETs.

3.7 CONCLUSIONS AND OUTLOOK

In this chapter we have outlined a concept for the rationalization of NTFET and spectroscopic behavior of SWNTs through the use of frontier orbital and band theory. We have proposed that SWNT spectroscopic and electronic behavior, upon molecular interaction, can be described in terms of the electronic density in the valence band. Through electronic donation or withdrawal

the relative position of the SWNT valence band will be altered with respect to the Fermi level, and the subsequent change in the electronic band gap and carrier density will modify the SWNT spectroscopic and electronic transistor behavior. The qualitative correlation between SWNT thinfilm spectroscopic shifts and NTFET transfer characteristics can provide a more in depth analysis of molecular interactions occurring at the SWNT surface. Future chapters will describe work using this approach to investigate the interactions between SWNTs and adsorbing chemical species.

4.0 INTERACTIONS BETWEEN SINGLE-WALLED CARBON NANOTUBES AND TETRAPHENYL METALLOPORPHYRINS: CORRELATION BETWEEN SPECTROSCOPIC AND FIELD-EFFECT TRANSISTOR MEASUREMENTS

4.1 CHAPTER PREFACE

The aim of this work was to provide experimental evidence that the combination of optical spectroscopy and NTFET measurements produced complementary information about the interaction between SWNTs and adsorbing molecular species, building upon the concepts presented in Chapter 3.0

Tetraphenyl metalloporphyrins (M-TPP) have been shown to noncovalently attach to the sidewalls of SWNTs,[51] presumably resulting in the donation of electronic density from M-TPP into the SWNT. Previously, the donation of electronic density into the SWNT valence band had only been measured using electronic NTFET measurements.[34] However, we hypothesized that the attachment of M-TPP onto the sidewall of SWNTs would also result in complimentary modifications to the spectroscopic signature of the SWNT S_{11} electronic transition. The added electronic density should serve to increase the transition intensity and decrease the band gap, resulting in a red shift in the absorption wavelength. By observing independent changes in the electronic NTFET and spectroscopic properties of the SWNTs after functionalization with M-TPP species, we hoped to correlate the two characterization techniques and demonstrate that they both originated from modification of the electronic density in the SWNT valence band. While the SWNT/M-TTP complex has been relatively well studied, the correlation between solid-state

electronic and spectroscopic measurements had not yet been shown. Therefore, this system provided a good starting point to demonstrate the relationship between optical spectroscopy and electrical transport measurements of SWNTs.

The material contained in this chapter was published as a research paper in *The Journal of Physical Chemistry C*; the figures and table in this chapter have been reproduced with permission from *J. Phys Chem. C* **2007**, *111*, 3539. Copyright 2007 American Chemical Society; the full citation is listed as reference 52 in the bibliography section.

List of Authors: Douglas R. Kauffman, Oleksandr Kuzmych and Alexander Star.

Author contributions: DRK and AS designed the experiments and wrote the paper. Optical spectroscopy was conducted by DRK and field-effect transistor work was performed by DRK and OK.

4.2 ABSTRACT

Noncovalent functionalization of single-walled carbon nanotubes (SWNTs) with metallotetraphenyl porphyrins (M-TPPs) was monitored with UV-vis-NIR absorption spectroscopy and electroanalytical measurements using nanotube field-effect transistors (NTFETs). By comparing the experimental data that we have obtained using both techniques, we have found that M-TTPs donate electron density exclusively into semiconducting SWNTs. Moreover, thin-film UV-vis-NIR absorption spectroscopy on SWNT/M-TPP complexes provides a well-resolved picture of the interaction between the SWNT valence band and the electron-donating M-TPP. In total, the electron donating properties of four different M-TPPs containing Mn(III), Co(II), Cu(II), and Zn(II) were compared, and the electronic affects of each are discussed.

4.3 INTRODUCTION

Porphyrins are an extensively studied group of organic molecules and much interest has been generated in exploiting their natural biochemical behavior.[53] Research into this rich field has produced developments such as solid-state[54] and electrochemical sensors,[55] as well as the design of integral components for solar energy conversion.[56] Compared to porphyrin research the field of carbon nanotube (CNT) chemistry is still in its infancy,[2] and much can be learned from coupling the well-studied porphyrins to the relatively new CNT system. Interest has been gaining in CNT research due, in part, to the potential for such applications as molecular electronics,[39] sensing devices[57] and catalytic platforms,[58] to name a few. Due to the CNT's environmentally

sensitive electronic properties, which can be probed by various spectroscopic[59] and electrical[21,39,60] methods, they represent an ideal candidate for nano-scale devices for extremely sensitive applications. Pairing the CNT with a system having photoactive properties, molecular selectivity, and electron-donating characteristics invites the possibility for the development of ultra-sensitive and compact devices for a host of energy conversion, analyte sensing, and catalytic capabilities.

Several studies have been conducted on the functionalization of single-walled carbon nanotubes (SWNTs) with porphyrin systems.[51] Recently, the interaction between SWNTs and porphyrins has lead to the creation of supramolecular assemblies[61] and the study of light-induced charge transfer[62] for applications in solar energy conversion. In light of the budding interest in SWNT-porphyrin hybrids, it is important to understand the result of the complexation between the two species in terms of the impact on the SWNT electronic structure. Combining two techniques such as optical spectroscopy and electroanalytical measurements using nanotube field effect transistors (NTFETs) creates a powerful tool for probing SWNT electronic structure. The extreme sensitivity of these techniques has been illustrated in recent studies monitoring the hybridization[63] and conformational changes[64] of DNA molecules immobilized on SWNT surfaces. In this chapter, we combine UV-Vis-NIR thinfilm absorption spectroscopy and NTFET measurements to address the consequences of porphyrin complex formation on the SWNT electronic structure. Specifically, we seek to determine how complexation with M-TPPs affects the electronic transitions and electrical transport properties of the SWNTs.

4.4 EXPERIMENTAL

As purchased SWNTs (Carbon Solutions) were sonicated into DMF for approximately 30 minutes until the solution became uniform in color, indicating good nanotube dispersion. 5,10,15,20-Tetraphenyl-21H,23H-porphine manganese(III) chloride (MnTPP), zinc(II) (ZnTPP), copper(II) (CuTPP), and cobalt(II) (CoTPP) tetraphenyl porphyrins (Sigma-Aldrich) were dissolved in DMF and introduced in excess to the SWNT solution. An additional 5-minute sonication was conducted to ensure even distribution of SWNT and M-TPP and facilitate complex formation. After stirring overnight, the solution was then filtered and rinsed with copious amounts of DMF, water and acetone to remove any free M-TPP, and finally dried in vacuum. The dried SWNT/M-TPP filtrate was re-dispersed in DMF by brief sonication and used for solution UV-Vis absorption spectroscopy or sprayed onto a heated quartz substrate with a commercial air brush (Iwata) to create SWNT/M-TPP thinfilms, which afterwards were dried in vacuum and used for spectroscopic measurements on a Lambda 900 UV-Vis-NIR Spectrophotometer (Perkin Elmer). NTFET devices were constructed as described elsewhere,[63a] but briefly, SWNTs were grown *via* a CVD process onto Si wafers and interdigitated Au/Ti electrodes were photolithographically patterned onto the SWNT network creating multiple devices on the Si chips. For experiments, chips were wire-bonded and packaged in a 40-pin Ceramic Dual-Inline Package (CERDIP) and tested using a custom NTFET electronic test fixture.[63a] NTFET devices were complexed with M-TPP by dropcasting a small volume of metalloporphyrin solution (1 μL; 10^{-4} M in THF or DMF) onto the NT network. NTFET source drain conductance *versus* gate voltage (G-VG) transfer characteristics were recorded with a V_G sweep frequency of 3 Hz at V_{SD} = 0.05 V using *LabView* data acquisition software.

4.5 RESULTS

In DMF, free MnTPP has major and minor peaks at 466 and 436 nm, that are known as the Soret and Q-bands and correspond to allowed and forbidden porphyrin ring π-π^* transitions, respectively.[65] The ability of the M-TTP to complex with ligands, such as nitric oxide (NO), has been known for some time, and ligation events typically result in modification to the M-TTP UV-Vis absorption spectra.[66] To investigate the affect of chemical ligation on the M-TTP absorbance spectrum, N_2 saturated solutions were bubbled with either 10 ppm NO or 10 ppm nitrogen dioxide (NO_2) for 60 seconds. Figure 4-1A shows the results of bubbling the N_2 saturated MnTPP solution (MnTPP / N_2; black curve) with 10 ppm NO (MnTPP / NO; red curve) or 10 ppm NO_2 (MnTPP / NO_2; blue curve). Initially, MnTPP had two Soret band peaks, with a less intense peak at 436 and a more intense peak at 466 nm. Bubbling with NO gas creates a clear increase and blueshift of the 436 nm peak, shifting it to 427 nm, while the 466 nm peak experiences a significant decrease in absorption intensity. This phenomenon has previously been explained as NO donating an electron from its singly occupied $2\pi^*$ orbital to the central Mn atom in the MnTPP.[66a,b] This has been suggested to create a Soret band blueshift by placing a negative charge on the porphyrin ring and pushing the porphyrin π and π^* orbitals further apart.[65] Upon exposure to NO_2, a similar increase in the 436 nm peak occurs; however, no blueshift was seen, and a small decrease in the 466 nm peak is also observed. This phenomenon has been observed in other porphyrin species, and recent reports have suggested that NO_2 molecules engage in π–π interaction with the porphyrin ring.[67] CoTPP, CuTPP and ZnTPP were also exposed to 10 ppm NO and NO_2 gases (not shown), with CoTPP showing a slight decrease

in its Soret Peak upon NO exposure, and the formation of a new lower wavelength peak in the presence of NO_2; CuTPP and ZnTPP did not show any response to either NO or NO_2.

The reaction of MnTPP with NO and NO_2 exposure is a useful starting point when investigating the interaction with SWNTs. Figure 4-1B shows the UV-Vis absorbance spectra of MnTPP (dashed black), bare SWNT (solid black) and the SWNT/MnTPP complex (red) in DMF. Pristine SWNTs do not show prominent spectroscopic features in the MnTPP Soret absorption region, but after complexation with MnTPP, filtration, rinsing and resuspension, two small peaks developed at 436 and 466 nanometers. Interestingly, these features correspond to the ligated form of MnTPP, showing a larger peak at 436 nm and a smaller peak at 466 nm in accordance with literature results, [54b,c,68] and correspond to the attachment of M-TPP species onto the sidewalls of SWNTs.[69] In addition SWNT/CoTPP, SWNT/ZnTPP and SWNT/CuTPP complexes were investigated, but it was found that only CoTPP demonstrated a behavior to MnTPP in the Soret region in the presence of SWNTs, which probably resulted from solvent effects.

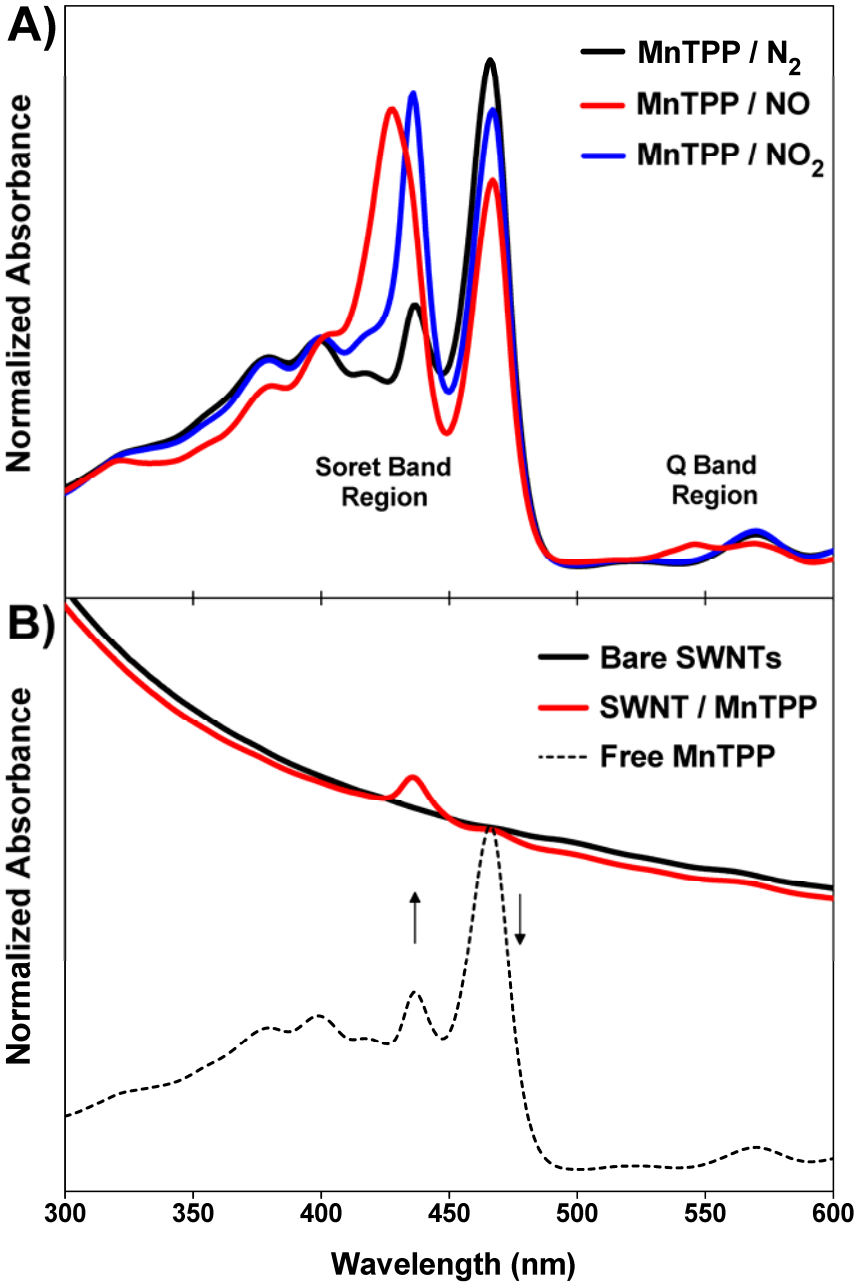

Figure 4-1. Mn tetraphenyl porphyrin (MnTPP) and SWNT absorbance spectra. A) UV-Vis Spectra of a DMF solution of MnTPP saturated with N_2 (MnTPP / N_2; black curve), 10 ppm nitric oxide (NO) gas (MnTPP / NO; red curve) or 10 ppm nitrogen dioxide (NO_2) gas (MnTPP / NO_2; blue curve). B) UV-Vis absorbance spectra of MnTPP (Free MnTPP; black dashed curve), bare SWNTs (black solid curve) and MnTPP functionalized SWNTs (SWNT / MnTPP; red curves) in DMF.

Thinfilms of SWNT/M-TPP complexes were made in order to investigate the NIR region of the SWNT S_{11} transition. Spectroscopic measurement of SWNT solutions in the NIR region is greatly complicated in solution for two main reasons; (1) water shows strong optical absorbance in this region and unless the experiments are conducted in a completely dry environment ambient water vapor will dissolve into the DMF solvent and mask the SWNT S_{11} band, and (2) the SWNT S_{12} transition is highly sensitive to the local solvent environment, and so-called solvatochromic effects can influence the absorption and fluorescent wavelengths.[70] The problems of dissolved water and solvatochromic effects were avoided entirely by probing the SWNT S_{11} region in the solid state. Moreover, the interconnected network of SWNTs obtained by spraying a film on quartz more closely resembles the nanotube environment present in NTFET devices, as compared to a solution of SWNTs.

Figure 4-2A compares the normalized UV-Vis-NIR absorption spectra of thinfilms of bare SWNTs (black curve) and the SWNT / MnTPP complex (red curve); spectra were normalized at 1500 nm (marked with blue asterisk). This comparison highlights the obvious change in the SWNT S_{11} absorbance band, which we suggest arose from the added electronic density in the SWNT valence band. Moreover, we proposed that the added electronic density would also serve to decrease the transition band gap, resulting in a redshift in the S_{11} band wavelength of maximum absorbance. Interestingly, we also observed an increase in the SWNT S_{22} absorption band, which is somewhat surprising because it is not expected to experience any change from the charge transfer. This phenomenon has been reported before but it was attributed to changes in the local solvent environment surrounding the SWNT,[71] and the SWNT S_{22} absorption in our particular case could be a change in the local dielectric environment from a layer of attached MnTPP molecules. MnTPP functionalization did not result in significant

modification to the SWNT M_{11} absorption band, which has been reported before.[72] CoTPP, CuTPP, and ZnTPP porphyrins all had equivalent effects on the SWNT S_{11} absorption band, as listed in Table 4-1.

Electronic NTFET measurements were conducted on the SWNT/M-TPP systems. Figure 4-2B presents the G-V_G transistor characteristics of a NTFET before (black curve) and after (red curve) MnTPP functionalization. The results of drop casting dilute MnTPP solutions onto the surface of the NTFET device were consistent regardless if the solvent was THF or DMF. However, DMF required a much longer drying time and THF was used for experimental convenience. Drop casting MnTPP onto the SWNT network of the NTFET device resulted in a shift in the transfer characteristic towards more negative gate voltages and decreased device conductance. This behavior is indicative of electronic donation into the SWNT network of the NTFET device. Furthermore, no significant change in the positive extreme of the gate voltage sweep occurred after the addition of the MnTPP, indicating no interaction with the metallic component of the SWNT network. CoTPP, CuTPP and ZnTPP all had effects on the NTFET transfer characteristic similar to MnTPP, such that functionalization resulted in a negative shift in gate voltage and a decrease in device conductance. The average shifts in gate voltage of NTFET devices functionalized with different M-TPPs are listed in Table 4-1; due to variations in device-to-device performance, the gate voltage shift can only be viewed as a general trend and we did not try to place any emphasis on the magnitude of the shift. These results corroborate the spectroscopic evidence of selective interaction between MnTPP and semiconducting SWNTs, and give experimental evidence that both the spectroscopic and electronic response to MnTPP functionalization resulted from electronic donation into the SWNT valence band.

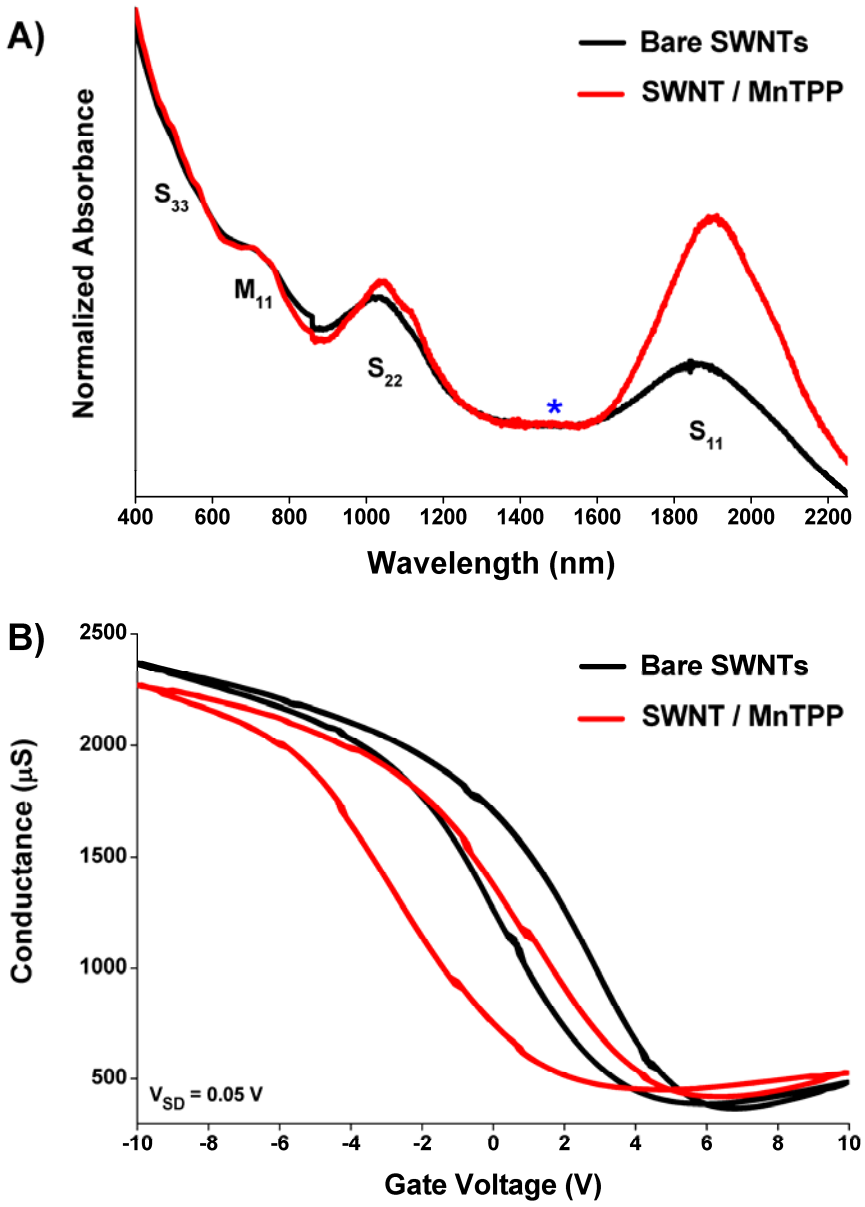

Figure 4-2. Solid-state porphyrin-SWNT absorption spectra and transistor behavior. A) Normalized thinfilm UV-Vis-NIR absorbance spectra of bare SWNTs (black curve) and the SWNT/MnTPP complex (red curve); the spectra were normalized at 1500 nm (marked with a blue asterisk). B) NTFET transfer characteristic showing the G-V_G curves of bare SWNTs (black curve) and MnTPP functionalized SWNTs (red curve); V_{SD} = 0.05 V.

Table 4-1. Summary of SWNT / M-TPP properties. The average gate voltage shifts (ΔV_G) were calculated from four individually tested devices functinoalized with the same M-TPP.

Complex	**S_{11} Band Redshift (meV)**	**Gate Voltage Shift (ΔV_G)**
SWNT / MnTPP	16	-2.2 ± 0.1
SWNT / ZnTPP	16	-4.3 ± 0.2
SWNT / CuTPP	15	-2.0 ± 0.5
SWNT / CoTPP	15	-4.3 ± 0.1

4.6 DISCUSSION

Upon complexation with M-TPP the SWNTs demonstrated a spectral redshift in the S_{11} band and to a lesser extent in the S_{22} band, whereas the M_{11} and S_{33} bands were un-shifted. Previous studies have concluded certain molecules preferentially interact with either semiconducting or metallic SWNTs[41] and metalloporphyrins have been shown to selectively interact with semiconducting SWNT.[72] Our spectroscopic results support this finding in that complexation only significantly modified the S_{11}. It is well established that metalloporphyrins are electron donating systems,[62,69,73] and, as SWNTs are hole doped in ambient conditions,[60a,b] the S_{11} band will be partially vacant.[48] As a result, electronic transfer is expected to occur at the top of the SWNT valence band,[45,48,48,74] meaning the S_{11} transition should be strongly effected. As M-TPP donates electronic density into the SWNT valence band the transition will redshift and become more intense due to the added electronic density and the decreased band gap (Figure 4-3). The small redshift in the S_{22} absorbance band has been reported previously in charge transfer experiments and has been attributed to noncovalent interactions between the charge transfer molecule and the SWNT sidewall.[71] However, unlike previous experiments, the S_{11} band did not experience bleaching, because the noncovalent π–π electron interactions prevent destruction of the SWNT electronic structure.

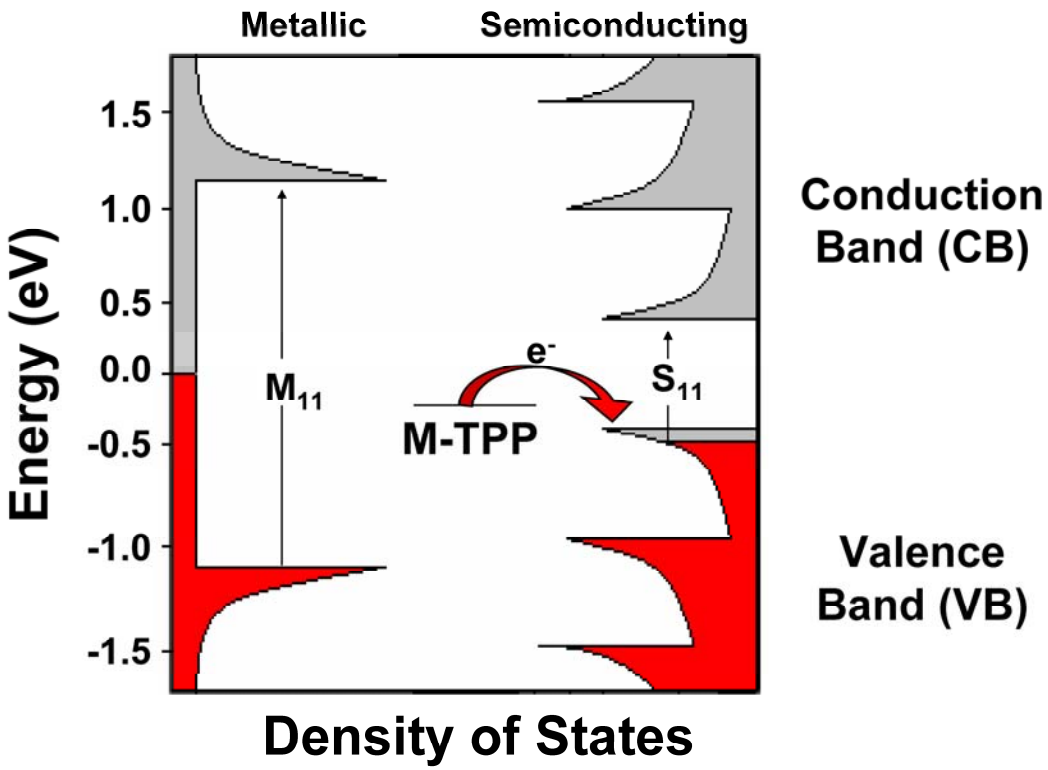

Figure 4-3. Porphyrin-SWNT interaction. Density of states (DOS) diagram showing electron donation from M-TTP into the partially vacant SWNT S_{11}.

From NTFET G-V_G measurements we observed a negative shift in gate voltage and no significant change in minimum conductance. Under ambient conditions NTFET devices are p-type,[16,60] meaning electron donation from M-TPP results in a decrease of the carrier concentration. The negative gate voltage shifts in M-TPP functionalized NTFETs G-V_G transfer characteristics are in line with previous findings.[34] The observed negative shift in gate voltage corroborates spectral redshifts resulting from electronic donation into the SWNT S_{11} valence band. We found that the NTFET gate voltage shifts are consistent for all device geometries functionalized with the same M-TPP, indicating device geometry did not play a role in charge transfer.

In the evaluation of this data we assumed surface adsorption of M-TTP on the SWNT, which is in line with previous porphyrin-functionalized SWNT studies.[51] The ability of porphyrins to maintain intimate contact with the SWNT sidewall is due to π–π stacking between the SWNT and aromatic porphyrin, and previous STM studies have found excellent porphyrin adsorption on HOPG,[75] which is an accepted model for nanotube sidewalls. Controversy does exist, however, on the orientation of adsorbed porphyrins. Previous studies have concluded that porphyrins in aqueous solutions can assemble in monolayers, or form extended rod-like aggregates on HOPG.[76] To address this controversy, we contend that porphyrin aggregation was avoided in thinfilm preparation due to thorough rinsing of SWNT/M-TTP complex filtrate; however, we followed a previous method for functionalizing NTFETs with M-TPP,[34] which may have allowed the formation of aggregate porphyrin structures on the nanotube surface due to solvent evaporation. Regardless of M-TTP aggregation in NTFET devices, all measurements indicated in electronic donation into the semiconducting SWNT valence band.

4.7 CONCLUSIONS

We have demonstrated that upon complexation with metalloporphyrins SWNTs experience an injection of electronic density into the S_{11} band, while confirming spectroscopically and electronically that M-TPP species donate electronic density into semiconducting SWNTs. Thinfilm UV-Vis-NIR absorption spectroscopy was employed to directly monitor the electronic changes in the lower energy SWNT transitions resulting from the complexation with the electron donating M-TPP. A better understanding of the fundamental charge transfer events present in the interaction between SWNT and M-TPP will hopefully lead to further progress in the study and applications such complexes for a host of novel sensing and optoelectronic platforms.

Acknowledgement. We thank Nanomix Inc. for supplying the NTFET devices used in this study.

5.0 SIMULTANEOUS SPECTROSCOPIC AND SOLID-STATE ELECTRONIC MEASUREMENT OF SINGLE-WALLED CARBON NANOTUBE DEVICES

5.1 CHAPTER PREFACE

The aim of this work was to build upon our concept of combining optical spectroscopy and electrical transport measurements that was discussed in Chapters 3 and 4. Specifically, we provided experimental evidence that the two measurement techniques can provide complementary information in real time. We chose the well-studied interaction between bare SWNTs and NH_3 and NO_2 to show that gas adsorption, and subsequent charge transfer, will produce simultaneous and complementary changes to the SWNT absorption spectrum and electrical transport properties. This approach is presented as a means to differentiate between two hotly debated sensor response mechanisms; charge transfer *versus* Schottky barrier modification at the SWNT-electrode interface. The material contained in this chapter was published as a research paper in *The Journal of Physical Chemistry C*; the figures and table contained in this chapter have been reproduced with permission from *J. Phys Chem. C* **2008**, *112*, 4430. Copyright 2008 American Chemical Society; the full citation is listed as reference 77 in the bibliography section.

List of Authors: Douglas R. Kauffman and Alexander Star

Author contributions: Both authors designed the experiments and wrote the paper. Experimental work was performed by DRK.

5.2 ABSTRACT

We describe simultaneous spectroscopic and solid-state electronic operation of a single-walled carbon nanotube (SWNT) thinfilm device under the influence of NH_3 and NO_2 gases. Using this simultaneous approach we show that both the optical absorbance and network conductance show a shared time dependency upon exposure to NH_3 or NO_2 gas. We show that the device behavior is dominated by gas adsorption on the SWNT network, and we explore the role of network density in regards to device behavior under gas exposure. Lastly, we provide evidence to suggest that the device sensitivity towards a particular analyte can be tuned by simply varying the density of the SWNT network.

5.3 INTRODUCTION

The development of gas and vapor sensors based on single-walled carbon nanotubes (SWNTs) has attracted considerable attention in recent years.[78] Despite the rapid progress in SWNT-based sensors, fundamental questions concerning the mechanism of the device response still remain. One widely held opinion is that charge transfer between the analyte molecule and SWNT is responsible for sensor response. A second argument is that molecular interaction with the device electrodes may actually produce sensor response. More specifically, molecular adsorption on the electrode could alter the metal's work function and modify the Schottky barrier (SB) at the SWNT-metal interface. The distinction between SB modification and charge transfer is a daunting task, and a good deal of debate surrounds this argument because both phenomena produce similar results. For example, Dai and coworkers[21b] first reported that exposing a SWNT

based device to NH_3 or NO_2 produced opposing sensor response, presumably from electron donation or withdrawal, respectively. However, Avouris and coworkers[18] have shown that similar results could be achieved by simply varying the work function of the device electrodes.

While NH_3 and NO_2 are widely considered the prototypical electron donating and withdrawing species, respectively, theoretical and experimental values of binding energy and charge transfer between SWNTs and these two gases varies widely.[20,25,29,79] For example, infrared[80] and x-ray photoelectron[81] spectroscopic studies have concluded that NO_2 and NH_3 adsorb onto SWNTs and subsequently effect their electronic structure. However, despite the many experimental examples of NO_2 and NH_3 interaction with SWNTs,[78] computational studies disagree on the exact adsorption geometries[82] and selectivity towards semiconducting or metallic SWNT types.[83] A simultaneous spectroscopic and electronic measurement technique would be an advantageous approach because it would allow one to consider the SWNT as a molecule by probing the electronic transitions spectroscopically while operating the sample as a chemically sensitive network resistor. By spectroscopically monitoring a working electronic device and adopting a molecular orbital (MO) based description of the chemical interactions occurring at the SWNT surface,[41a] one could begin to develop a more complete understanding of the mechanisms prompting the device response that either technique may not provide independently. The aim of this type of combined spectroscopic and electronic approach is to help identify significant mechanisms present in electronic SWNT devices. Understanding the processes that govern solid-state SWNT-based sensor response will help researchers develop device architectures that can exploit dominant phenomenon, and will provide another tool towards the goal of realizing more sensitive, and possibly selective sensors.

Recently, Haddon and coworkers[84] reported the simultaneous measurement of the optical spectroscopic and solid-state electronic properties of a sample of poly(m-aminobenzenesulfonic acid) (PABS) functionalized SWNTs in the presence of NH_3 gas and HCl vapor. In this report we detail the simultaneous spectroscopic and electronic behavior of devices composed of random networks of SWNTs in the presence of NO_2 and NH_3 gases. While some groups have utilized passivation techniques to chemically insulate device electrodes,[20,29] inconsistency in passivation layers and the possibility of gas diffusion through pinholes has created some confusion about the origin of device response. Here, we report on a technique to use changes in the optical absorption spectra of SWNTs to understand the electronic response of large area (~3.8 cm^2) SWNT network-based electronic devices. We present this technique as an additional route towards investigating molecular interaction with SWNTs without the need for complicated passivation schemes, and we provide evidence that strongly suggests the response of large area devices to NH_3 and NO_2 is dominated by gas adsorption on the SWNT network. Additionally, we show data that suggests more subtle effects, such as modification of inter-SWNT potential barriers, or interaction with the SWNT hydration layer or defect sites, may also contribute to the device response.

5.4 EXPERIMENTAL

A cartoon representing the setup for conducting *in situ* spectroscopic and electronic measurements on a single SWNT sample is shown in Figure 5-1A. SWNT thinfilm devices were created by spray casting a DMF suspension of SWNTs (Carbon Solutions P2 SWNTs; Batch # 02-170) onto a 1” x 1” quartz plate heated to 185 ^oC using a commercial air gun (Iwata, Inc.).

Electrodes were created using Al tape and conductive Ag paint (SPI Supplies),[85] and were spaced 1.5 cm apart. This ensured an unobstructed optical path through the device and separated the spectroscopically probed area a macroscopic distance from the electrodes—therefore removing it from any far-reaching SB effects.[29] A finished device is shown in Figure 5-1B, where the University of Pittsburgh emblem is clearly visible through the device.

Gas exposure experiments were conducted in a custom built gas flow chamber constructed out of Teflon (shown in Figure 5-1C) that was housed inside of a Perkin Elmer Lambda 900 UV-Vis-NIR spectrophotometer. After purging the chamber with dry N_2 for 30 minutes, either 10 ppm NO_2 or 100 ppm NH_3 (both in N_2) were introduced for a period of 90 minutes at a constant flow rate of 300 SCCM. UV-Vis-NIR absorption spectra of the SWNT films were continuously measured with a cycle time of 9 minutes. Network conductance versus time, G(t), measurements were conducted with a constant bias voltage of 500 mV using a Keithley 2400 Sourcemeter. Scanning electron microscopy was performed with a Phillips XL30 FEG microscope.

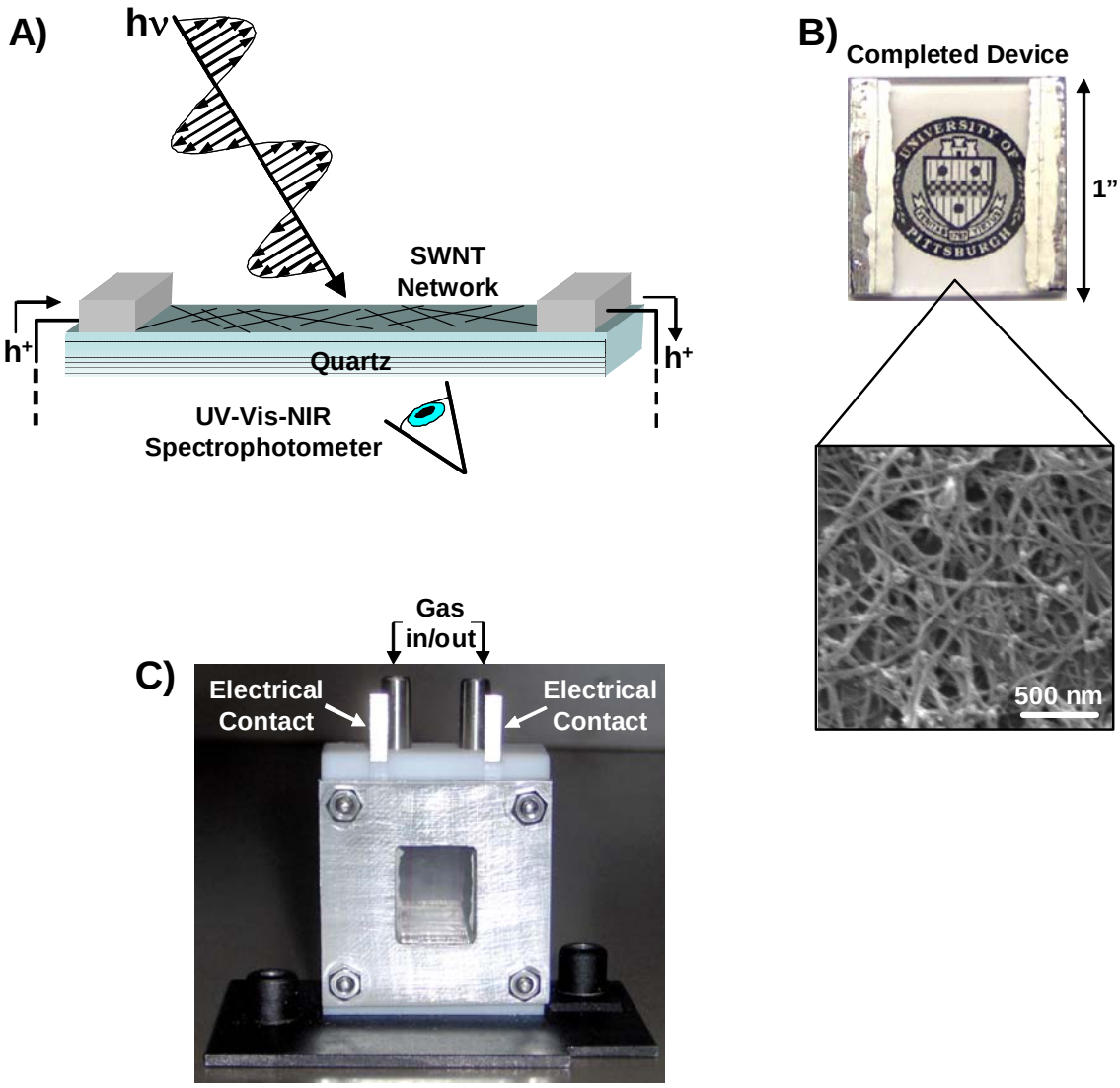

Figure 5-1. Experimental setup for simultaneous optical spectroscopy and electrical transport measurements of SWNTs. A) Cartoon describing the experimental setup where a SWNT network connects two electrodes on an optically transparent quartz substrate. This allows simultaneous measurement of the network conductance and UV-Vis-NIR absorbance spectra. B) A digital image of a completed device where the bulk Al tape contacts and conductive Ag paint are shown. The University of Pittsburgh emblem is clearly visible through the SWNT network, illustrating the optical transparency of this electronic device. C) A digital image of the gas flow chamber with a completed device housed inside where the gas inlet and outlet ports, and stainless steel electrical contacts are labeled.

5.5 RESULTS AND DISCUSSION

SWNTs can be broadly classified as semiconducting or metallic, and a sample will contain both varieties. Electronic transitions between spikes in the SWNT density of states (DOS),[40] called van Hove singularities, produce peaks in the SWNT UV-Vis-NIR absorption spectra that correspond to either metallic or semiconducting SWNTs.[6] Three semiconducting transitions, called the S_{11}, S_{22}, and S_{33}, and one metallic transition, called the M_{11}, are typically observed in the UV-Vis-NIR absorption spectrum of a sample of SWNTs, and it has been reported that the intensity of these transitions can be modified *via* doping the SWNT with holes or electrons.[50] We found that the SWNT absorption spectrum remained constant regardless of the applied bias voltage. As expected, the conductance and absorbance spectrum of the SWNT sample remained constant (excluding minor electronic drift) under pure N_2; however, the device showed significant electronic and spectroscopic response to NH_3 and NO_2. If a molecule engages in electronic interaction with p-type semiconducting SWNTs, then it must donate or withdraw electronic density from the top of the valence band,[41,71,74a] and should produce complementary changes in the electronic and spectroscopic properties of the SWNT sample.[37] This occurs because the redox potentials of the p-type semiconducting SWNT and adsorbing molecules are such that electronic interaction with the semiconducting SWNT valence band is favorable.[86]

Figure 5-2, panels A and B show the absorption spectra of independent SWNT devices as a function of exposure time to either NH_3 or NO_2, respectively. In both experiments, the introduction of the particular gas resulted in exclusive modification of the SWNT S_{11} transition intensity such that it increased as a function of NH_3 exposure time and decreased as a function of NO_2 exposure time. Furthermore, NH_3 exposure produced a small (~3 nm) redshift while NO_2

exposure produced a small (~3 nm) blueshift in the S_{11} peak absorption wavelength. While gas adsorption on metallic SWNTs is likely, there was no observable change in the M_{11} transition intensity. The SWNT M_{11} transition is relatively insulated from the effects of charge transfer,[87] owing to the finite electronic density at the Fermi level. Subsequently, any influence that NO_2 or NH_3 adsorption may have had on the electronic structure of metallic SWNTs was not visible by absorption spectroscopy.

Because the S_{11} transition intensity is directly proportional to the electronic density in the semiconducting SWNT valence band, we hypothesize that interaction with the gas molecules serves to modify the electronic density of the semiconducting SWNT valence band. More specifically, MO overlap must occur such that an NH_3 MO with finite electronic density must reside energetically above the semiconducting SWNT valence band edge, and a partially vacant NO_2 MO must reside energetically lower than the semiconducting SWNT valence band edge; this is depicted in the insets of Figure 5-2, panels C and D. Moreover, the change in electronic density could serve to move the absolute position of semiconducting SWNT valence band edge, and may explain the small shift in the peak absorption wavelength.

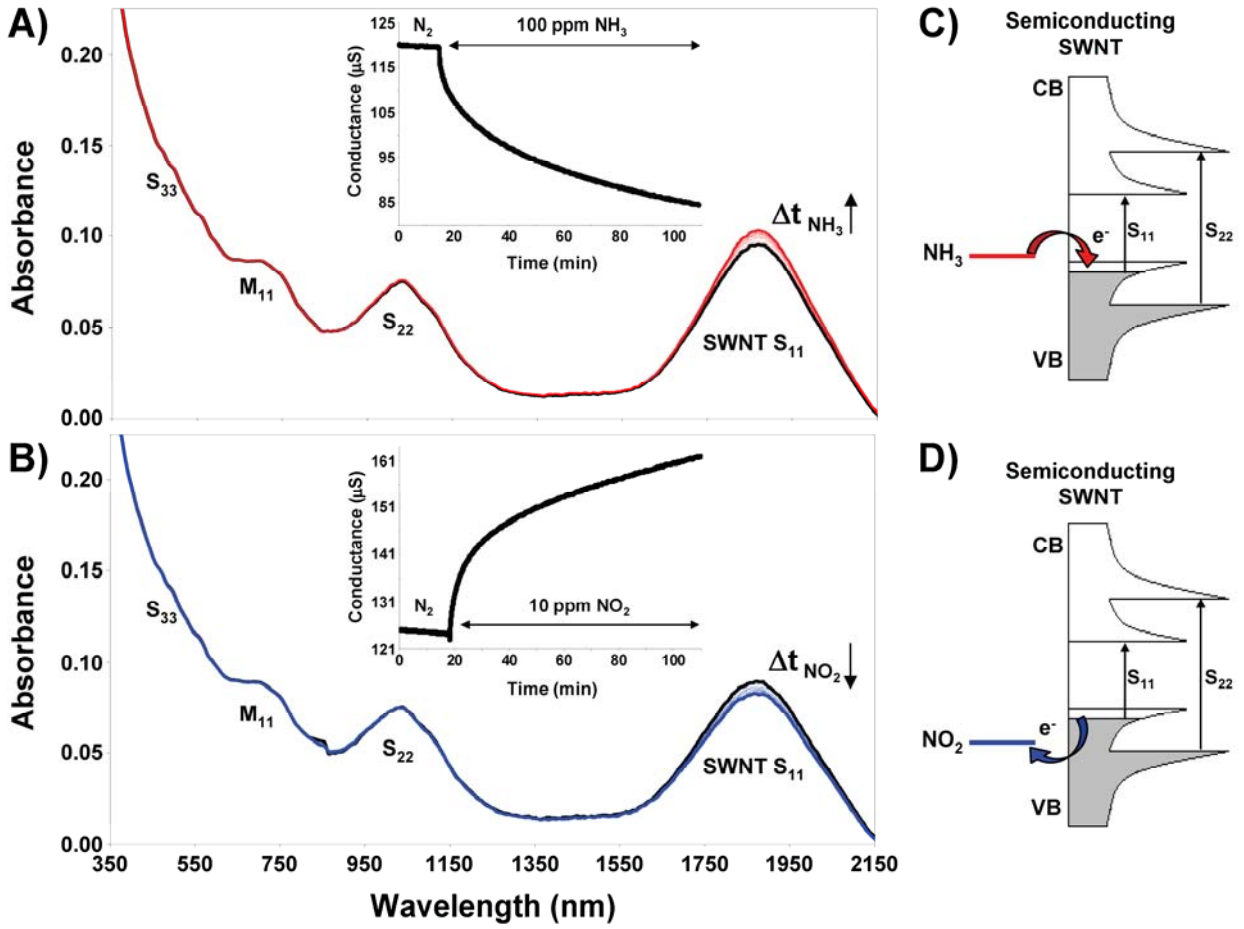

Figure 5-2. SWNT response to NH_3 and NO_2 gases. UV-Vis-NIR absorption spectra of SWNT films under exposure to (A) 100 ppm NH_3 and (B) 10 ppm NO_2 (both in N_2) where spectroscopic changes are limited exclusively to the SWNT S_{11} transition. Δt_{gas} corresponds to a 90-minute gas exposure time and the insets show the corresponding gas interacting with the top of the semiconducting SWNT valence band. The insets show the simultaneously recorded electrical conductance measurements of the SWNT films during NH_3 and NO_2 exposure, respectively. Diagram depicting charge transfer between (C) NH_3 and (D) NO_2 and the SWNT valence band (VB). Here the donation or removal of electronic density modifies the electronic density of the VB, affecting the S_{11} transition, as shown in panels (A) and (B).

We previously reported a strong correlation between the electrical and spectroscopic behavior of a noncovalently functionalized sample of SWNTs.[52] Here, the spectroscopic response was accompanied by a simultaneous change in the network conductance of the SWNT device. However, the electrical and spectroscopic responses, ΔG and Δabs, respectively, will be of opposite sign because semiconducting SWNTs demonstrate p-type behavior under ambient conditions.[14] The origin of p-type doping is still under debate, however, it is widely believed to result from oxygen adsorption on the SWNT[60a] or at the SWNT-electrode interface.[14b] The insets of Figure 5-2, panels A and B, show that NH_3 or NO_2 exposure independently decreased or increased network conductance, respectively. After approximately 90 minutes of gas exposure there was a ~3% change in the S_{11} absorbance and ~30% change in the network conductance in either direction, depending on the gas used. For both gases the combined response seemingly corresponding to charge transfer with the SWNT network. For example, NH_3 exposure increased the S_{11} transition intensity and decreased the network conductance—both of these results could be explained in terms of refilling the partially depleted SWNT valence band with electronic density. Conversely, the decreased S_{11} transition intensity and increased network conductance after NO_2 exposure could be attributed to electronic withdrawal.

Three sets of devices were created with “high”, “medium” and “low” density networks to determine if the network composition influenced the device response. Medium and low density devices had approximately 2/3 and 1/3 the network density of the high density device, respectively; network densities were estimated from scanning electron microscope (SEM) images and S_{11} band absorbance intensities (Figure 5-3, panels A and B). The response of these devices under NH_3 and NO_2 are summarized in Table 5-1. In all cases, the spectroscopic (Δabs) and electronic (ΔG) responses shared a time dependency which suggests that gas adsorption on

the SWNT network dominates the device response. Another similarity between devices of differing network density is that the spectroscopic response to both gases decreased with decreasing network density; this is most apparent in the spectroscopic response of the low density device to NH_3, where the Δabs (~0.12%) was just within the sensitivity of the spectrophotometer.

We contend that the difference in magnitude between the spectroscopic and electronic measurements stems, at least in part, from the cross section of sample measured by each technique. For example, conductance of SWNT networks of this size is dominated by a few percolation pathways that depend on inter-SWNT potential barriers.[84,88] On the other hand, the spectroscopic response is an average value measured over a large number of SWNTs. This difference is conceptually illustrated in Figure 5-3C where the dominant percolation pathway is represented with bold lines and the area probed spectroscopically is contained inside the dashed rectangle. Consequently, the electronic response is inherently more sensitive than the spectroscopic response because of the smaller number of pathways contributing to the network conductance. While charge transfer appears to influence the device response, we acknowledge that the presence of a hydration layer[21a,89] or defect sites[90] on the SWNT surface may play a role in device response to a particular analyte. However, the discrepancy in response to NO_2 and NH_3 suggests that analyte sensitivity (and possibly selectivity) may be further tuned by simply varying the network density in typical SWNT-based sensor architectures. Lastly, if device response were dominated by Schottky barrier modification we contend that significant electronic response would occur with negligible spectroscopic response. However, if Schottky barrier affects dominated the response of a device, one could consider developing a geometry that could exploit this phenomenon by maximizing the area of the SWNT-metal electrode interface.

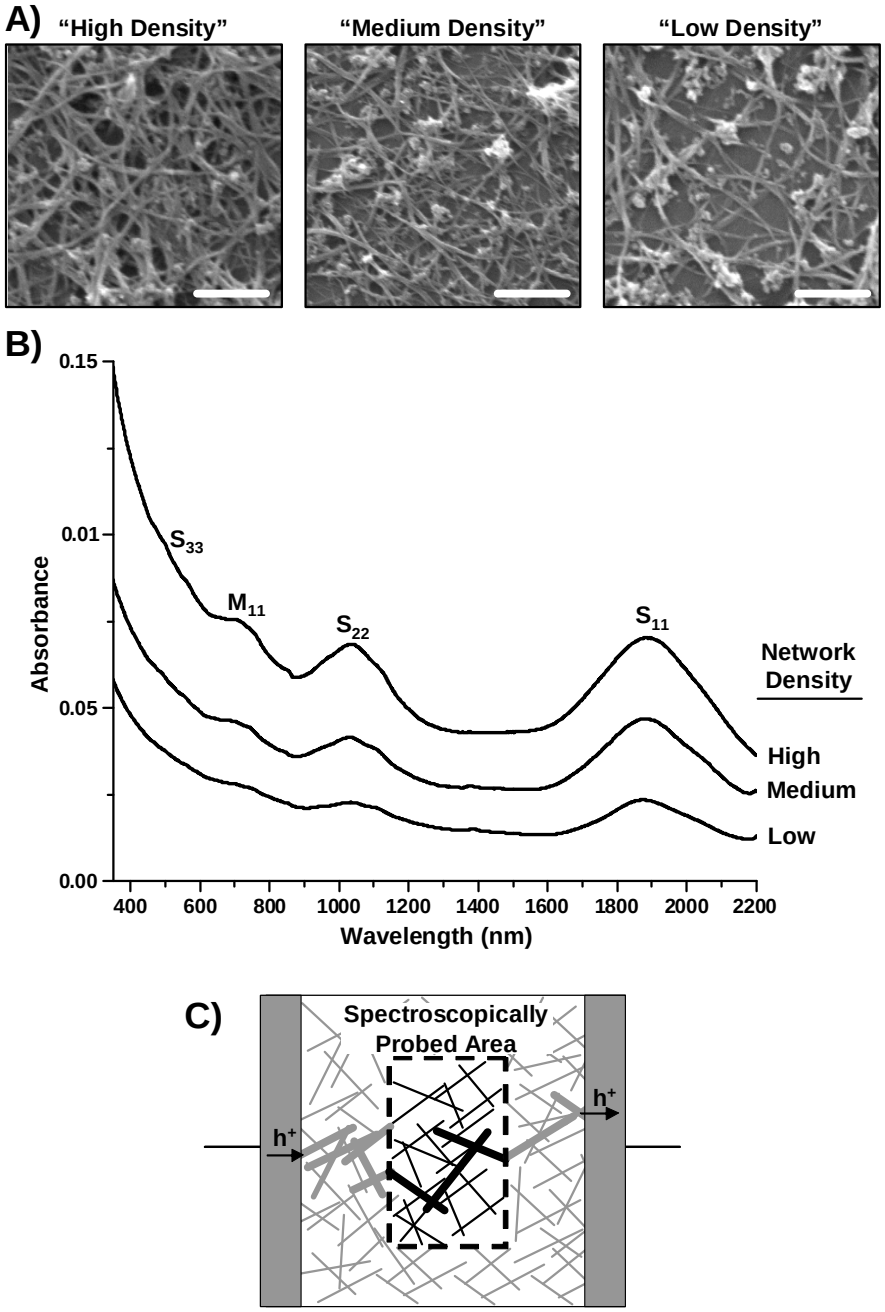

Figure 5-3. SWNT films of different thickness. A) Scanning electron microscope (SEM) images of the "high", "medium" and "low" density SWNT networks; scale bars correspond to 500 nm in all three images. B) UV-Vis-NIR absorption spectra of the films imaged in panel A. C) Conceptualized illustration of the difference in electronic and spectroscopic measurement cross section areas. Here the dominant percolation pathway is represented with bold lines and the area probed spectroscopically represented by the darker lines contained inside the dashed rectangle.

Table 5-1. Summary of the electronic (ΔG) and spectroscopic (Δabs) response of devices of differing SWNT network density to NH_3 and NO_2 gases.

	NH_3 Exposure		**NO_2 Exposure**	
Network Density	**ΔG (%)**	**Δabs (%)**	**ΔG (%)**	**Δabs (%)**
High	-19.5	3.8	40.1	-3.2
Medium	-15.5	1.1	47.9	-1.9
Low	-5.00	0.12	68.0	-1.1

5.6 CONCLUSIONS

We have described the combined spectroscopic and electronic operation of a SWNT thinfilm-based solid-state device under the influence of NH_3 and NO_2 gases. We have shown that the device response seems to be intimately related to the overall composition of the SWNT network. Our observations suggest that gas adsorption on the SWNT network seems to dominate both the spectroscopic and electronic response; however, modification of potential barriers at inter-SWNT junctions, or interaction with the SWNT hydration layer or defect sites, may also have an important role in the response of the device. Furthermore, we have shown that the analyte sensitivity of a device may be tuned by simply varying the density of the SWNT network. This type of combined spectroscopic and electronic (spectronic) approach will hopefully lead to a more fundamental understanding of the chemical processes occurring on the device surface, ultimately leading to the design of more sensitive and possibly selective chemical sensors.

Acknowledgement. The authors would like to thank Profs. David Pratt and Shigeru Amemiya for their insightful suggestions, as well as the University of Pittsburgh's Department of Materials Science and Engineering for the provision of access to the electron microscopy instrumentation and for assistance with the execution of this part of our research.

6.0 UNDERSTANDING THE SENSOR RESPONSE OF METAL DECORATED CARBON NANOTUBES

6.1 CHAPTER PREFACE

The aim of this work was to revisit the sensor response of metal nanoparticle decorated SWNTs (Chapter 2) with the use the combined spectroscopic and electrical transport measurement techniques that were described in Chapters 3 through 5. In addition to our experimental work, we engaged in a collaboration with computational chemists to further understand the behavior of the metal decorated SWNTs. The material contained in this chapter has been published in the journal *Nano Letters*; the figures in this chapter have been reproduced with permission from *Nano Lett.*, **2010**, *10*, 958. Copyright 2010 American Chemical Society; the full citation is listed as reference 91 in the bibliography section.

List of Authors: Douglas R. Kauffman, Dan C. Sorescu, Daniel P. Schofield, Brett L. Allen, Kenneth D. Jordan, Alexander Star.

Author contributions: All authors contributed to design of experiments. All experimental work was performed by DRK, except for Raman spectroscopy, which was performed by BLA. Computational work was performed by DCS, DPS and KDJ.

6.2 ABSTRACT

We revisit the metal nanoparticle (NP) decorated single-walled carbon nanotube (NP-SWNT) system with a combination of solid-state optical spectroscopy, electrical transport measurements and electronic structure calculations using density functional theory (DFT). Specifically, we have explored the effects of metal nanoparticle (MNP) deposition on the electronic structure of single-walled carbon nanotube (SWNT) networks, and we study the response mechanism towards carbon monoxide (CO) gas exposure. Using optically transparent and electrically conductive SWNT networks immobilized on quartz substrates, we find that the deposition of Au NPs creates a decrease in the intensity of the first semiconducting SWNT absorbance band indicating electron transfer out of the SWNT valence band. CO exposure induces simultaneous changes in the absorbance spectrum and network conductance of SWNT networks decorated with various species of metal nanoparticles, which indicate electron donation back into the SWNT upon CO adsorption. We show that combination of optical spectroscopy, solid-state electrical measurements and DFT calculations can provide mechanistic information about the room temperature and ambient pressure behavior of supported nanoparticle species, which may provide a valuable tool for exploring catalytic abilities and sensor response of nanoparticle-based systems.

6.3 INTRODUCTION

Recent years have seen an explosion of interest in carbon nanotubes (CNTs) for applications in advanced electronics,[14] biotechnology/medicine,[92] fuel cells[93] and sensors.[78,94] Along these lines,

the interaction between metal nanoparticles (NPs) and CNTs[95,96] has also attracted much attention because NP-CNT systems show unique or enhanced sensitivity towards gaseous species such as H_2,[25,27] CH_4,[27,97] H_2S, [27,96c] CO,[27,98] NO_2,[98,99] and NO.[22] Despite their application in gas sensing, little is actually known about the electron transfer events that occur between the NP and CNT during gas adsorption. Previous computational efforts have investigated the interaction between CNTs, NPs and adsorbing gas molecules,[100] but a combination of computation and experimental measurement could provide more information on the NP-CNT system during gas adsorption.

Carbon monoxide (CO) gas can serve as a chemical probe because it has the ability to bind to a variety of surfaces at low temperatures.[101] Accordingly, CO adsorption should be useful in studying the interactions that occur between single-walled carbon nanotubes (SWNTs) and NPs. SWNTs are an interesting platform to study such interactions because they maintain their electrical conductivity even in thin, optically transparent networks. Herein, we demonstrate the use of optically transparent SWNT networks to study the electronic interactions between the MNPs and SWNTs under the influence of CO gas, and we use DFT-based electronic structure calculations to further explore the system. This approach is significant because we can probe the chemical interactions occurring at the surface of the MNP-decorated SWNT networks at ambient temperature and pressure, which is useful for understanding the processes occurring at operating fuel cell catalysts and chemical sensor elements. While we focus primarily on the interaction between CO and Au-SWNTs, we demonstrate that SWNTs decorated with Pt and Rh NPs show similar behavior, and we contend that the insights gained from this system may extend to a wide range of other supported NP systems.

6.4 EXPERIMENTAL

Materials. Single-walled carbon nanotubes (SWNTs) were obtained from Carbon Solutions (type P2; ~1.4 nm average diameter)[10] and used without further purification. All chemicals were used as received from Sigma-Aldrich. For gas exposure experiments, grade 5.0 N_2 (Valley National Gas) was used as the reference gas before exposure to 2500 ppm CO (in grade 5.0 N_2; Liquid Technology Corporation).

MNP Deposition on SWNT Networks. SWNT networks were fabricated as previously described by spraycasting DMF suspended SWNTs onto heated 1" x 1" electrically insulating quartz substrates with an air brush (Iwata).[77] The application of a sufficiently cathodic electrochemical potential in an appropriate metal salt solution will induce the nucleation and growth of metal NPs at the nanotube surface.[102,103] Electrochemical NP deposition was accomplished by using the spray-cast SWNT networks as working electrodes in aqueous solutions of 1.0 mM $HAuCl_4$, H_2PtCl_6 or Na_3RhCl_6 with a supporting electrolyte of 0.1 M HCl. Specifically, the SWNT network working electrodes were connected to an electrochemical potentiostat (CH Instruments, model 604C) as the working electrode with Ag/AgCl reference and Pt wire counter electrodes completing the cell.

The electrochemical deposition of NPs onto a SWNT network results in the formation of a density gradient that decreases as a function of distance from the potential source.[103a] To create more uniform NP coverage across the SWNT network surface we adopted a procedure to form opposing deposition gradients. For example, a potential of –1.0 V was applied for a predetermined duration to a SWNT network in a particular metal salt solution, it was then dipped in DI water several times and blown dry with air. The opposite end of the network was then

connected to the potentiostat as the working electrode and the deposition process was repeated. As a control, –1.0 V was applied to a SWNT network in an identical manner in an aqueous solution of 0.1 M HCl for a total of 200 seconds.

Physical characterization. All measurements were performed with the NP-SWNT networks supported on quartz substrates. Scanning electron microscope (SEM) imaging and energy dispersive X-ray (EDX) spectroscopy were performed with a Phillips XL30 FEG microscope equipped with an EDAX assembly; samples were sputter coated with Pd prior to imaging and EDX spectroscopy to eliminate charging of the quartz substrate. X-ray diffraction (XRD) patterns were recorded on a Phillips MPD-1880 multipurpose diffractometer system. Raman spectra were recorded under ambient conditions with a Renishaw Inviva Raman microscope using a 633 nm excitation wavelength; the reported spectra are the average of five individual scans. X-ray photoelectron spectroscopy (XPS) was performed with a PHI 5600ci spectrometer employing Al Kα X-rays with a base pressure lower than 1 x 10^{-8} torr; an electron flood gun was used to neutralize surface charging of the substrate. XPS binding energies were corrected using the Si 2p peak of the quartz substrate at a binding energy 103.4 eV,[104] and the reported spectrum is the average of 20 individual scans.

Electrochemical measurements. Cyclic voltammetry (CV) and spectroelectrochemical measurements of SWNT networks (on quartz) were performed in a custom built Teflon measurement chamber[77] with a supporting electrolyte of N_2 saturated 0.5 M NaOH. The Au-SWNT networks were secured in the chamber such that they contacted two stainless steel electrodes (which were not in contact with the supporting electrolyte) while leaving an

unobstructed optical path. In this configuration, the SWNT networks were connected to the electrochemical analyzer as a working electrode with Ag/AgCl reference and Pt counter electrodes completing the cell. For spectroelectrochemical measurements of the Au-SWNT network, the chamber sat inside of a Perkin Elmer Lambda 900 UV-Vis-NIR spectrophotometer and absorbance spectra were recorded while holding an electrochemical potential corresponding to the Au NP oxidation or reduction.

Gas exposure measurements. NP-SWNT networks were placed inside the Teflon measurement chamber for simultaneous spectroscopic and electrical conductance measurements.[77] The NP-SWNT networks were secured in the chamber such that they contacted two stainless steel electrodes (which were not in contact with the gas) while leaving an unobstructed optical path, and the chamber was cycled between N_2 and 2500 ppm CO at room temperature and ambient pressure. The chamber sat inside of the spectrophotometer for acquisition of the UV-Vis-NIR absorbance spectra. Network conductance data were collected at a bias voltage of 0.5 V with a Keithley 2400 SourceMeter interfaced to LabVIEW 7.1 software. The response of the Au-SWNTs to CO gas exposure was fit using OriginPro 7.5 software.

Computational methods. The adsorption properties of Au_{20} clusters on (14,0) SWNTs, as well as the interaction of the Au_{20}-SWNT system with molecular CO, have been studied using density functional theory (DFT) in conjunction with periodic slab models. Calculations were performed using the Vienna *ab initio* simulation package (VASP) code,[105] which evaluates the total energies of periodically repeating geometries based on plane-wave basis sets and the pseudopotential approximation. The electron-ion interactions were described by the projector

augmented wave (PAW) method of Blöchl[106] and implemented in VASP code by Kresse and Joubert.[107] The generalized gradient approximation (GGA) with the Perdew, Burke and Ernzerhof (PBE)[108] functional has been used for description of exchange and correlation. In the case of adsorption on the defective nanotube surface spin-polarized calculations were employed.

The selection of the (14,0) SWNT with a diameter of 1.096 nm was motivated by the need to use a semiconducting nanotube within the diameter range of the experimentally examined SWNTs. The supercell model used in the calculations contained four repeating SWNT units along the tube axis leading to a system with 224 carbon atoms. A supercell model with dimensions 21.0 × 17.04 × 30 $Å^3$ was used for description of Au_{20} clusters adsorbed on the nanotube surface where the nanotube was placed along the shortest supercell direction, *i.e.* the O_y axis. The relatively large dimensions of the supercells were necessary in order to separate the lateral interaction between the (Au_{20}-CO) species adsorbed on nanotube surface and their periodic images.

Solution of the Kohn-Sham equations was accomplished using a plane wave basis set with a cutoff energy of 400 eV. This value gave adequate energy convergence for the systems examined in this study. The Brillouin zone was sampled using a single k-point at the Γ point, which is a reasonable choice given the large size of the supercell employed. The equilibrium configurations were determined by relaxation of all the atoms in the supercell excepting the bottom two layers of the SWNT C atoms, which were kept frozen.

For the adsorption configurations identified in this study, we report the corresponding adsorption energies. For Au_{20} clusters these have been determined based on the equation $E_{ads} = (mE_{(X)} + E_{(slab)} - E_{(slab+X)})/m$, where $E_{(X)}$ is the energy of the isolated Au_{20} cluster, m=1 and $E_{(slab)}$ is the total energy of the relaxed nanotube. In the case of adsorption of *m* CO molecules on the

(Au_{20}-SWNT) system, $E_{(X)}$ is the energy of the isolated CO molecule, $E_{(slab)}$ is the total energy of the (Au_{20}-SWNT) system and $E_{(slab+X)}$ is the energy of the entire system composed of the SWNT, Au_{20} cluster and *m*CO molecules. ***Note:*** In the sign convention described above, positive adsorption energies correspond to stable adsorption configurations. Charge transfer upon adsorption of an Au_{20} cluster on a SWNT, or CO adsorption on the Au_{20} decorated SWNT have been determined using the set of Bader charges.[109] In these cases the electronic charge density decomposition was obtained using the algorithm developed by Henkelman *et al*.[110]

A non-equilibrium Green's function (NEGF) approach combined with DFT was used to determine the electronic structure of the system when a bias voltage is applied.[111] Specifically, we used this approach to model the electrical conductance of a single (14,0) SWNT decorated with an Au_{20} cluster as a function of CO coverage. The four unit cell system described above was used as a scattering region placed between two semi-infinite (14,0) nanotube electrodes. We chose this arrangement to avoid any influence from SWNT-metal Schottky barriers.[14] The self-energy of the electrodes was determined from separate bulk calculations with periodic boundary conditions, a k-point grid of $1\times1\times50$ and a mesh cutoff of 150 Ry. The LDA functional along with a double-zeta polarized (C, O) and single-zeta polarized (Au) basis set was used. All electron transport calculations were performed using the NEGF-DFT formalism in the Atomistix Tool Kit (ATK).[112]

6.5 RESULTS AND DISCUSSION

The application of –1.0 V for 100 seconds per side (200 seconds total) to a SWNT network in a solution of $HAuCl_4$ resulted in the deposition of Au NPs. We found that the application of –1.0 V for 200 s deposited polycrystalline Au^0 NPs between ~50-150 nm in diameter onto the SWNT network (Figure 6-1, panels A and B, and Figure 6-2),[104,113] giving it a pink color due to the Au NP surface plasmon resonance (SPR).[114] The absence of detectable Au-oxide peaks, which would be expected at ~86 eV and ~90 eV in the XPS spectrum (Figure 6-1C),[104,113] indicates that O_2 dissociation and subsequent formation of surface oxide species did not occur with our Au-SWNT samples. Using identical deposition times and potentials we also found equivalent NP size, distribution, and polycrystallinity with Pt (Figure 6-3) and Rh (Figure 6-4) NP decorated SWNT networks.

Optical spectroscopy is a valuable tool for probing electron transfer within SWNT systems. Electron confinement around the SWNT circumference produces a unique electronic structure with several spikes due to van Hove singularities in its density of states (DOS).[40] Electronic transitions between singularities in the SWNT valence and conduction bands correspond to optical absorbance bands in the UV, visible, and NIR spectral regions (Figure 6-5A),[6a] where semiconducting SWNTs typically show three absorbance bands, termed S_{11}-S_{33}, while metallic SWNTs show one, termed M_{11}. Our group[37,52,77] and others[44,71,84] have shown that the magnitude of the S_{11} absorbance band can vary with the addition or removal of electrons from semiconducting SWNTs because it originates from states at the top of the valence band.[48] Subsequently, observing changes in the absorbance of the S_{11} band is a good way to qualitatively monitor charge transfer with the semiconducting component of the SWNT network. Conversely, the M_{11} transitions of metallic SWNTs are relatively unaffected by charge transfer.[42,43,87,115]

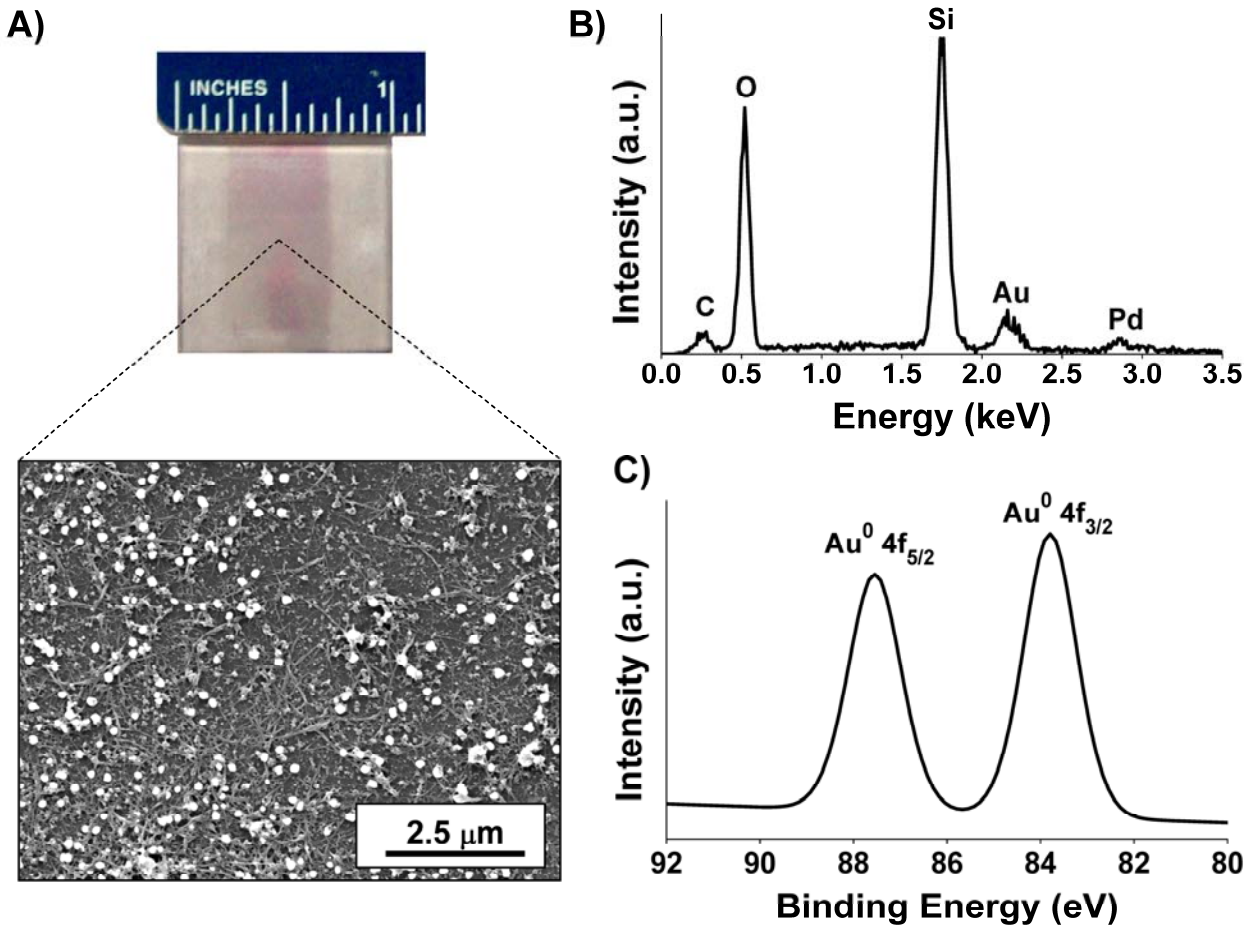

Figure 6-1. Au NP decorated SWNTs (Au-SWNTs). A) Digital photograph of an Au-SWNT network on quartz; the expanded view shows a scanning electron microscope (SEM) image of the Au-SWNT network surface. B) Energy dispersive X-ray (EDX) spectroscopy and (C) X-ray photoelectron spectroscopy (XPS) of the Au-SWNT network. The strong O, Si, and Pd signatures in the EDX spectrum are due to the quartz substrate (SiO_2) and Pd sputter coating process, respectively.

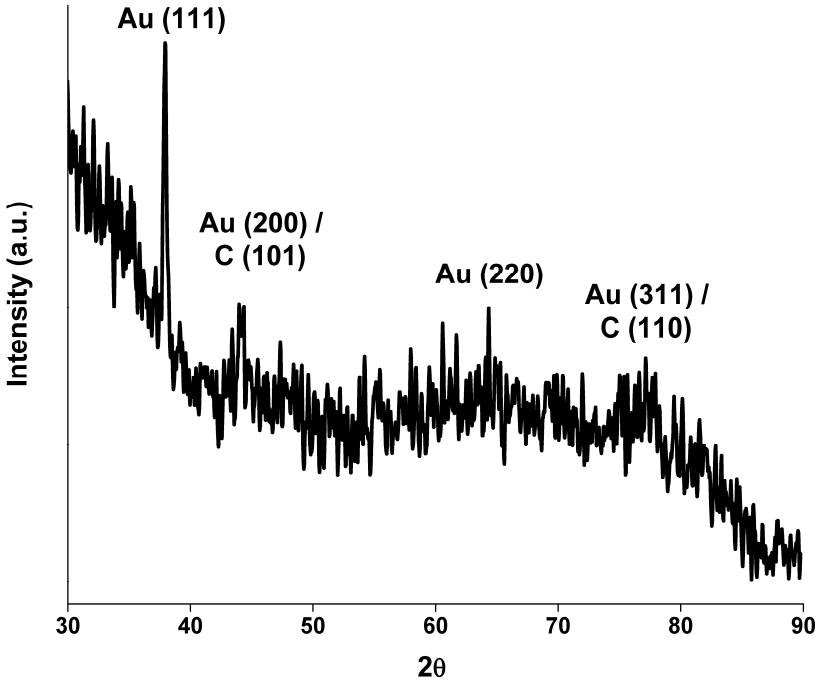

Figure 6-2. X-ray diffraction (XRD) pattern of an Au-SWNT network on quartz. The XRD pattern is somewhat noisy due to the thin Au-SWNT sample and the large background signal from the quartz substrate.

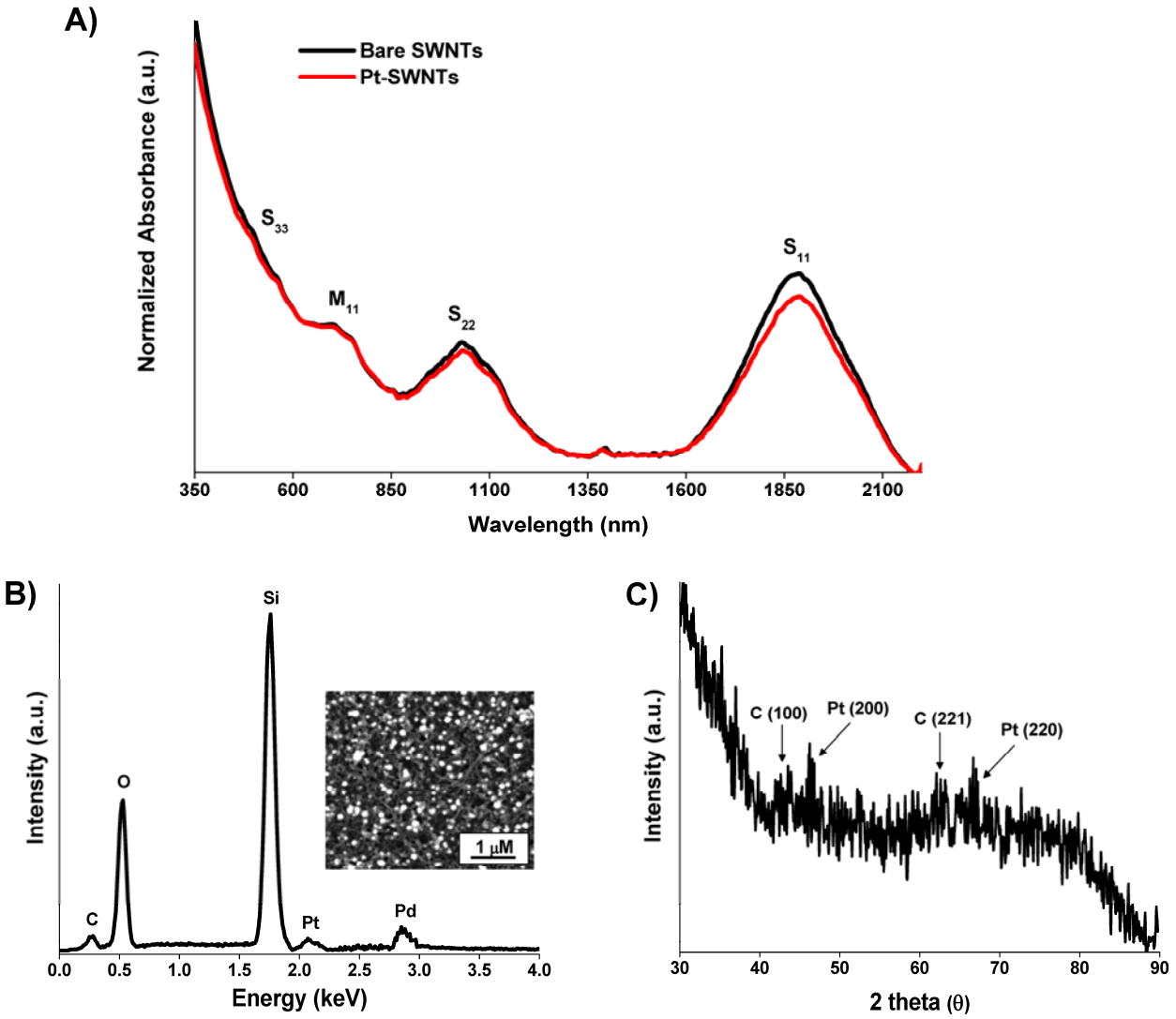

Figure 6-3. Pt-SWNT characterization. A) Normalized UV-vis-NIR absorption spectra of a SWNT network before (black curve) and after (red curve) deposition of Pt NPs for 200 seconds at –1.0 V in an aqueous solution of 1 mM H_2PtCl_6 with a supporting electrolyte of 0.1 M HCl; spectra were normalized at 1350 nm. B) EDX spectrum and SEM image of the Pt- SWNT network—the O, Si and Pd signals are from the quartz substrate and Pd sputtering process, respectively. C) XRD pattern of the Pt-decorated SWNT network; the XRD pattern is somewhat noisy due to the thin Pt-SWNT sample and the large background signal from the quartz substrate.

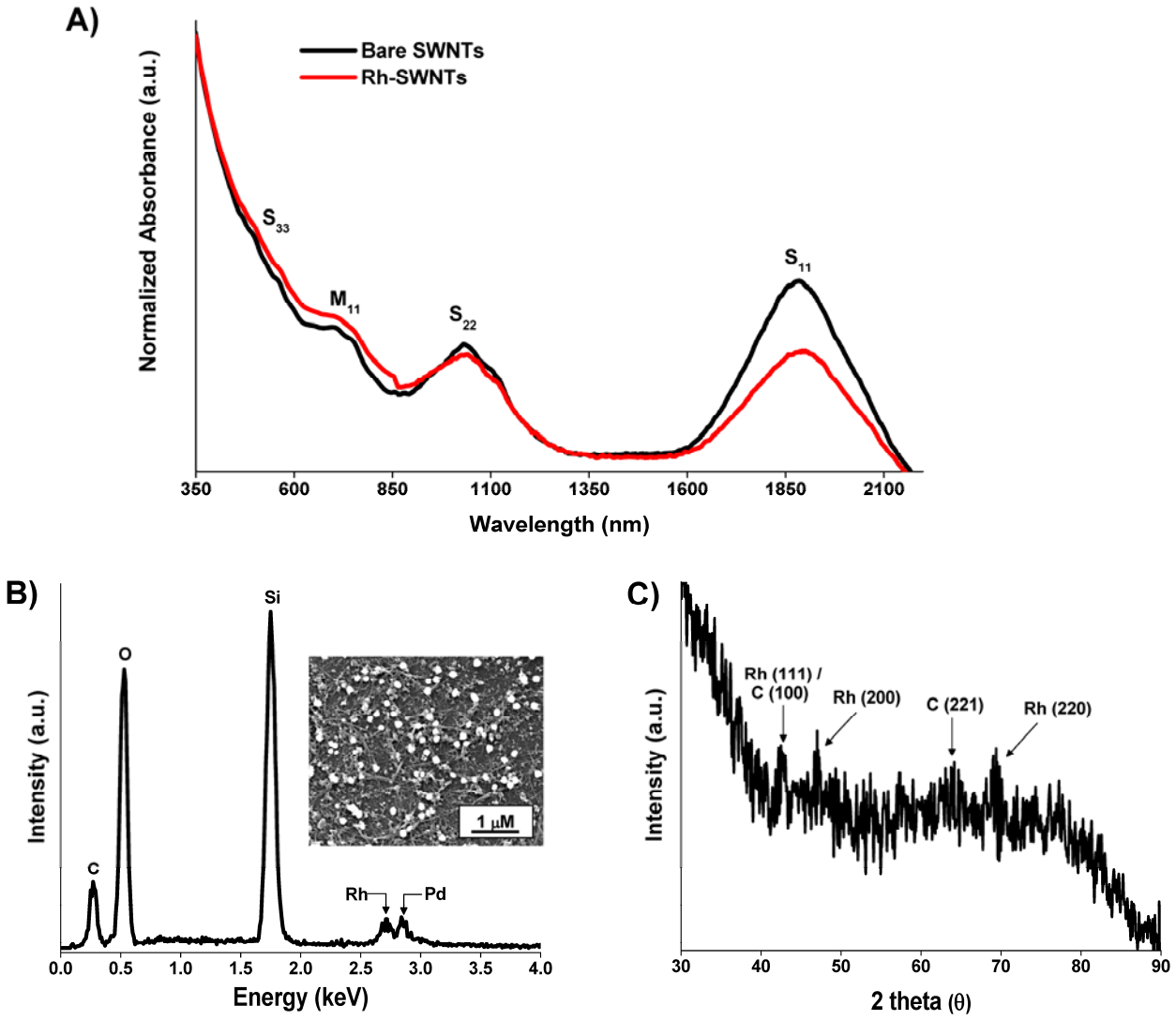

Figure 6-4. Rh-SWNT characterization. A) Normalized UV-vis-NIR absorption spectra of a SWNT network before (black curve) and after (red curve) deposition of Rh NPs for 200 seconds at –1.0 V in an aqueous solution of 1 mM Na_3RhCl_6 with a supporting electrolyte of 0.1 M HCl; spectra were normalized at 1350 nm. B) EDX spectrum and SEM image of the Rh-decorated SWNT network. C) XRD pattern of the Rh-decorated SWNT network; the XRD pattern is somewhat noisy due to the thin Rh-SWNT sample and the large background signal from the quartz substrate.

Figure 6-5A shows the absorbance spectra of a SWNT network before (black curve) and after (red curves) Au NP deposition at –1.0 V for times of 100, 150 and 200 s. In addition to the development of the Au NP SPR centered around 530 nm,[114] we also observed a ~30% decrease in the absorbance of the SWNT S_{11} band. The decrease in the S_{11} absorbance after Au NP deposition is consistent with the removal of electronic density from the SWNT valence band.[48,77,84] Moreover, the magnitude of the Au SPR and the SWNT S_{11} band change linearly with respect to the Au NP deposition time (Figure 6-6); SWNT networks decorated with Pt or Rh NPs also experience a comparable decrease in the S_{11} band absorbance (Figure 6-3 and Figure 6-4). As a control, a SWNT network was held at –1.0 V for 200 s in 0.1 M HCl (no metal salt), after which the S_{11} band absorbance increased by ~14% (Figure 6-7). This result shows that the growth of metal NPs, and not the application of a cathodic potential, produced the decrease in the SWNT S_{11} band absorbance.

Raman spectroscopy also suggests that NP deposition modifies the electronic structure of the SWNT, as observed through changes in the radial breathing mode (RBM) and G band (representative of the SWNT graphitic structure[116]) regions. For example, in Figure 6-5B the RBM of the Au-SWNT network (red curve) is broadened and shifted towards lower wavenumbers, as compared to that of the bare SWNT network (black curve). Furthermore, Figure 2c shows that the SWNT G band experiences a decrease in the intensity of the lower wavenumber shoulder (boxed region, ~1550 cm^{-1}). The intensity decrease in both the RBM and G band of the SWNT Raman spectrum have been attributed to removal of electronic density,[44,71,96b,117] which is consistent with the decrease in the S_{11} absorbance band after Au NP deposition.

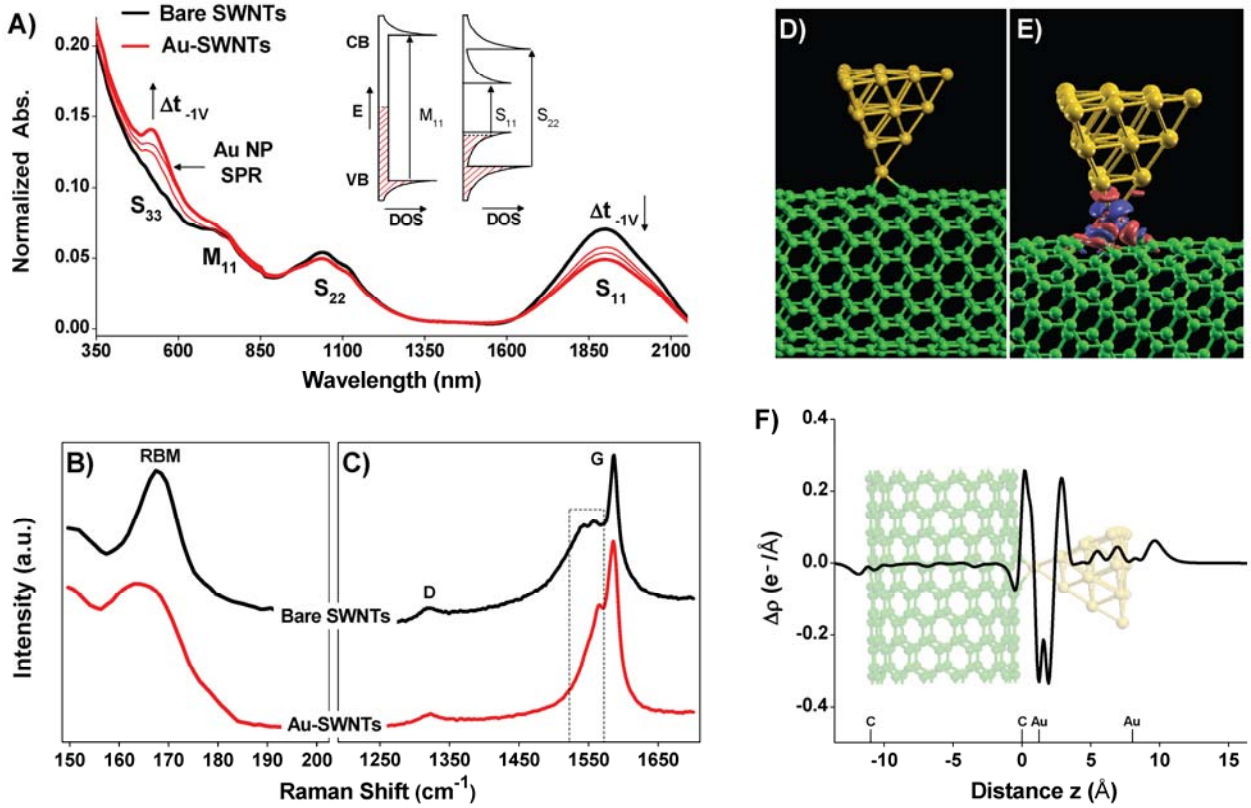

Figure 6-5. Au-SWNT optical spectroscopy and DFT calculations. A) Normalized UV-vis-NIR absorption spectra of a SWNT network before (black curve) and after (red curves) being held at -1.0 V (vs. Ag/AgCl) in a 1 mM $HAuCl_4$ / 0.1 M HCl solution for a total of 100, 150, and 200 seconds; spectra were normalized at 1350 nm. The inset contains a density of states (DOS) diagram for metallic and semiconducting SWNTs and shows their respective optical transitions. B) Radial breathing mode (RBM) and (C) D and G band regions of the Raman spectrum for a bare SWNTs (black curve) and Au-SWNTs (red curve); $\lambda_{ex.}$ = 614 nm and the spectra have been offset for clarity. D) Adsorption configuration and (E) charge variation maps depicting "corner-on" adsorption of an Au_{20} clusters on a defective (14,0) SWNT; the indicated isosurfaces correspond to values of +0.02 $e^-/Å^3$ (red) and -0.02 $e^-/Å^3$ (blue)—Au atoms are yellow and C atoms are green. F) Charge difference plot of the Au-SWNT couple at different z planes; for clarity, an image of the Au-SWNT couple is shown behind the plot.

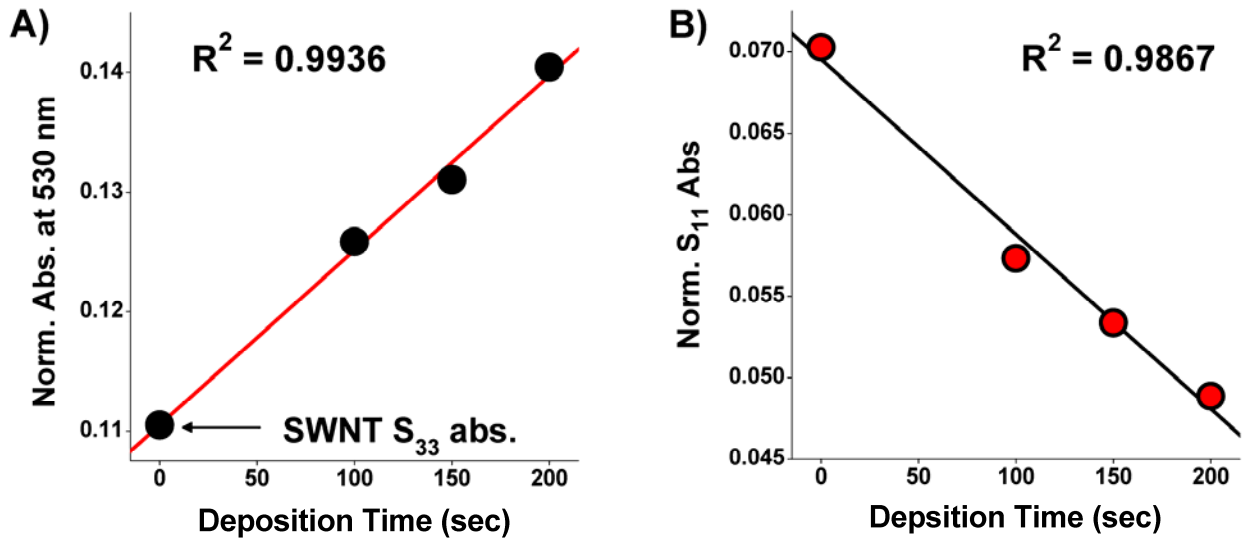

Figure 6-6. Spectroscopic changes during Au NP deposition. Normalized absorbance of the (A) Au NP SPR (530 nm) and (B) SWNT S_{11} band (1895 nm) as a function of Au NP deposition time at -1.0 V in a 1 mM HAuCl4 / 0.1 M HCl solution. The non-zero absorbance at a deposition time of 0 seconds in panel A is from SWNT S_{33} band; see Figure 6-5A.

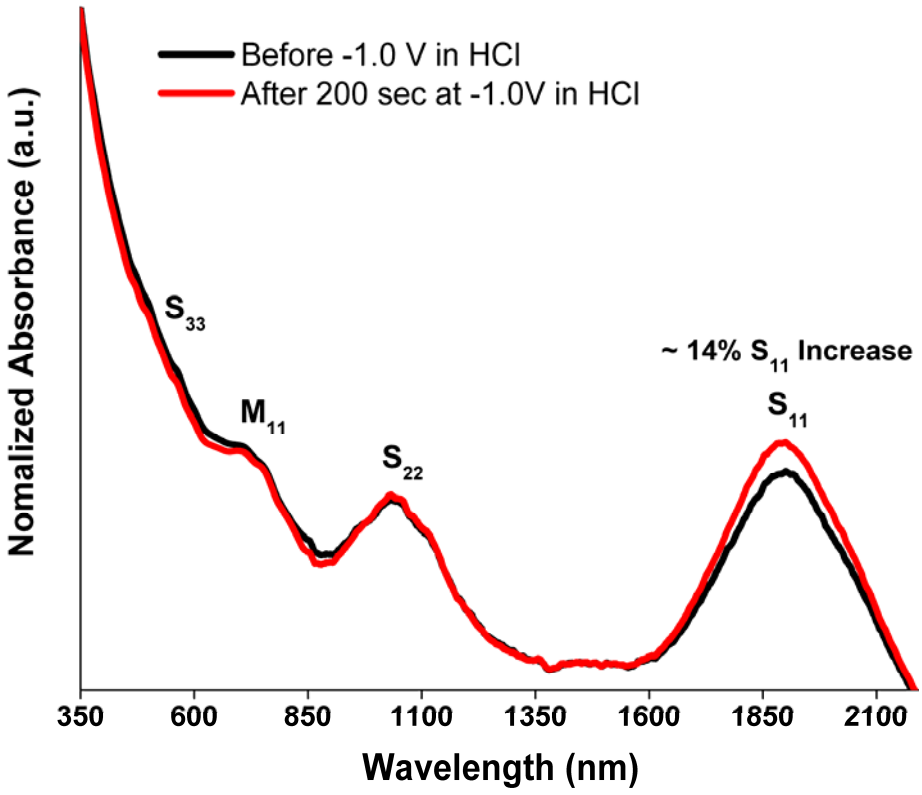

Figure 6-7. Control sample to evaluate the effect of holding a cathodic electrochemical potential on a SWNT network. The normalized UV-vis-NIR absorbance spectra of a SWNT network before (black curve) curve and after (red curve) holding it at –1.0 V for 200 seconds in an aqueous solution of 0.1 M HCl; the spectra were normalized at 1350 nm. The increased S_{11} band absorbance indicates donation of electronic density into the SWNT valence band.

In our theoretical studies, we employed a (14,0) SWNT and an Au_{20} cluster to model the Au-SWNT system. In the absence of defects, the gold cluster is calculated to bind only weakly with an adsorption energy of only 6.1 kcal/mol for attachment in a "corner-on" configuration to the SWNTs; this value is in agreement with the reported low binding energy of Au_{13} on pristine (5,5) SWNTs.[118] The Au-SWNT systems relevant to the experiments are expected to have the NPs bound at defect sites, where the binding can be appreciably stronger. Figure 6-5, panels D and E, show the adsorption configuration, and charge variation maps of an Au_{20} cluster attached to a semiconducting (14,0) SWNT with a missing carbon atom defect. The calculations show that "corner-on" attachment at the SWNT defect site is most energetically favorable with an adsorption energy of 39.8 kcal/mol, supporting Collins and coworkers'[95a] report of preferential NP deposition at SWNT defect sites. Attachment of the Au_{20} cluster at this site is accompanied by transfer of 0.050 e^- from the SWNT to the gold cluster. Figure 6-5F presents the average charge difference of the Au_{20}-SWNT couple taken at different z-axis planes parallel to the SWNT axis; for clarity, an image of the Au_{20}-SWNT couple is shown behind the charge difference plot. This data shows a depletion of electronic density from the SWNT immediately before the Au-SWNT interface, followed by large fluctuations at the interface, and finally an accumulation of electronic density on the Au_{20} cluster. The computational prediction of large fluctuations in electronic density at the Au-SWNT interface supports our previous suggestion of NP-SWNT interfacial potential barriers,[22] and the prediction of electron transfer from the SWNT into the Au NP is consistent with the observed changes in the absorbance and Raman spectroscopy of the SWNTs upon metal NP deposition.

We used a simultaneous combination of absorbance spectroscopy and electrochemistry (spectroelectrochemistry) to investigate the optical properties of the Au-SWNT system as a

function of the applied electrochemical potential. Figure 6-8A presents the stabilized cyclic voltammograms (CVs) of a SWNT network in N_2 saturated 0.5 M NaOH before (dashed curve) and after (solid curve) the electrochemical deposition of Au NPs. In NaOH, bare SWNTs show a relatively featureless CV typical of CNT double layer capacitive behavior.[119] However, after Au NP deposition, we observed peaks centered around 0.5 V (anodic sweep direction) and 0.0 V (cathodic sweep direction) that correspond, respectively, to oxidation and reduction of the Au NP.[113a] The wavelength and intensity of the Au NP SPR could be modified by applying electrochemical potentials.[120] Figure 6-8B shows the SPR region of a Au-SWNT network absorbance spectrum in 0.5 M NaOH. Initially (dashed black curve), the SPR maximum was approximately 564 nm, which is somewhat redshifted from the peak in air (or N_2) due to the different dielectric environment.[120] After applying an oxidizing potential (0.5 V; solid black curve) for 700 s we observed a redshift and decrease in intensity of the SPR, whereas the subsequent application of a reducing potential (0.0 V; solid red curve) for 700 s returned the SPR maximum to its initial wavelength and intensity. This spectroelectrochemical behavior, supported by the XPS measurements, suggests that the Au NPs are initially in a non-oxidized state, and it demonstrates how the addition or removal of electrons affects the Au NP SPR.

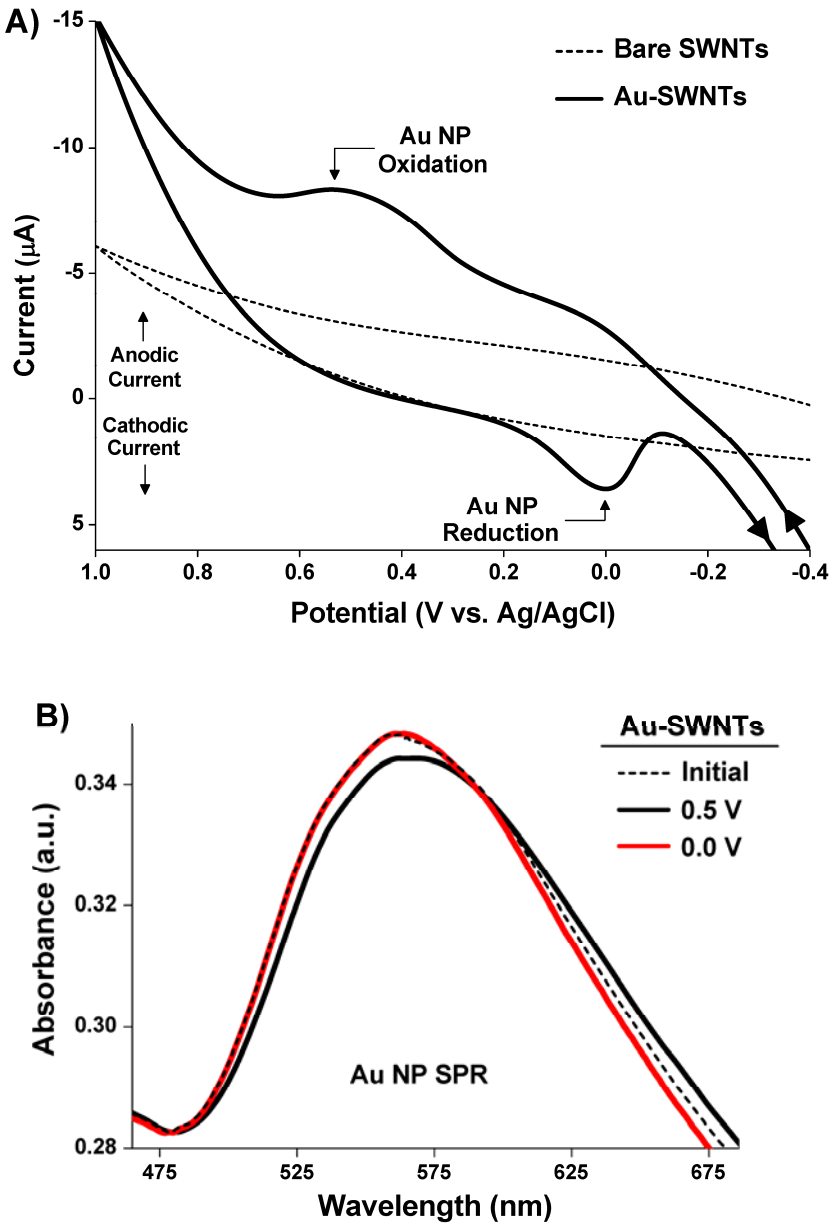

Figure 6-8. Au-SWNT electrochemical properties. A) Cyclic voltammogram (CV) of a SWNT network (on quartz) in N_2 saturated 0.5 M NaOH before (dashed curve) and after (solid curve) Au NP deposition. B) Au NP surface plasmon resonance (SPR) region of the Au-SWNT absorption spectrum as a function of applied electrochemical potential.

Figure 6-9A shows the UV-vis-NIR absorption spectra of an Au-SWNT network in flowing N_2 (black curve) and after a 30 min exposure to flowing 2500 ppm CO at room temperature and ambient pressure (red curve). During CO exposure, the Au NP SPR (Figure 6-9A, inset) increased in intensity and slightly blueshifted. Based on our spectroelectrochemical results (Figure 6-8B) we interpret this as being caused by a donation of electrons into the Au NP, which agrees with previous findings of electron donation into Au surfaces from the 5σ orbital of adsorbed CO molecules.[121] During CO exposure we also observed a simultaneous increase in the magnitude of the Au-SWNT S_{11} absorbance band (Figure 6-9B) and a decrease in the electrical conductance (Figure 6-9C), both of which are a consequence of electron donation into the SWNT network.[77,84] The 3% increase in the Au-SWNT S_{11} absorption band after CO exposure was approximately 70 times larger than the baseline noise, and it is comparable to the response of bare SWNTs to 100 ppm NH_3.[77] Furthermore, the room temperature electrical response of approximately 6% after CO exposure is in line with other reports of SWNTs decorated with Au[96c] or Rh[27] NPs. As shown in Figure 6-9C and Figure 6-10, bare SWNTs did not respond to CO gas; however, we found that SWNT networks decorated with Pt and Rh NPs showed similar electrical and spectroscopic responses to CO gas (Figure 6-11).

Our density functional theory (DFT) calculations indicated that O_2 dissociation at the Au NP surface was energetically unfavorable, and our model proceeds with the hypothesis that the Au-SWNT system transduces the adsorption of CO at the Au NP surface. We contend this approach is valid because XPS and spectroelectrochemical measurements did not indicate the presence of oxidized Au species, and CO gas exposures were conducted in an O_2 free atmosphere. Figure 6-9, panels D and E, show that CO adsorption at Au_{20} corner (i) and edge (ii, iii) sites is possible, with all adsorption configurations leading to electron donation into the

SWNT. However, our results showed that adsorption at the Au_{20} corner sites was the most energetically favorable configuration with an adsorption energy of 20.1 kcal/mol and a donation of 0.049 e^- into the SWNT for the adsorption of three CO molecules.

Non-equilibrium Green's function – DFT calculations[111] were performed on a single (14,0) SWNT decorated with a Au_{20} cluster to model the electrical transport properties of the Au-SWNT system during CO adsorption. For example, Figure 6-9F shows the normalized electrical conductance of a 0.1 V biased Au_{20}–(14,0) SWNT with zero, three and nine CO molecules adsorbed on the Au_{20} cluster. Specifically, the calculations predict that the adsorption of more CO molecules on the Au_{20} NP will decrease the SWNT conductance due to electron donation, effectively driving it into an electrically "off" state. Notably, this model qualitatively agrees with our experimental results presented in Figure 6-9C, insomuch as continued CO adsorption decreases the electrical conductance of the Au-SWNT system. We should note that the Au_{20} clusters considered in the calculations are smaller than those present in the experimentally measured Au-SWNT samples, but they should be suitable as models because the corner and edge sites that they contain will also be present in larger particles.[122] Qualitatively, we obtain agreement between the experimental and computational results, such that CO adsorption at the Au-SWNT couple results in a donation of electronic density into the SWNT.

Typically, gas adsorption on surfaces can be described by a Langmuir adsorption isotherm (Equation 1). [123]

$$\Gamma = \Gamma_{\max}\left(\frac{kC}{1+kC}\right)$$

Equation 1

Here, Γ represents the amount of adsorbed gas a particular time, Γ_{max} is the maximum amount of adsorbed gas, k is an equilibrium constant, and C is the concentration or partial pressure of the gas. However, in our specific case the pressure and concentration of CO remains constant. To fit our data with a Langmuir-type equation we have replaced the Γ and Γ_{max} terms with the measured Au-SWNT response, S and S_{max}, respectively, and we have replaced the C term with gas exposure time, x. We based these changes on the hypothesis that the Au-SWNT response is proportional to the amount of adsorbed CO, and that the CO coverage (*i.e.* concentration) on the Au NP surface will increase as a function of exposure time, giving Equation 2.

$$S = S_{\max}\left(\frac{kx}{1+kx}\right)$$

Equation 2

Using this approach, and taking S_{max} as the response of the Au-SWNT at the end of the exposure period, we were able to fit the response of the Au-SWNT S_{11} absorbance band and network conductance (red dashed curves in Figure 6-9, panels B and C). The departure of the Au-SWNT conductance from the ideal Langmuir-type response may stem from the presence of metallic SWNTs because they can attenuate the electrical response of SWNT networks to particular analytes.[21b] This approach also allowed us to fit the Au NP SPR response to a Langmuir-type curve, as shown in Figure 6-12, but this response appeared to require much longer to show saturation during CO exposure.

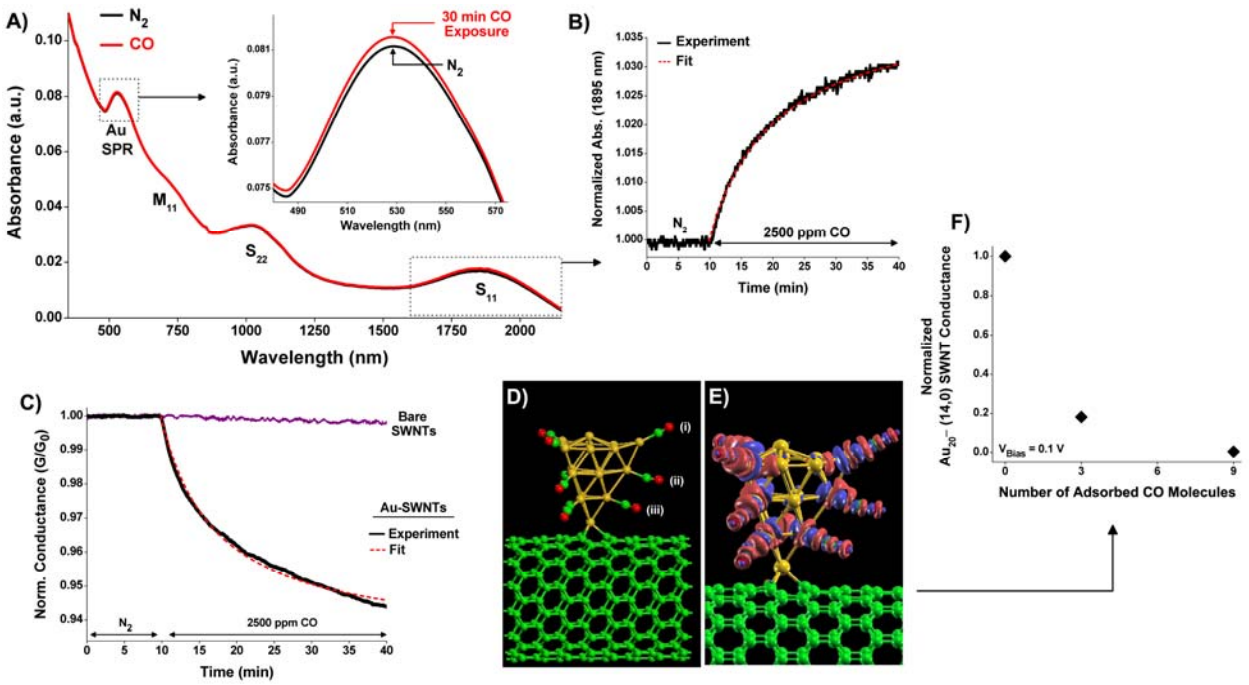

Figure 6-9. Au-SWNTs during CO exposure. A) UV-vis-NIR absorption spectra of a Au- SWNT network under N_2 (black curve) and after thirty minutes of exposure to 2500 ppm CO gas (red curve). The inset depicts the enlarged Au NP SPR region before and after CO exposure. B) The absorbance of the Au-SWNT network S_{11} band at 1895 nm during CO exposure. C) Normalized network conductance (G/G_0) of a bare SWNTs and Au-SWNTs during exposure to CO gas. The red dashed lines in panels (B) and (C) represent the fitted response using the Langmuir-type adsorption isotherm. D) Adsorption configuration and (E) charge variation map depicting nine CO molecules attached to the corner (i) and edge (ii, iii) sites of a Au_{20} cluster on a defective (14,0) SWNT; Au atoms are yellow, C atoms are green and O atoms are red. F) The calculated electrical conductance of a single (14,0) SWNT decorated with an Au_{20} cluster as a function of adsorbed CO molecules; a bias voltage of 0.1 V was considered.

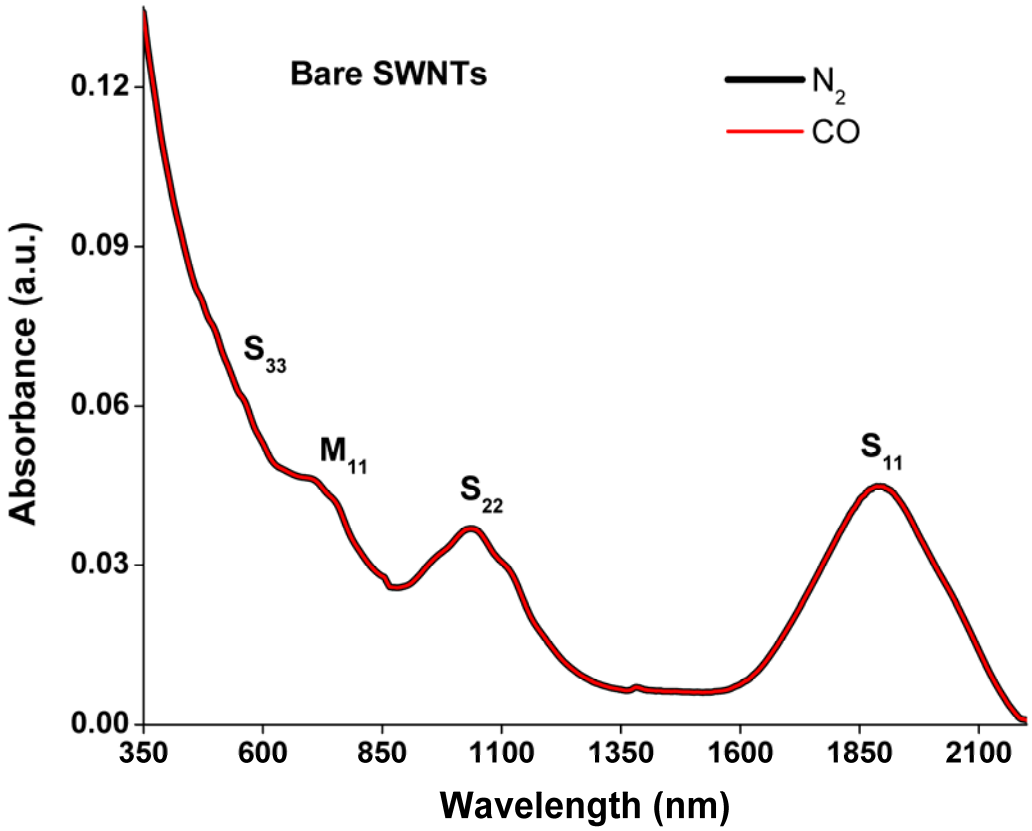

Figure 6-10. Spectroscopic response of bare SWNTs to CO gas. UV-vis-NIR absorbance spectra of a bare SWNT network under flowing N_2 (black curve) and after exposure to 2500 ppm CO for 30 minutes (red curve). As seen from the spectra, the SWNT S_{11} absorbance band did not change during CO exposure.

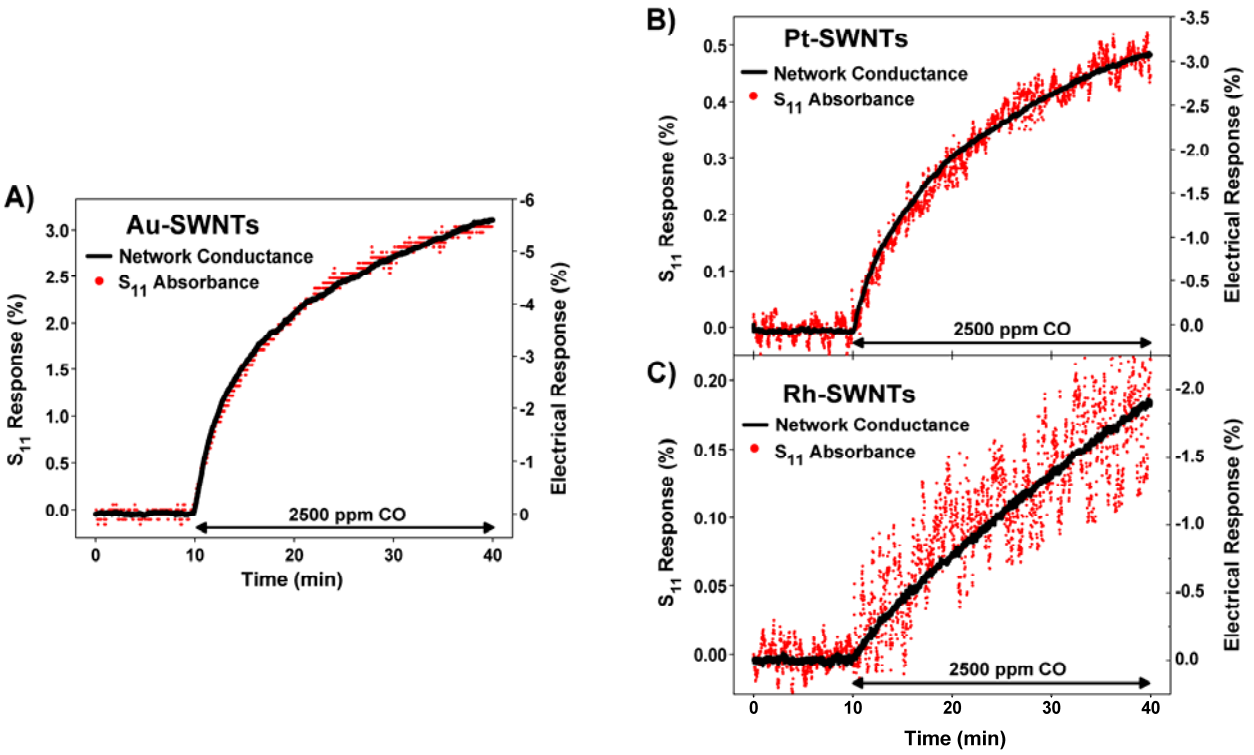

Figure 6-11. NP decorated SWNT response to CO. Combined spectroscopic S_{11} band absorbance (left axis; red labels) and electrical conductance (right axis; black curve) response for (A) Au-SWNTs, (B) Pt-SWNTs and (C) Rh-SWNTs during exposure to 2500 ppm CO gas. For all three experiments the samples were in flowing grade 5.0 N_2 before CO exposure. The spectroscopic S_{11} band response is substantially smaller than the electrical response for Pt-SWNTs and Rh-SWNTs during CO exposure.

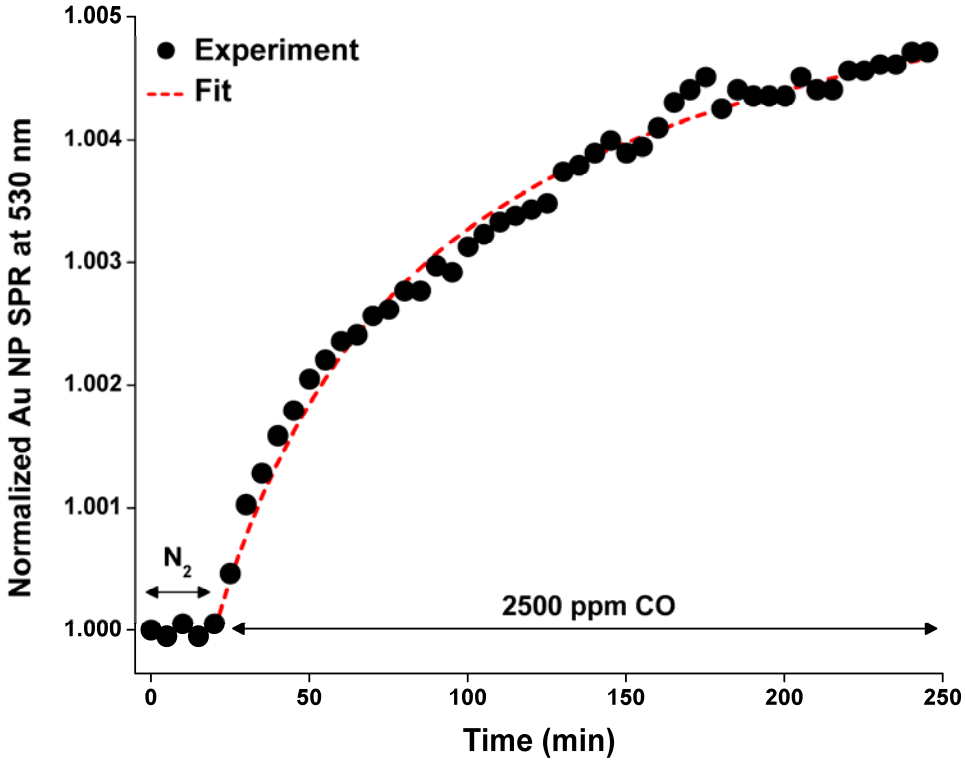

Figure 6-12. Response of the Au NP Surface plasmon resonance (SPR) during CO exposure. Normalized Au NP SPR absorbance at 530 nm (black labels) during exposure to 2500 ppm CO gas and fitting (red dashed curve) to the Langmuir-type adsorption isotherm.

The donation of electrons into the Au-SWNT system upon CO exposure is in accordance with previous results.[27] However, it is interesting that the response of the Au NP SPR is on a longer timescale than the response of the SWNT S_{11} absorbance band and electrical conductance. We hypothesize that this phenomenon stems from an increase of the Au-SWNT interfacial potential barrier upon CO adsorption.[22] Eventually these potential barriers become large enough that electron donation into the SWNT will slow, and eventually lead to a saturation of both the S_{11} band and electrical conductance response.

Another factor that we expect to contribute to the longer response of the Au NP SPR than the SWNT S_{11} band absorption and electrical conductance is the presence of Au NPs with diameters greater than the electron mean free path, which is approximately 50 nm in bulk Au.[31,124] Specifically, electron transfer into Au NPs from CO adsorption sites more than ~50 nm away from the Au-SWNT interface will lose too much energy through electron-phonon and electron-interface scattering[125] to overcome the interfacial potential barrier and transfer into the SWNT. Ultimately, these electrons may become localized on the Au NPs and promote the SPR response even after the SWNT response has saturated. Based on the observations presented here, we suggest that large gains in SWNT-based sensor response or catalyst efficiency could be made through utilization of well-dispersed NPs that are substantially smaller than the respective electron mean free path.

6.6 CONCLUSIONS

We have demonstrated a technique using optically transparent SWNT-based devices to investigate the electronic interactions between SWNT networks and metal NP species under the

interaction of CO gas under ambient pressure and temperature. Moreover, we have obtained consistent agreement between the measurements on the impact of CO adsorption on the electronic properties of Au NP / SWNT systems and electronic structure calculations on a model system with a Au_{20} cluster attached to a carbon vacancy defect on a (14,0) carbon nanotube. While we focused primarily on the Au-SWNT system, the similar response of Pt- and Rh-SWNT networks in the presence of CO gas indicates that this approach could provide equally fruitful results with other systems. These findings show that electronic structure calculations, in conjunction with experimental studies, can provide insight into the behavior of SWNT-supported NP species.

ACKNOWLEDGMENTS. D. R. K. acknowledges a graduate student fellowship through the Bayer Corporation. D. P. S. acknowledges the New Zealand Foundation for Research, Science and Technology for a postdoctoral fellowship. This work was performed in support of ongoing research in sensor systems and diagnostics at the National Energy Technology Laboratory (NETL) under RDS contract DE-AC26-04NT41817. We thank John Baltrus at the NETL for access to the XPS instrumentation, as well as Albert Stuart and the Department of Materials Science and Engineering at the University of Pittsburgh for access to and assistance with the XPS, SEM, TEM and XRD instrumentation. We gratefully acknowledge the computational resources provided by Pittsburgh Supercomputer Center. Disclaimer: reference in this work to any specific commercial product is to facilitate understanding and does not necessarily imply endorsement by the United States Department of Energy.

7.0 DECORATED CARBON NANOTUBES WITH UNIQUE OXYGEN SENSITIVITY

7.1 CHAPTER PREFACE

The overall scope of this work was quite serendipitous, inasmuch that we did not set out to create a room temperature SWNT-based O_2 sensor. However, by applying the techniques outlined in Chapters 3 – 6 we were able to deduce that this particular SWNT system was reversibly sensitive towards O_2 at room temperature and ambient pressures. This work can be viewed as the culmination of the previously described work because it is the most complex and sophisticated SWNT-based system described in this document, and we addressed both the mechanistic and practical aspects of developing a SWNT-based sensor system. The material contained in this chapter was published as a research paper in the journal *Nature Chemistry*, and the 2009 copyright is retained by the authors listed below. The chapter contents have been reproduced with permission from the Nature Publishing Group, and the full citation is listed as reference 126 in the bibliography section.

List of Authors: Douglas R. Kauffman, Chad M. Shade, Hyounsoo Uh, Stéphane Petoud, Alexander Star.

Author contributions: All authors contributed to the design of the experiments and preparation of the paper. DRK fabricated devices, performed electron microscopy, optical absorption

spectroscopy, EDX spectroscopy, electrical conductance measurements, and gas sensor studies. CMS performed photoluminescence spectroscopy and luminescence lifetime measurements. HU synthesized and characterized the Eu_8 dendrimer.

7.2 ABSTRACT

The relatively simple and robust architecture of carbon nanotube (CNT) based microelectronic devices, in conjunction with their environmental sensitivity, places them among the leading candidates for incorporation into ultraportable or wearable chemical analysis platforms. We use single-walled carbon nanotube (SWNT) networks to establish a mechanistic understanding of the solid-state O_2 sensitivity of a Eu^{3+}-containing dendrimer complex. The Eu^{3+} dendrimer-decorated SWNT networks show bimodal (optical spectroscopic and electrical conductance) sensitivity towards O_2 gas at room temperature under ambient pressure after illumination with 365 nm light. Through time-resolved and steady state optical spectroscopy, analysis of excited-state luminescence lifetimes, and solid-state electrical transport measurements, we investigate the mechanism of this unique O_2 sensitivity. We demonstrate a potential application of this system by showing a reversible and linear electrical response to O_2 gas in the tested range of 5-27%.

7.3 INTRODUCTION

Molecular oxygen is a ubiquitous requirement for human safety, and the need for ultraportable or wearable personal safety devices for ambient level O_2 monitoring is paramount for a wide array of civilian and military applications. Such sensor platforms could operate as personal safety

devices for workers in confined spaces or ambient level O_2 sensors for enclosed working environments. As a result, researchers have worked to develop microelectronic sensor platforms based on chemically sensitive resistors (chemiresistors) for the room-temperature detection of O_2 gas. The advantage of a room temperature O_2 sensor design over state of the art O_2 sensor technology, including optical spectroscopy,[127] solid-state or solution phase electrochemistry,[128] and resistive metal-oxide semiconductors,[129] is the potential for the miniaturization of robust low power devices without the requirement of maintaining high operating temperatures. While progress has been made,[130] the complicated fabrication techniques required to produce the sensing elements inhibit wide-scale adoption of this technology. Towards this end, ultra-small and low power carbon nanotube-based microelectronic devices,[14,131] especially those composed of networks of single-walled carbon nanotubes (SWNTs),[16] have shown great promise as candidates for the development of robust and low cost chemical detection platforms.[78] However, SWNTs have only shown reversible O_2 sensitivity with the aid of vacuum instrumentation,[60a,132] illustrating a fundamental limitation towards the development of this technology.

Here we describe the spectroscopic and electrical behavior of simple chemiresistor devices composed of SWNT networks decorated with an oxygen sensitive Eu^{3+}-containing dendrimer complex, abbreviated here as Eu_8 and illustrated in Figure 7-1, panels A and B. Lanthanide-containing complexes show solution-phase sensitivity towards O_2,[133] which we exploit by immobilizing Eu_8 on highly conductive and optically transparent SWNT-based devices,[77] as shown in Figure 7-1, panels C-E. We use the combined approach,[77,84] of optical spectroscopy and electrical transport measurements on SWNT-based devices to show that the O_2 sensitivity of the solid-state Eu_8 does not rely on the typical excited state quenching phenomena observed in the solution phase.[133] Specifically, we show that a preliminary illumination with UV

light (365 nm) is required to populate electron traps in the substrate surface. This approach is different from other solid-state techniques because we have used simple chemiresistor devices to transduce chemical events in the overlying molecular layer. Lastly, the Eu_8-decorated SWNT (Eu_8-SWNT) devices demonstrate a linear sensitivity towards O_2 gas in the environmentally relevant concentration range of 5-27% while operating at room temperature and ambient pressure, which represents an important step in the development of small scale and low power room temperature O_2 detection platforms.

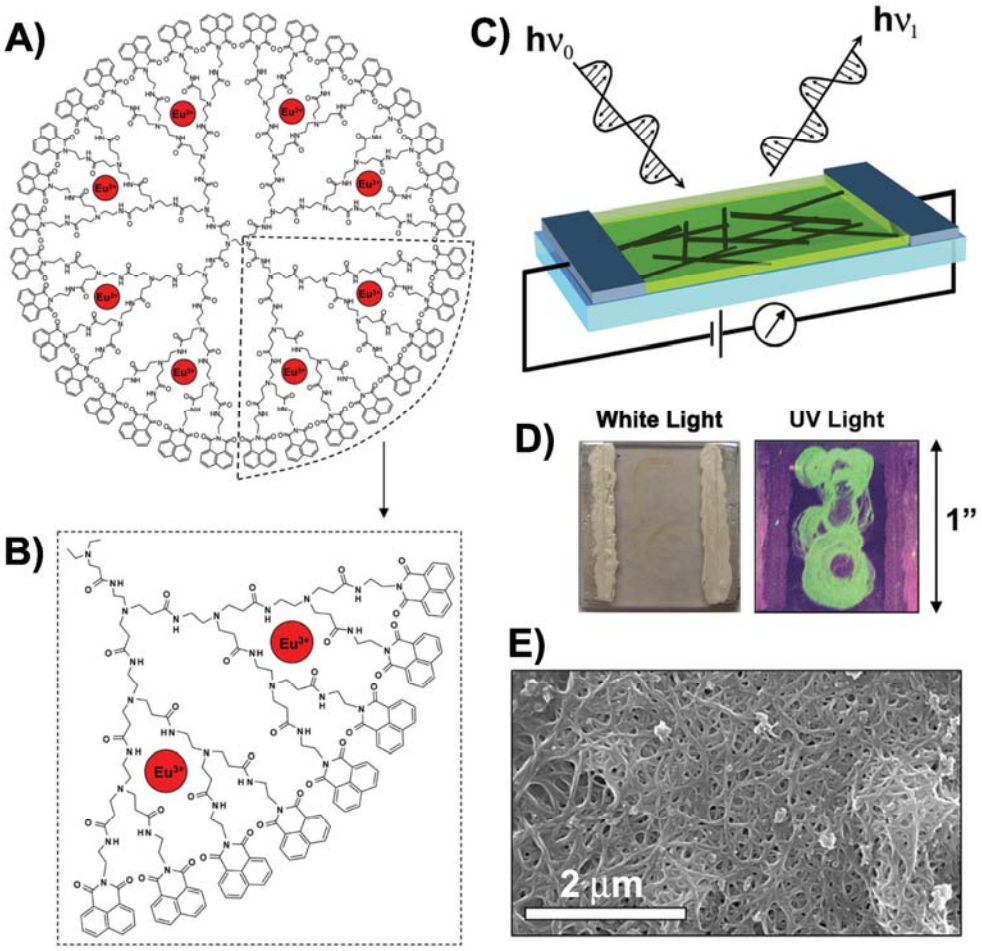

Figure 7-1. Chemical structure of the Eu^{3+}-containing dendrimer complex (Eu_8) and presentation of decorated SWNT devices. A) Chemical structure of the Eu_8 complex which contains eight Eu^{3+} cations (red) coordinated inside of a 1,8-naphthalimide terminated, generation-3 poly(amidoamine) (G3-PAMAM) dendrimer core. B) Expanded view of the Eu_8 structure illustrating the coordination of the Eu^{3+} ions. C) Cartoon representation of an optically transparent and electrically conductive Eu_8-SWNT device composed of a SWNT network decorated with Eu_8 (green layer) for simultaneous spectroscopic and electrical conductance measurements. D**)** Digital photographs of 1”×1” Eu_8-SWNT devices decorated with a dropcast layer of Eu_8 under white light (left) and 365 nm light (right); the green color of the Eu_8 layer is the complex photoluminescence. E) Scanning electron microscope (SEM) image of a typical device surface showing the Eu_8-decorated SWNT network; here, the Eu_8 molecules coat the underlying SWNT network. Energy dispersive x-ray (EDX) spectroscopy confirmed the presence of Eu on the Eu_8-SWNT device surface, and for comparison a SEM image and EDX spectrum of a typical bare SWNT network are presented in Figure 7-2.

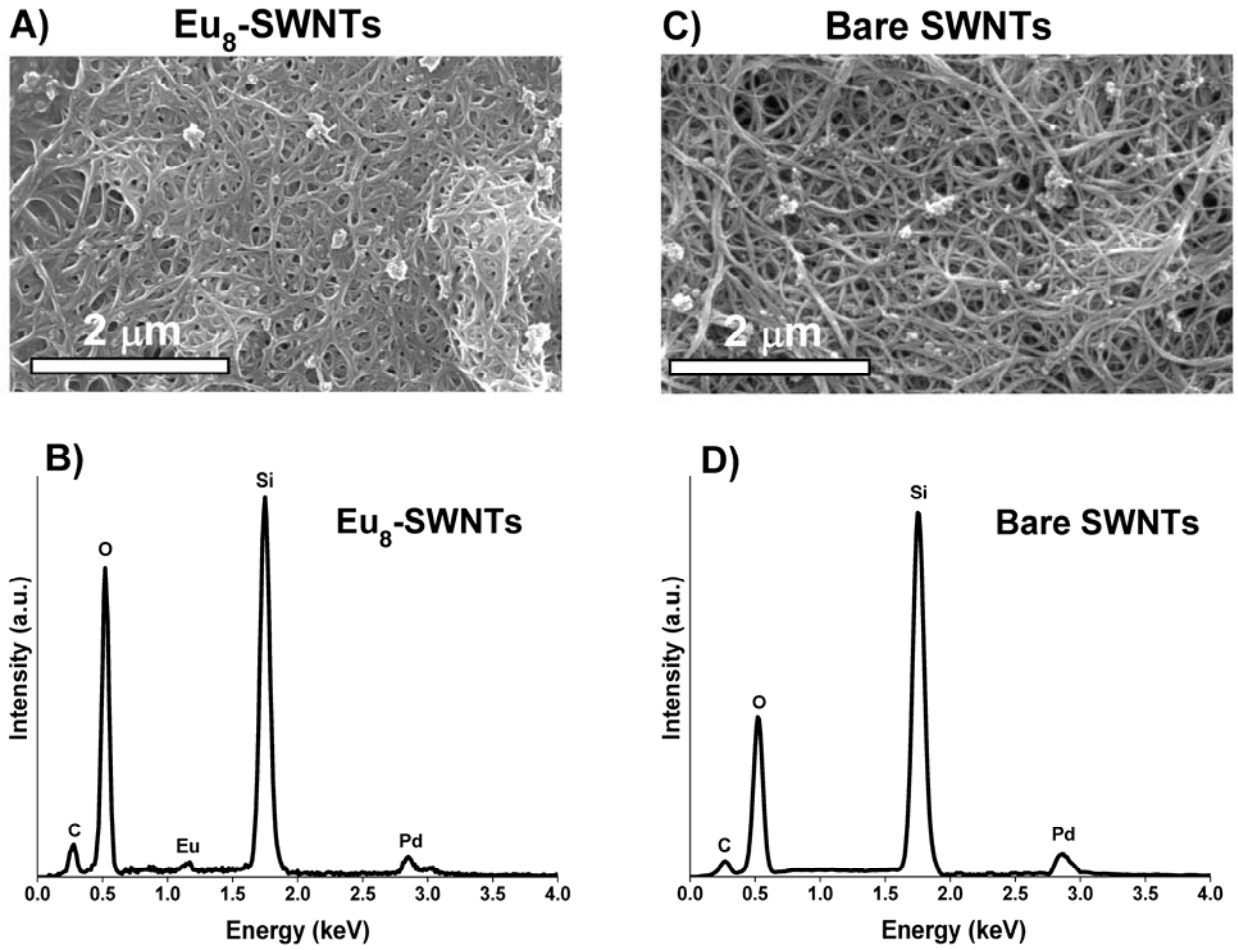

Figure 7-2. Characterization of Eu_8-SWNTs and bare SWNTs—scanning electron microscope (SEM) images and energy dispersive X-ray (EDX) spectroscopy of Eu_8-SWNTs and bare SWNTs. The SEM image of the Eu_8-SWNT network (panel A) shows a coating of Eu_8 on top of the SWNT network, and the EDX spectrum (panel B) confirms the presence of Eu at approximately 1.2 keV. The bare SWNT network (panel C) is composed of bundles of individual SWNTs, and as expected, the Eu signature is absent from the EDX spectrum (panel D). In the EDX spectra of both samples, the strong O and Si signatures are due to the underlying quartz (SiO_2) substrate; the Pd signature results from sputter coating the sample with Pd prior to imaging, which was done to prevent charging of the insulating quartz substrate during SEM operation.

7.4 EXPERIMENTAL

Synthesis of G3-PAMAM-(1,8-naphthalimide)$_{32}$. Poly(amidoamine) (PAMAM) dendrimer G(3)-NH_2 (390.5 mg, 0.0565 mmol) and 1,8-naphthalic anhydride (447.9 mg, 2.26 mmol) were suspended in DMF (25.0 mL) and stirred at 95^{o}C for 48 hours under a N_2 atmosphere. The compound was purified by dialysis using a regenerated cellulose membrane (Fisher; nominal MWCO 12,000-14,000) in DMSO for three days. The solution in the dialysis membrane was dried in a vacuum oven to yield the title product as a brown solid (517.6 mg, 72.4%); ^{1}H NMR (300MHz; $CDCl_3$, δ): 8.23 (br s, 64H, Ar H), 7.97 (br s, 64H, Ar H), 7.69 (m, 60H, -NH), 7.49 (br s, 64H, Ar H), 4.12 (br s, 64H, –N(CO)$_2$C*H*$_2$–), 3.51 (br s, 64H, -NHC*H*$_2$-), 3.19 (m, 56H, -NHC*H*$_2$-), 2.90–2.40 (m, 60H, –NC*H*$_2$CH$_2$NH–), 2.27 (m, 120H, –NC*H*$_2$CH$_2$CO–), 1.93 (m, 120H, –COC*H*$_2$–).

Synthesis of Eu$_8$-G3-PAMAM-(1,8-naphthalimide)$_{32}$, Eu$_8$. The preparation of the dendrimer complex was adapted from a synthesis protocol that we have described previously for a parent dendrimer ligand.[135] G3-PAMAM-(1,8-naphthalimide)$_{32}$ (16.81 mg, 1.326×10^{-6} mol) was dissolved in DMSO (5.0 mL) and a solution containing 1.397 mM of $Eu(NO_3)_3$ solution in DMSO (7.593 mL, 1.061×10^{-5} mol) was added. The mixture was incubated for seven days. DMSO was then evaporated in a vacuum oven, and the residual solid was dissolved in 10.0 mL of DMF to obtain a 1.40×10^{-4} M solution.

SWNT Device Fabrication. Optically transparent and electrically conductive SWNT network devices were fabricated and measured as previously described.[77] Briefly, commercially available

SWNTs (Carbon Solutions, Inc. P2 SWNTs; reported purity 70-90 percent) were suspended in DMF *via* sonication without further purification. 1 $in^2 \times 1/16^{th}$ in thick fused quartz (SiO_2) plates (Quartz Scientific; reported specific resistance of 10×10^{18} Ohm/cm^3 at 20 ^oC) served as the device substrates, and were cleaned prior to SWNT deposition with acetone, rinsed with water and dried under compressed air. After spraycasting the SWNT networks with a commercial air brush (Iwata) onto the heated quartz plates, Al tape and Ag paint were used to form the device electrodes. To create devices with two SWNT networks a cotton tipped applicator soaked in acetone was used to wipe clean a section of the spray-cast SWNT network. Two devices were created from the bisected SWNT network by individually connecting electrodes to each section with Al tape and Ag paint. Quartz plates with additional hydroxyl surface groups were created by soaking overnight in Piranha solution (1:3 H_2SO_4:H_2O_2 v/v; **CAUTION:** Pirahna is a vigorous oxidant and proper caution should be taken when handling this solution). Nanotube field-effect transistor (NTFET) devices consisted of interdigitated Au electrodes (10 μm pitch size) on a Si/SiO_2 substrate; dilute suspensions of Carbon Solutions P2 SWNTs in DMF were dropcast onto heated devices to form the conduction channel.

Device Decoration and Measurement. SWNT devices were decorated as follows: the devices were heated to just above the solvent boiling temperature and 200 μL (4 μL for NTFETs) of a particular molecule was dropcast evenly onto the surface of the device. For NTFET devices, all measurements were conducted under ambient conditions with a drain-source bias voltage of 100 mV using two Keithley model 2400 SourceMeters interfaced to LabVIEW 7.1 software.

UV-vis-NIR absorption spectra were recorded with a Perkin Elmer Lambda 900 UV-vis-NIR spectrophotometer, and steady-state excitation and emission spectra, as well as the

luminescence lifetime measurements, were recorded using a custom designed JY Horiba Fluorolog-322 spectrofluorimeter and a Tektronix TDS model 754D oscilloscope. At least 1000 luminescence decay traces, each containing 50,000 points were averaged and treated to calculate the lifetimes using Origin 7.0 software. The reported lifetime for a particular excited state is the average of at least two independent measurements. For multi-exponential fittings, we used the amplitude of the major component as a criterion for isolating the values reported in Table 7-1; components with amplitudes less than 1% were discarded. Time-resolved excitation and emission spectra of the Eu_8 solutions were measured using a Varian Cary Eclipse spectrofluorimeter.

For the optically transparent SWNT devices, the UV-exposure and gas sensitivity measurements were performed in a custom-built gas delivery chamber[77] that was housed inside of the spectrometers for simultaneous electrical and optical measurements. The device conductance was measured at a bias voltage of 500 mV with a Keithley model 2400 SourceMeter interfaced to LabVIEW 7.1 software. The network conductance of two devices on a single quartz substrate was simultaneously measured at 500 mV with a Keithley 2602 SourceMeter and a Keithley 708A switching matrix using Zephyr data acquisition software. The atmosphere inside the chamber was controlled with flowing research grade gases at a constant flow rate of 1000 standard cubic centimeters per minute (SCCM); all gases were dry unless otherwise noted. Atmospheres of 43 % RH were created by passing the gases over the headspace of sealed container of saturated K_2CO_3 solution; literature RH: 43.2 ± 0.3 % at 20 ^{o}C.[134] The UV lamp used for device illumination was a UVP, Inc. Model UVGL-55 hand held unit (365 nm; 250 $\mu W/cm^2$). **Caution**: UV light can be dangerous and appropriate eye protection should be worn. All measurements were conducted at room temperature and ambient pressure. Scanning

electron microscopy (SEM) and energy dispersive X-ray spectroscopy (EDX) were conducted on a Phillips XL30 FEG microscope operated at an accelerating voltage of 10 kV; samples were sputter coated with Pd prior to imaging to prevent charging of the insulating quartz substrate.

7.5 RESULTS

Solution Phase Behavior of Eu_8. Figure 7-3A presents the emission spectra of a Eu_8 solution (in DMF) saturated with either Ar or O_2, where O_2 saturation results in a decrease of the apparent emission intensity. The Eu_8 emission profile contains a broad band arising from the excited states of 1,8-naphthalimide groups centered around 469 nm, and three narrow emission bands located at lower energy that are characteristics of the Eu^{3+} centered transitions. In the Eu_8 structure, the 1,8-naphthalimide groups act as sensitizing agents (Figure 7-4). Specifically, photoexcited electrons in the excited naphthalimide singlet state undergo intersystem crossing into a triplet state, and subsequent energy transfer into the accepting levels of the Eu^{3+} ions produces the sharp Eu^{3+} centered emission bands.[135] The reversible and reproducible quenching effect of O_2 on the solution phase Eu_8 emission intensity is in accordance with its predicted behavior.[133] However, we found that the Eu^{3+} centered emission bands show a larger sensitivity to O_2 in comparison to the 1,8-naphthalimide band. For example, Figure 7-3B shows the relative emission intensity of the naphthalimide centered (469 nm; square labels) and Eu^{3+} $^5D_0 \rightarrow {}^7F_2$ (615 nm; circular labels) bands in a solution cycled several times between O_2 and Ar saturation. The larger relative change in the Eu^{3+} emission suggests that O_2 more effectively deactivates the Eu^{3+} excited state, as compared to the 1,8-naphthalimide, through the introduction of non-radiative pathways.[133]

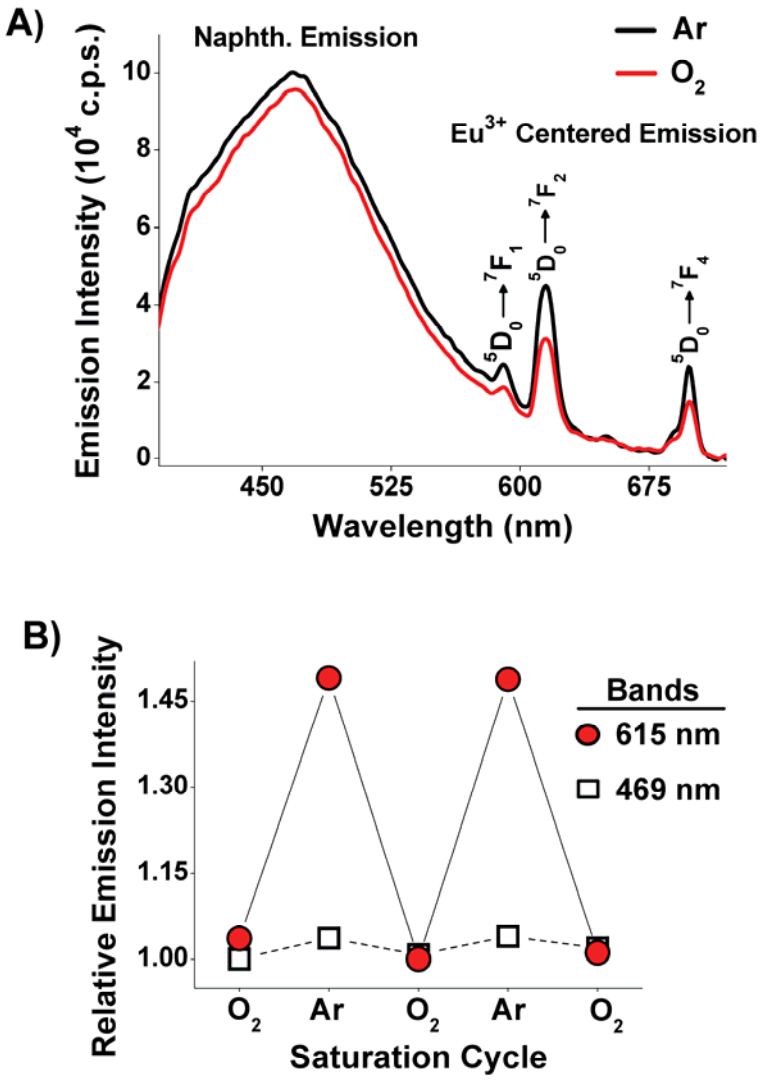

Figure 7-3. Solution phase O_2 sensitivity of the Eu_8 complex. A) Steady state emission spectrum of a Eu_8 solution (in DMF, 1.45×10^{-5} M; $\lambda_{excitation}$ = 354 nm) saturated with Ar (black curve) and O_2 (red curve). B) Relative emission intensity of the 1,8-naphthalimide ($\lambda_{emission}$ = 469 nm; hollow square labels) and Eu^{3+} $^5D_0 \rightarrow {}^7F_2$ ($\lambda_{emission}$ = 615 nm; solid circular labels) centered emission bands cycled between Ar and O_2 saturation.

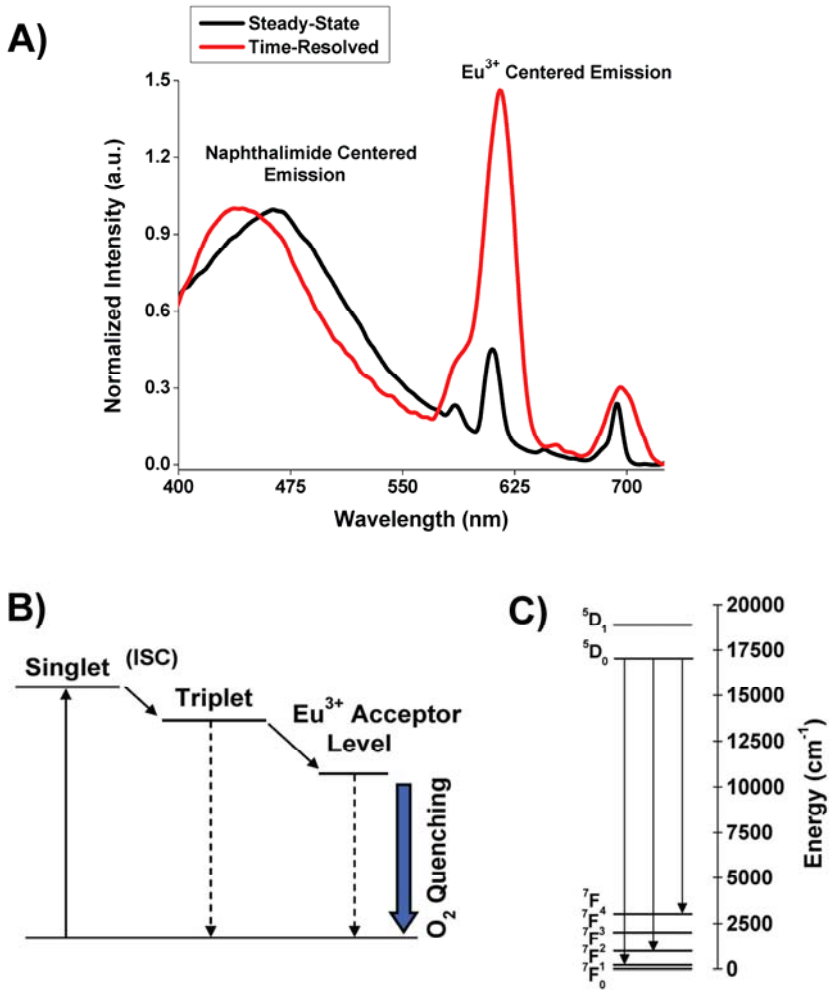

Figure 7-4. Emission spectra and energy diagram of Eu_8. A) Normalized steady-state (black curve) and time-resolved (red curve; delay of 4 ms) emission spectra of a solution of Eu_8 (in DMF; 1.45×10^{-5} M) recorded under ambient conditions; $\lambda_{excitation}$ = 354 nm. The spectra were normalized at the height of the apparent maximum of the naphthalimide emission band. B) Diagram of Eu_8 describing energy transfer from the naphthalimide triplet state into accepting levels of Eu^{3+}, as well as the proposed location of the O_2-induced non-radiative relaxation pathway for solution phase Eu_8. C) Energy level diagram showing the Eu^{3+} centered transitions.

Solid-State Behavior of Eu_8. In the solid state, the relative intensity of the Eu^{3+} centered transitions were greatly attenuated, and as shown in Figure 7-5A, we could only resolve the $^5D_0 \rightarrow {}^7F_2$ transition. The decreased emission intensity and apparent absence of distinguishable $^5D_0 \rightarrow {}^7F_1$ and $^5D_0 \rightarrow {}^7F_4$ transitions may result from less efficient sensitization through a decrease in the efficiency of energy transfer into the accepting levels of Eu^{3+}. The relative emission intensity of solid-state Eu_8 (dropcast onto a quartz substrate) was constant when cycled between atmospheres of pure O_2 and Ar (Figure 7-5A), highlighting a fundamental difference between the behavior of solid-state and solution phase samples. However, after illuminating the sample with 365 nm light for 30 minutes (in flowing Ar), the emission profile of the solid-state Eu_8 developed a sensitivity towards O_2 such that the intensity was decreased after illumination and partially restored under flowing O_2, as shown in Figure 7-5, panels B and C. The observed behavior is quite interesting compared to the solution phase behavior of Eu_8, and to the solid-state behavior of other O_2 sensitive photoluminescent complexes.[136]

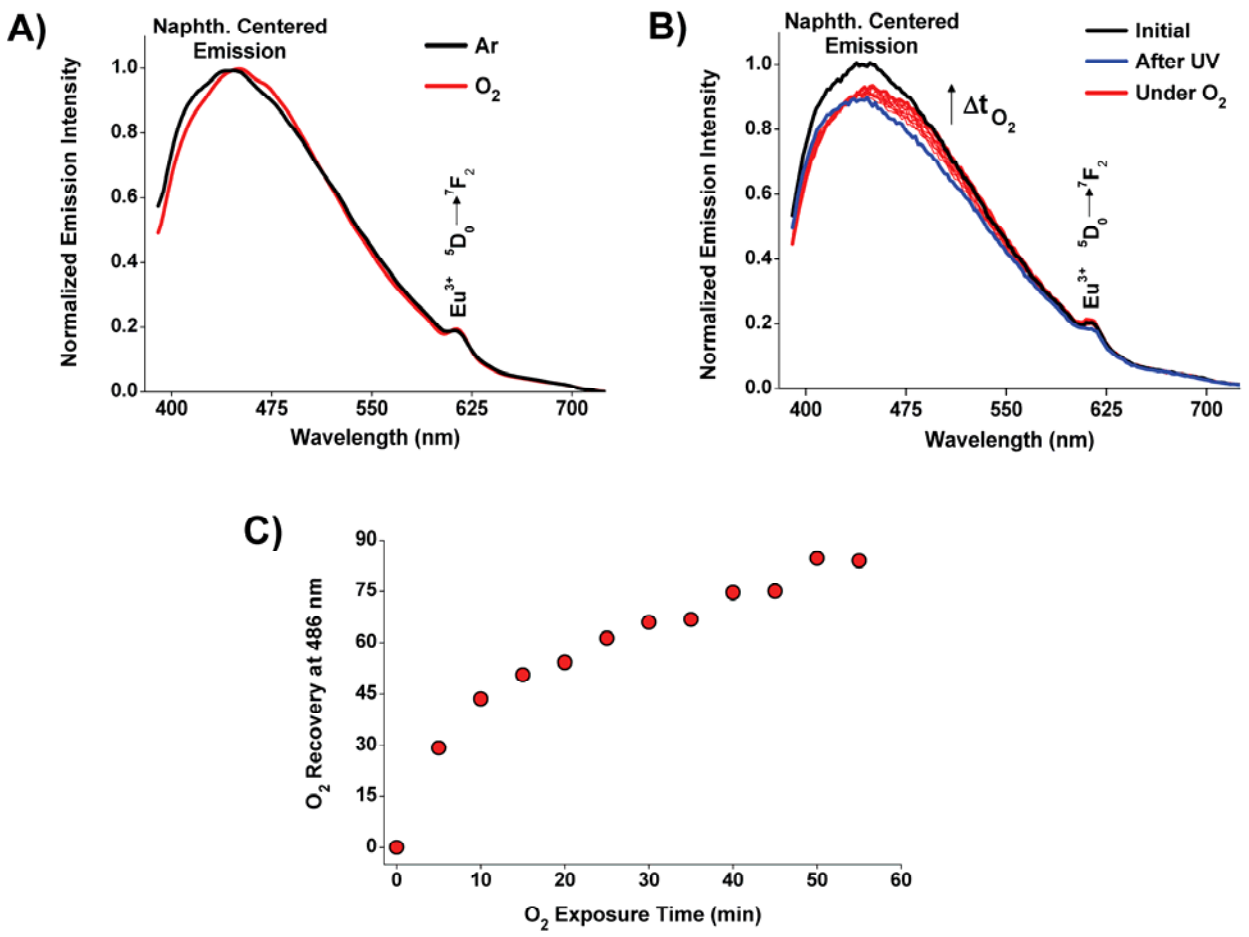

Figure 7-5. Solid-state Eu_8 O_2 response and recovery. A) Normalized emission spectra of Eu_8 (on quartz) in flowing Ar (black line) and pure O_2 (red line). B) Emission spectra of Eu_8 before (black line) and after (blue line) UV illumination in flowing Ar, and in flowing O_2 (red lines); spectra in flowing O_2 were recorded every minute. C) Naphthalimide centered emission intensity as a function of O_2 exposure time as measured at 486 nm. $\lambda_{excitation} = 354$ nm for all plots.

To further explore the solid-state behavior of Eu_8, we dropcast solutions onto optically transparent and electrically conductive SWNT devices.[77] We observed minimal changes in the spectroscopic signatures of both the SWNT network and the overlying Eu_8 layer after the devices were decorated, and separate field-effect transistor measurements of Eu_8-decorated SWNT networks suggest that the dominant effect of the overlying Eu_8 layer was to introduce charge scattering sites along the SWNT network (Figure 7-6).[137] Specifically, we found that Eu_8 decoration decreased the intensity of all the SWNT absorption bands (Figure 7-6A), and field-effect transistor measurements of a SWNT network dropcast onto interdigitated electrodes show a flattening of the drain-source current (I_{DS}) versus gate voltage (V_G) curve (Figure 7-6B), which has been suggested to indicate a reduction in charge mobility through the SWNT network.[137] On top of quartz immobilized SWNT networks, the Eu_8 absorbance spectrum was slightly blue shifted and broadened (Figure 7-6C). The excitation spectrum was slightly broadened, and the emission spectrum experienced a small redshift (Figure 7-6D). The spectroscopic characteristics of the system suggest that the electronic structure of the overlying Eu_8 molecule is not strongly effected by the presence of the SWNT network. Accordingly, we propose that Eu_8 acts as an overlying dielectric layer[64] that serves to reduce SWNT network charge mobility through the introduction of scattering sites.[137,138]

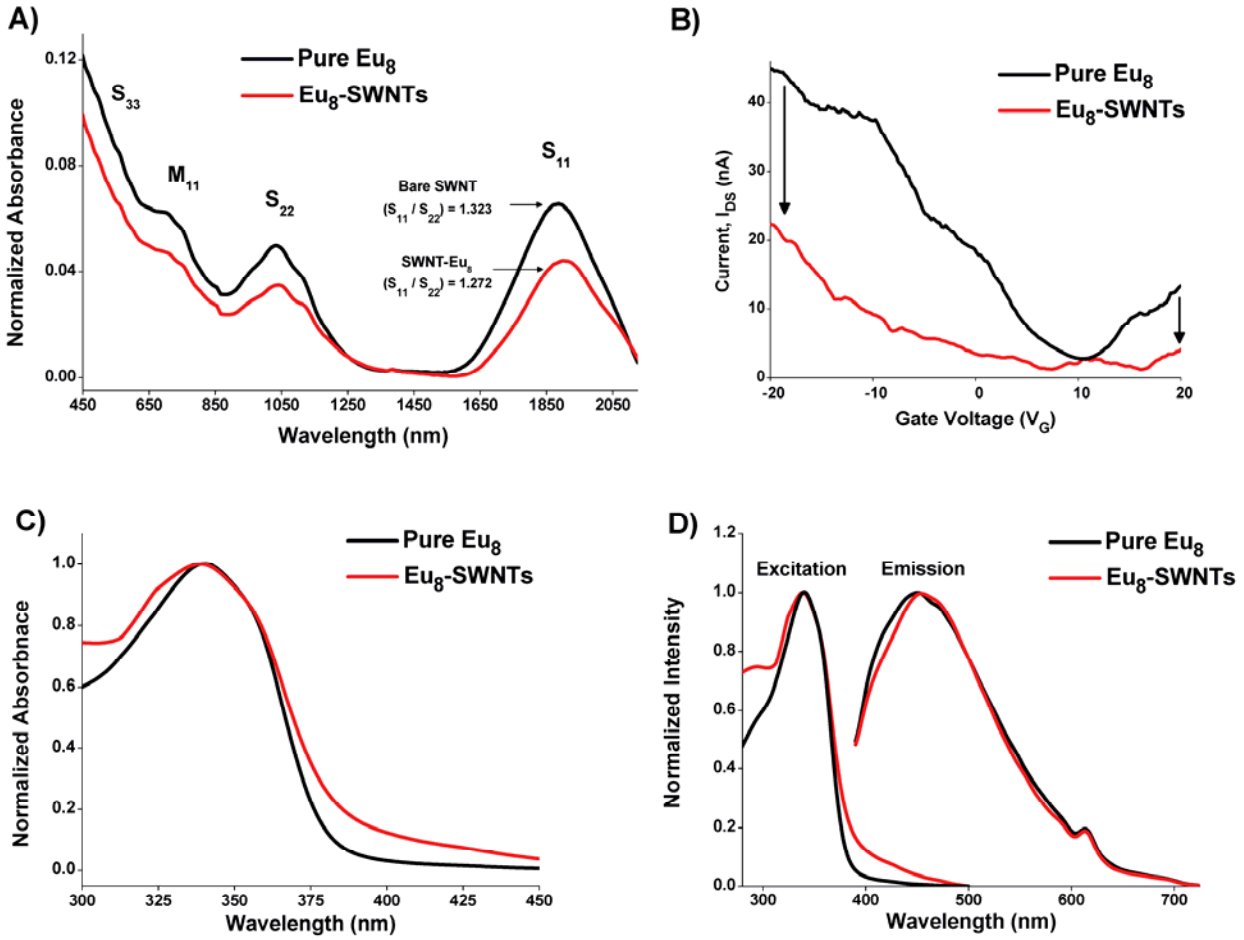

Figure 7-6. Characterization of Eu_8-decorated SWNT devices. A) UV-vis-NIR absorbance spectra of an optically transparent SWNT device (on quartz) before (black curve) and after (red curve) decoration with Eu_8; spectra were normalized at 1375 nm. B) Field-effect transistor transfer characteristics showing the drain-source current (I_{DS}) versus gate voltage (V_G) of a SWNT network dropcast onto interdigitated electrodes before (black curve) and after (red curve) decoration with Eu_8; the applied drain-source bias voltage was 100 mV. Normalized (C) absorbance as well as (D) excitation (λ_{em} = 615 nm) and emission (λ_{ex} = 354 nm) spectra of Eu_8 on quartz (black curve) and on top of a quartz-immobilized SWNT network (red curve).

Figure 7-7A shows the emission spectra of one Eu_8-decorated SWNT (Eu_8-SWNT) device before (black curve) and after (blue curve) exposure to 365 nm light, and during exposure to pure O_2 (red curves). After 30 minutes of illumination with 365 nm light (in flowing Ar) the Eu_8-SWNT device experienced a 25% decrease in the emission intensity of the naphthalimide band, and a 20% decrease in the emission intensity of the Eu^{3+} centered band. The spectroscopic behavior of Eu_8 after illumination and O_2 exposure was comparable on bare quartz as well as the SWNT networks, which strongly suggests that the observed behavior is an intrinsic property of solid-state Eu_8 on quartz.

Behavior of Eu_8 Decorated SWNT Networks. Using simultaneous UV-vis-NIR absorbance spectroscopy and network conductance measurements on Eu_8-SWNT devices, we found that the underlying SWNT network was able to transduce changes in the electronic properties of the Eu_8 layer during illumination with 365 nm light and exposure to pure O_2 gas. After a 30 minute illumination period, the device exhibited a decrease in the first semiconducting SWNT absorption band, labeled S_{11} in Figure 7-7B.[6a,40b] Additionally, illumination triggered an increase in the network conductance (Figure 7-7C), which we have termed the photogenerated ON-state. We found that the ON-state conductance abruptly increased after the termination of UV light and then slowly decayed as a function of time. To test the reproducibility of the Eu_8-SWNT response to UV light we exposed nine individual devices to 365 nm light for 30 minutes. Each device behaved qualitatively similarly, but we found that the magnitude of the response scaled inversely with the initial device conductance (Figure 7-8). This behavior differs drastically from the response of undecorated SWNTs to UV light,[139] which show a decrease in the SWNT network conductance and an increase in the S_{11} absorption band (Figure 7-9).

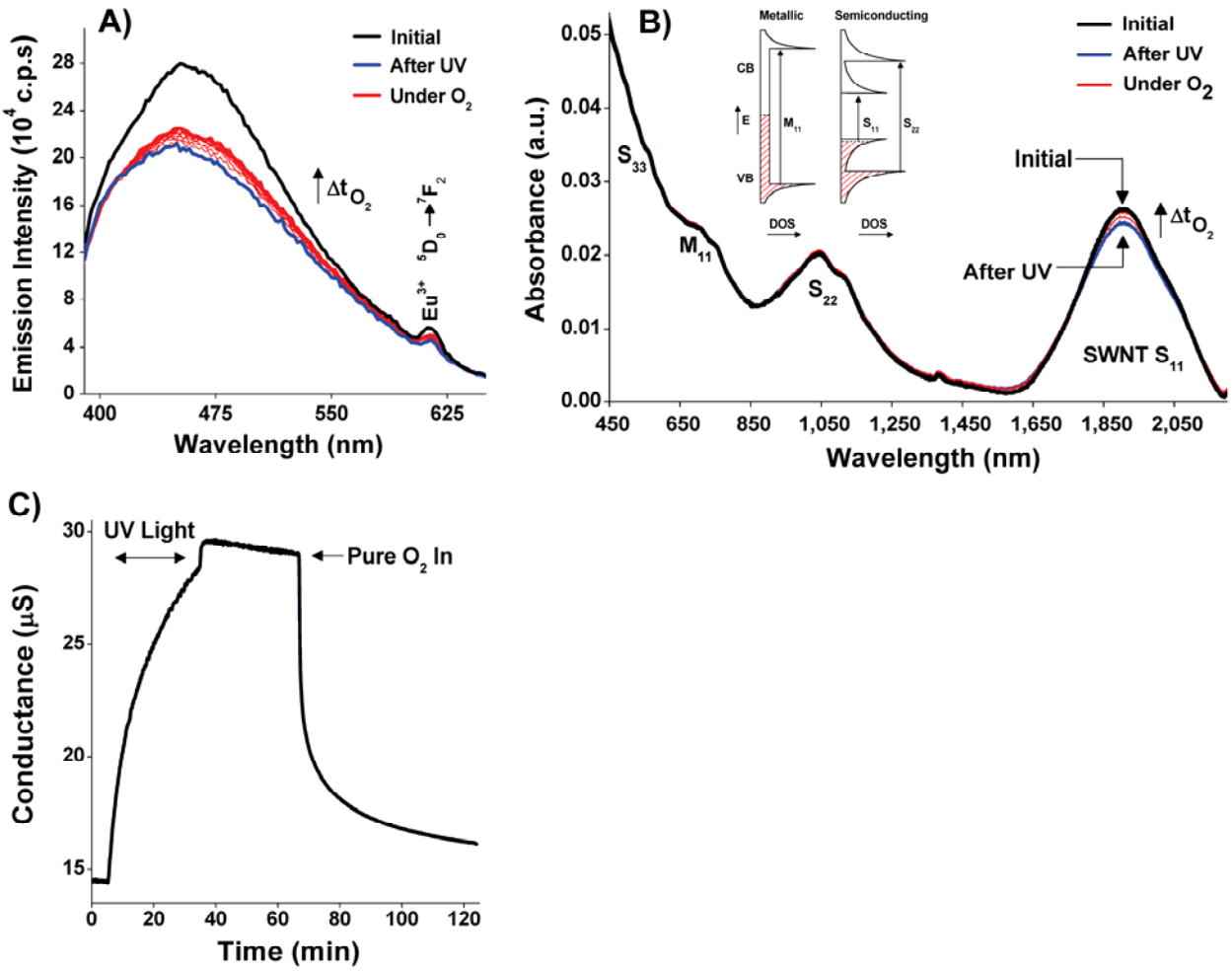

Figure 7-7. Bimodal O_2 sensitivity of the Eu_8 decorated SWNT devices. A) Emission ($\lambda_{excitation}$ = 354 nm) spectra of a Eu_8-SWNT device before (black curve) and after (blue curve) 30 minutes of illumination with 365 nm light (in flowing Ar) and during one hour of O_2 exposure (red curves); the UV and gas exposure times are identical in panels A-C. B**)** UV-vis-NIR absorbance spectra of the Eu_8-SWNT device before and after illumination with 365 nm light (in Ar) and during O_2 exposure; a partial density of states (DOS) diagram is presented in the inset. C) Network conductance of the Eu_8-SWNT device during 365 nm illumination and sustained photogenerated ON-state (in flowing Ar), followed by the introduction of pure O_2; the network conductance was measured simultaneously with the UV-vis-NIR absorption spectra (panel B).

After a 30 minute exposure to 365 nm light, we found that the device conductance decreased rapidly in the presence of O_2 (Figure 7-7C) such that nine individually tested devices experienced a 60 ± 10% decrease after a 200 second exposure to pure flowing O_2, regardless of the initial network conductance. After an hour-long exposure to pure O_2, we observed nearly 100 % restoration of the S_{11} band absorbance (Figure 7-7B) and approximately 90% recovery of the initial device conductance (Figure 7-7C). This electrical behavior was also reproducible, but we did notice that after 1 hour of O_2 exposure some devices demonstrated a larger than 100% response that stemmed from increased defect sites in the quartz substrate (*vide infra*). We found that the absorbance change of the SWNT S_{11} band displayed a time dependence like that of the network conductance during O_2 exposure (Figure 7-10), which indicates that the device response stems from perturbations in the electronic density of the SWNT valence band rather than a modification of the potential barriers at the interface between the SWNT network and device electrodes.[140] Throughout these experiments, the intensity of the M_{11} transition remained constant. While the metallic component of the SWNT network may contribute to the electrical response of the SWNT devices, the finite Fermi-level electron density of metallic SWNTs (inset; Figure 7-7B) renders the M_{11} transition intensity somewhat unaffected by changes in the local charge environment.[87]

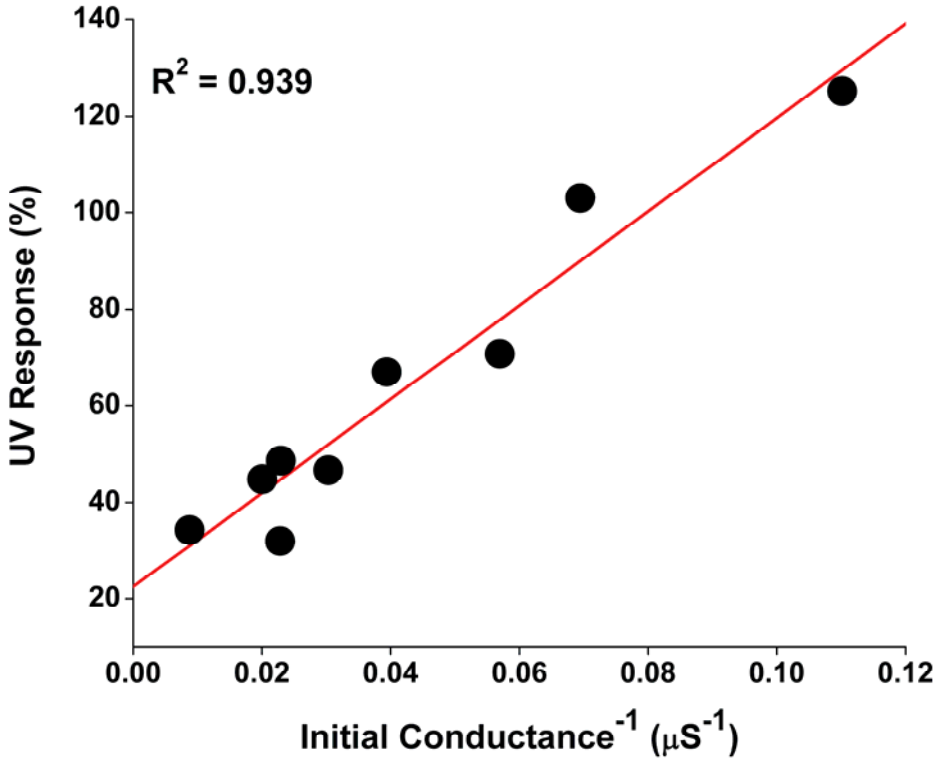

Figure 7-8. UV light response of multiple Eu_8-SWNT devices—response of nine individually tested Eu_8-SWNT devices after a 30-minute exposure to 365 nm light (in flowing N_2 or Ar). We found that all of the SWNT-Eu_8 devices showed qualitatively similar response towards UV light, however devices with lower initial conductance demonstrated a larger relative increase in conductance. The device conductance can be viewed as a measure of the SWNT network density, where higher conductance devices have a higher SWNT network density. We believe that lower density networks allowed more contact between Eu_8 and the electron traps at the quartz substrate—producing a larger response during illumination with 365 nm light. Furthermore, the lower SWNT network density of low-conductance devices may indicate a higher semiconducting SWNT contribution to the electrical properties. This observation follows the accepted hypothesis that semiconducting SWNTs show larger response to their local charge environment, as compared to metallic SWNTs.[21b]

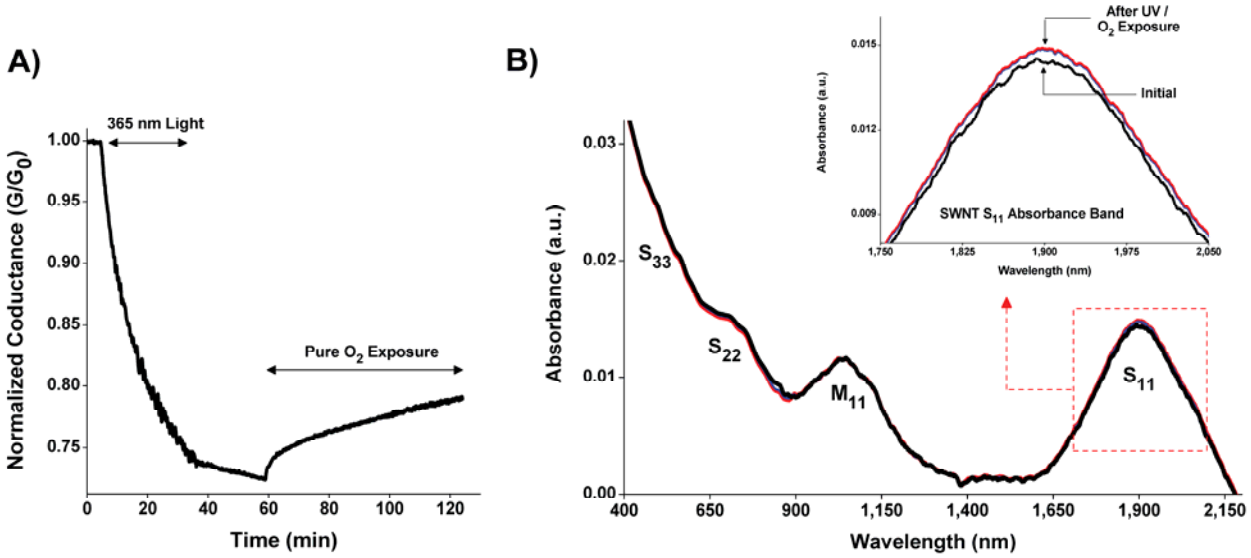

Figure 7-9. Response of bare SWNTs to UV light and O_2 gas. Simultaneously recorded (A) normalized network conductance (G/G_0) and (B) spectroscopic response (not normalized) of a bare SWNT network upon a 30 minute period of illumination with 365 nm light (in flowing Ar) and subsequent 60 minute exposure to pure O_2.

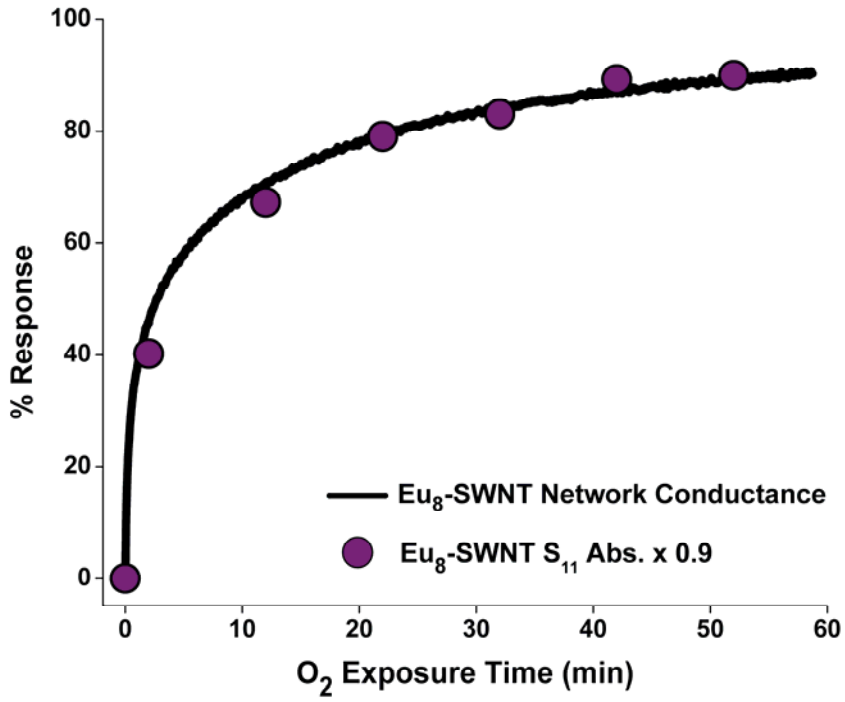

Figure 7-10. Spectroscopic and electrical response during O_2 exposure—simultaneously recorded spectroscopic and electrical behavior. The Eu_8-SWNT device network conductance (black line) and S_{11} band absorption (purple labels) are of the Eu_8-SWNT device shown in Figure 7-7; a scaling factor of 0.9 was applied to the S_{11} response. We have previously used scaling factors to compare the spectroscopic and electrical response of bare SWNT devices to gas phase analytes, but those values were typically larger than 5 (reference 77). Changes in the S_{11} transition intensity are proportional to changes in the electronic density of the semiconducting SWNT valence band, and a S_{11} scaling factor close to unity may indicate that semiconducting SWNTs dominated the device response to O_2.

Further control experiments were conducted on SWNT networks individually decorated with each component of Eu_8 complex, including the generation-three poly(amidoamine) (G-3 PAMAM) dendrimer with and without the 32 naphthalimide groups and the 1,8-naphthalic anhydride molecule by itself. Additionally, SWNT networks were decorated with an iron containing tetraphenyl porphyrin as an analog to a heme-containing moiety (Figure 7-11). We found that only the SWNT networks decorated with the 1,8-naphthalimide terminated G-3 PAMAM dendrimer demonstrated photo-response and O_2 sensitivity comparable to the Eu_8-decorated SWNT networks, indicating that the 1,8-naphthalimide terminated G-3 dendrimer component of Eu_8 was responsible for the observed behavior.

Luminescence Lifetimes. The presence of the Eu^{3+} ions in the Eu_8-SWNT networks allowed a quantitative comparison between the luminescence lifetimes of the Eu_8 triplet state and the Eu^{3+} acceptor level (abbreviated as T_3 and Eu^{3+}-AL, respectively). In essence, the presence of the Eu^{3+} emission serve as a spectroscopic beacon that can help identify the electronic processes that occur in the Eu_8-SWNT system by analyzing the two states' luminescence lifetimes. We measured the luminescence lifetimes of the Eu_8 T_3 and Eu^{3+}-AL before and after illumination with 365 nm light (in flowing Ar), and after the reintroduction of pure O_2 gas. The data presented in Table 7-1 shows that the luminescence lifetime of the T_3 state was not strongly affected by 365 nm illumination or the presence of O_2. However, we observed an increase in the lifetime of the Eu^{3+}-AL after 365 nm illumination, which began to decrease towards its initial value after 1 hour of O_2 exposure.

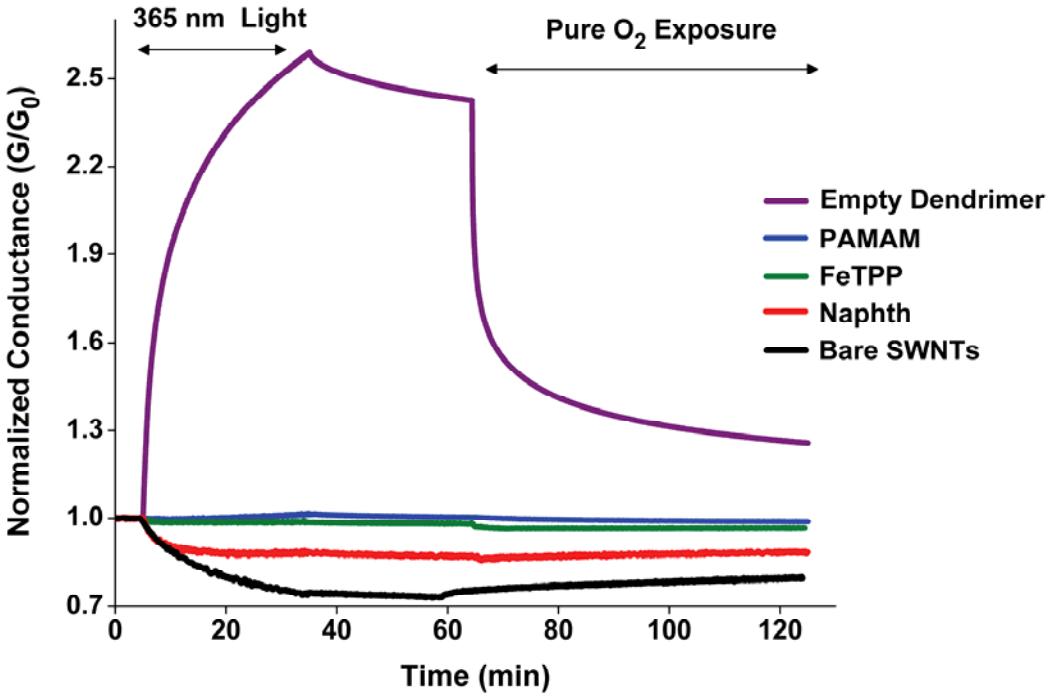

Figure 7-11. Effect of molecular decoration. Normalized conductance of SWNT networks decorated with various components of the Eu_8 complex including the 1,8-naphthalimide terminated G-3 PAMAM dendrimer (labeled Empty Dendrimer; purple curve), the G3 PAMAM dendrimer without the terminating 1,8-naphthalimide groups (labeled PAMAM; blue curve), and 1,8-naphthalic anhydride (labeled Naphth; red curve). Also presented is a SWNT device decorated with an iron containing porphyrin meso-Tetraphenylporphyrin Fe (III) chloride (labeled as FeTPP; green curve); a bare SWNT film is also presented for comparison (labeled Bare SWNTs; black curve). We found that only the SWNT devices functionalized with the empty dendrimer demonstrated behavior similar to the Eu_8-SWNT devices during 365 nm illumination and oxygen exposure. This observation strongly suggests that the 1,8-naphthalimide terminated PAMAM structure is responsible for the increased conductance after UV illumination and the sensitivity towards O_2 exposure.

Table 7-1. Luminescence lifetimes (τ) of the Eu8 triplet state (T_3) and Eu^{3+} acceptor level (Eu^{3+}-AL).

Measured Luminescence Lifetimes (ms)		
	T_3	**Eu^{3+}-AL**
Initial	0.3900 ± 0.0001	0.657 ± 0.001
After UV Light	0.370 ± 0.001	2.73 ± 0.07
After O_2 Exposure	0.4000 ± 0.0002	1.76 ± 0.07

7.6 DISCUSSION

Photoresponse. It has been reported that SWNTs will donate electronic density into the photodepleted ground state of an overlying chromophore during illumination with light.[34] The combined electrical and steady state spectroscopic behavior of the Eu_8-SWNT device fits this hypothesis (Figure 7-7, panels B and C), where the increased device conductance, and decreased SWNT S_{11} band absorbance during 365 nm illumination suggests that the photodepleted ground state of the Eu_8 complex exerted an attraction towards SWNT valence band electrons during illumination with 365 nm light.

The sustained Eu_8-SWNT photogenerated ON-state conductance after illumination with 365 nm light closely resembles the behavior of optoelectronic memory devices composed of polymer-decorated SWNTs.[141] In such systems, a so-called metastable ON-state persists after photoexcitation through the excitonic (separated electron-hole pairs) filling of electron traps at the SiO_2 surface.[141b,142] SiO_2 electron traps include SiOH groups,[143] water molecules hydrogen bonded to the device surface,[89] and a variety of other defects.[144] The abrupt increase in the network conductance immediately following termination of UV light has recently been described as a characteristic of photo-induced exciton separation and charge trap filling in polymer-decorated SWNT devices.[145] Moreover, the observation of a slight decay in the photogenerated ON-state conductance of the Eu_8-decorated SWNT networks is a consequence of the gradual recombination of spatially separated excitons.[146]

In contrast to polymer-decorated SWNT optoelectronic devices, which typically require an externally applied gate voltage to restore the initial conductance under ambient conditions,[141] the photogenerated ON-state of the Eu_8-SWNT system was sensitive towards O_2. To explain this

behavior, we propose a model based on the relative energy levels of the Eu_8 electronic states,[147] and electron traps in the quartz substrate, as described in Figure 7-12. For example, 365 nm illumination desorbs O_2 from the device surface,[139] whilst photoexciting electronic density from the ground singlet state (S_0) of the Eu_8 complex into an excited singlet state (S_1) results in energy transfer to the electron traps at the quartz surface.

After illumination, we observed a comparable decrease in both the intensity of the naphthalimide and Eu^{3+} centered emission bands, while the lifetime of the T_3 state was not strongly affected. This suggests that the electron traps are located close in energy to the S_1 state of the Eu_8 complex. In this configuration, the traps can accept energy from the S_1 state (red arrow) and inhibit intersystem crossing (ISC) into the T_3 state, thereby acting as an electronic bottleneck. The trap-induced inhibition of ISC serves to decrease the electronic population in both the T_3 and Eu^{3+}-AL, producing the observed decrease in emission intensities. Subsequently, a Coulomb attraction[148] develops between the photo-depleted S_0 state and electrons in the SWNT valence band, which effectively p-dopes the SWNT valence band. This phenomenon produces the increased Eu_8-SWNT network conductance during UV-illumination, sustained metastable ON-state conductance after the termination of UV-illumination, and decreased absorbance in the SWNT S_{11} band.

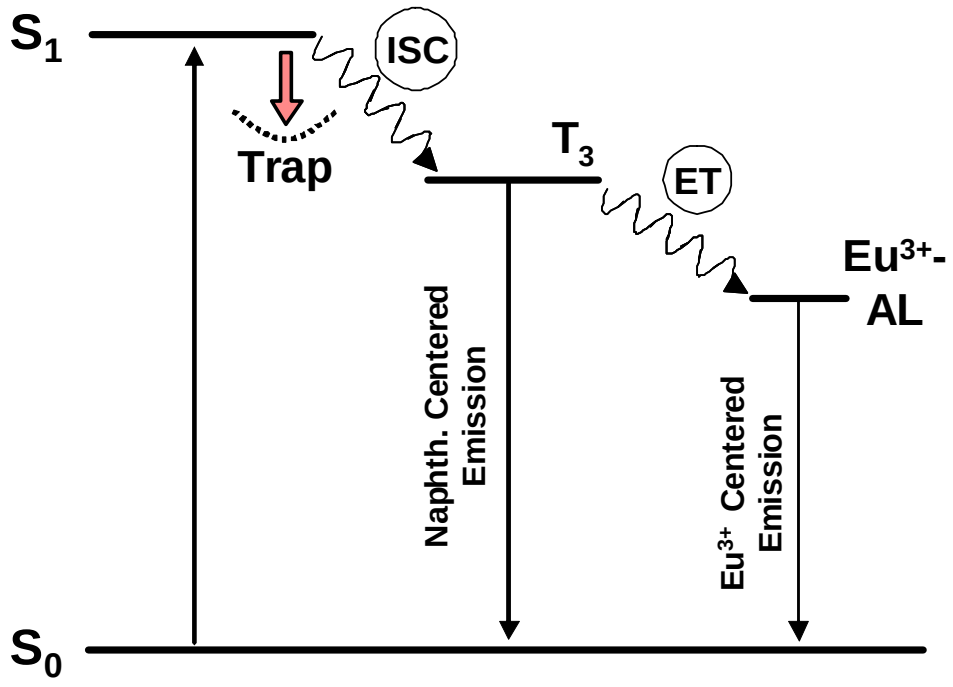

Figure 7-12. Proposed response mechanism describing the Eu_8-SWNT O_2 sensitivity in terms of the Eu_8 electronic structure. Here, the 1,8-naphthalimide ground and excited singlet (S_0 and S_1), and excited triplet (T_3) states are shown in relation to the Eu^{3+} acceptor level (Eu^{3+}-AL); the block arrow indicates energy donation into the trap states. ***ISC***: intersystem crossing, ***ET***: electron transfer.

O_2 Response. O_2 has been shown to passivate quartz charge traps, such as SiOH, through the introduction of non-radiative relaxation pathways.[149] Consequently, we suggest that the introduction of O_2 results in adsorption on the device surface and passivation of the electron traps through the addition of non-radiative pathways. The adsorption of O_2 removes the electronic bottleneck, increases ISC, and leads to the restoration of both the naphthalimide and Eu^{3+} centered emission band intensities. The increased lifetime of the Eu^{3+} centered transition after 365 nm illumination is a consequence of O_2 desorption, which removes any O_2-induced non-radiative pathways in the Eu^{3+} electronic structure. Finally, exciton recombination in the naphthalimide S_0 state eliminates the Coulombic attraction between the Eu_8 ground state holes and SWNT valence band electrons, which decreases the Eu_8-SWNT network conductance and increases the absorption of the SWNT S_{11} band.

To summarize the proposed response mechanism (Figure 7-12), we suggest that photoexcitation of the Eu_8-SWNT system promotes Eu_8 ground state electrons into an excited state, which subsequently fill electron traps at the quartz substrate surface. This leads to a Coulombic attraction between SWNT valence band electrons and the depleted Eu_8 ground state orbital, effectively p-doping the SWNT valence band. Upon the introduction of O_2 gas, non-radiative relaxation pathways allow electrons to return from the quartz electron traps back into the Eu_8 ground state. This alleviates the Coulombic attraction between the SWNT valence band and Eu_8 ground state and reverses the SWNT p-doping.

As a control, we modified the quartz surface to understand how an intentional increase in the number of surface electron traps (SiOH groups[143] and H_2O[89]) would affect the Eu_8-SWNT sensitivity to UV light and O_2 exposure in atmospheres of 0 % and 43 % relative humidity (Figure 7-13). We found that devices with increased trap sites behaved in a qualitatively similar

manner, but the response to an hour-long exposure to O_2 was consistently greater than 100%. We observed that this phenomenon was more pronounced in atmospheres with 43 % relative humidity, indicating that the density of charge traps has an important influence on device behavior in the presence O_2.

O_2 Detection. Using the Eu_8-SWNT devices in a chemiresistor configuration, we found a linear electrical response to O_2 in the concentration range tested (5-27%). By exploiting the stability of the Eu_8-SWNT photogenerated ON-state conductance, we were able to create a baseline for measuring O_2 response. For example, an initial 365 nm illumination in dry Ar (marked with a blue asterisk) established a baseline at an arbitrary network conductance (G_{ON}). Sequential pulses of dry O_2 gas (diluted in Ar) produced a concentration dependent decrease in the network conductance (Figure 7-14A). O_2 exposure (indicated with dashed lines) was followed by short periods of 365 nm illumination (marked with blue asterisks) to return the device to its arbitrarily defined ON-state conductance.

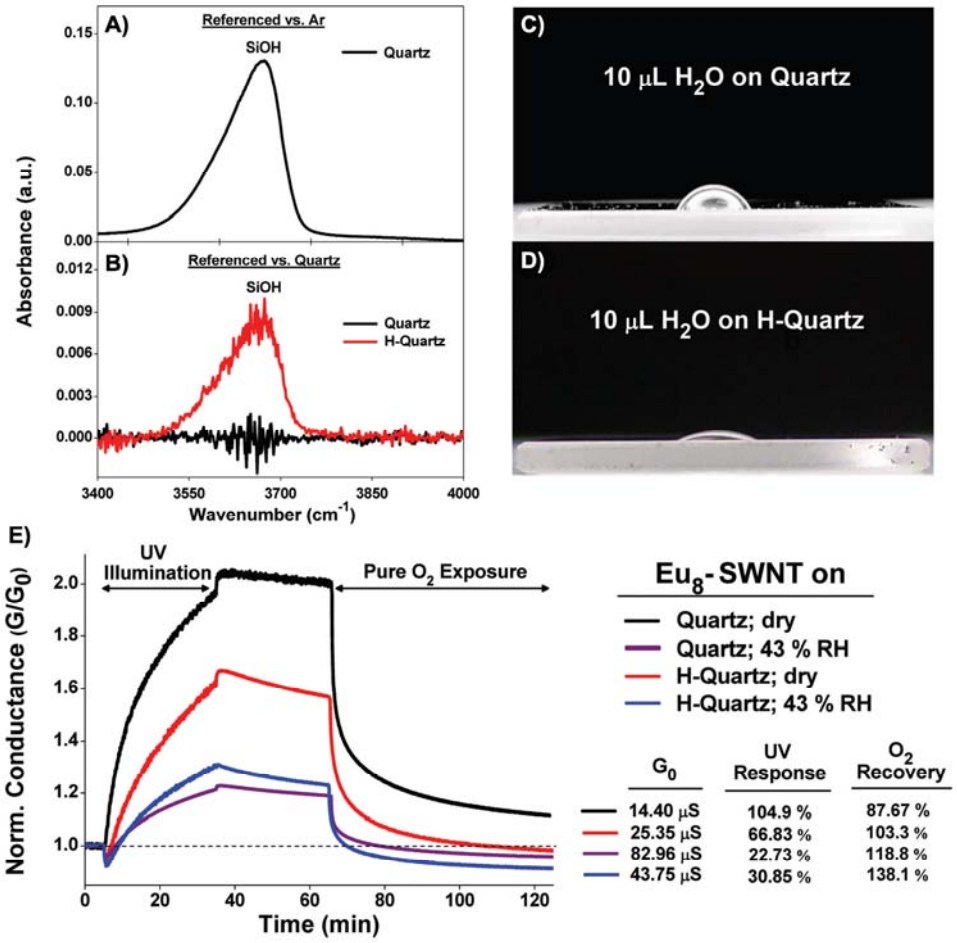

Figure 7-13. Introduction of defects onto quartz substrates—general affect on the device response. A) NIR absorption spectrum of quartz in Ar (referenced against Ar). B) NIR absorption spectra of quartz and hydroxylated quartz (H-quartz in Ar (referenced against quartz); the H-quartz was soaked in a 3:1 solution of conc. H_2SO_4 and 30% H_2O_2 overnight. Defects such as SiOH groups can be confirmed spectroscopically as increased absorbance at ~3650 cm^{-1}. After hydroxylation, the quartz shows increased absorbance at ~3650 cm^{-1}, indicating the presence of additional defect groups. Digital photographs of a 10 μL H_2O droplet on (C) quartz and (D) H-quartz, where the H-quartz appears less hydrophobic. E) Normalized response of Eu_8-SWNT networks on quartz in dry (black curve) and 43% relative humidity (RH; purple curve) atmospheres, as well as on H-quartz in dry (red curve) and 43% RH (blue curve) atmospheres. That data indicates that defect sites on the quartz surface, such as H_2O or SiOH groups, tend to produce larger than 100% response during O_2 exposure—highlighting the importance of the substrate on device performance.

During the 200 second O_2 exposure periods the device response did not saturate. However, we found that the rate of change in the network conductance scaled with the concentration of O_2. Figure 7-14B plots the rate of conductance change (ΔG relative to G_{ON}) during O_2 exposure cycles. Based on the standard deviation in the ON-state conductance before the first O_2 exposure, we have calculated the signal-to-noise ratio to be 3.89 for the device response to 5% O_2. The linear response to O_2, and repeated return to the ON-state conductance, indicates that the Eu_8-SWNT network did not experience any photo-degradation or chemical damage during operation. Using a value of three times the standard deviation of the ON-state conductance as the minimum detection limit (MDL), we have determined that the MDL of our un-optimized devices is less than 1 % O_2 for a 200 second exposure time, which is comparable to state-of-the-art, high temperature metal-oxide semiconductor sensor platforms for human safety applications.[150]

Lastly, the Eu_8-SWNT devices showed comparable photoresponse with N_2 as the carrier gas, demonstrated insignificant response to CO_2 and NH_3, were not adversely affected by relative humidity (0-43% RH; shown in Figure 7-13E), and retained good O_2 sensitivity even after storing the device in ambient conditions one week after the initial measurement. Typical of most solid-state O_2 sensors, we observed sensitivity towards NO_2. To identify false positives due to the presence of oxidizing species we created a device that contained both a Eu_8-SWNT network and a bare SWNT network (Figure 7-14C). Because bare SWNTs respond to oxidizing gases, such as NO_2,[21b,77] but do not respond to O_2 in ambient conditions, this device design provides an internal reference against the measurement of false positives. By monitoring the simultaneous conductance of both networks during UV, O_2 and NO_2 exposure we could determine the difference between a true O_2 response, and a false response due to the presence of NO_2.

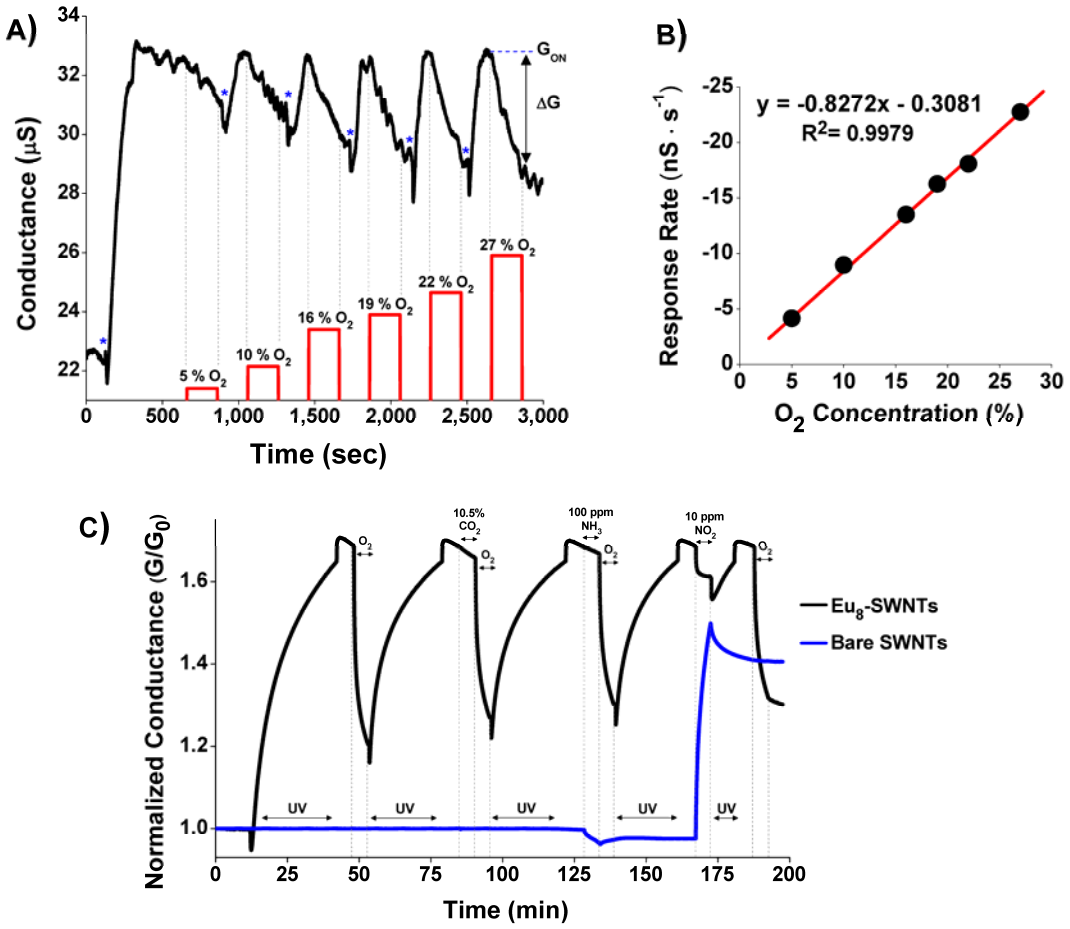

Figure 7-14. Eu_8-SWNT sensor response towards O_2. A) Electrical conductance of the Eu_8-SWNT device during 200-second gas exposure cycles of pure Ar and increasing O_2 concentrations (in Ar). The dashed lines represent the period of O_2 delivery, the red bars represent the delivered O_2 concentration, and the blue asterisks represent the initiation of brief UV-illumination periods (365 nm light; flowing Ar) that returned the device to a designated ON-state conductance (G_{ON}). B) Electrical response rate of the Eu_8-SWNT device to increasing O_2 concentrations during 200 second exposure cycles, where the response rate is defined as the change in network conductance (ΔG as measured from G_{ON}) during an O_2 exposure period. C) Simultaneously recorded conductance of a Eu_8-SWNT network (black curve) and bare SWNT network (blue curve) on a single quartz substrate during illumination with 365 nm UV light (in flowing N_2) and exposure to pure O_2, 10.5 % CO_2, 100 ppm NH_3 and 10 ppm NO_2. The bare SWNT device was masked as to eliminate illumination with UV light. After each UV light exposure the device remained in flowing N_2 for a period of five minutes, and each gas exposure was for a period of five minutes. After CO_2, NH_3 and NO_2 exposures, the device was exposed again to pure O_2, and the device conductance was returned to its ON-state conductance with UV light.

The insignificant sensitivity towards CO_2 and NH_3, identifiable response to an oxidizing species (NO_2), and comparable device operation in N_2 and humid atmospheres indicates that this system may hold promise as a low temperature platform for monitoring O_2 levels under ambient conditions. However, in the design of a field-usable platform one would need to take into consideration the need for a small reservoir of inert gas such as N_2 or Ar to purge the sample chamber during illumination with a compact UV light source.

7.7 CONCLUSIONS

We have used SWNT networks as a tool to establish a mechanistic understanding of the solid-state O_2 sensitivity observed in the Eu_8 system. When incorporated into electrically conductive and optically transparent devices, the Eu_8-SWNT system shows bimodal (optical spectroscopic and electrical conductance) sensitivity to O_2 gas at room temperature and ambient pressure. Using Eu_8-SWNT devices as chemiresistors, we have demonstrated a linear and reversible response to environmentally relevant O_2 concentrations between 5-27%, with a calculated minimum detection limit less of than 1% O_2. The response of Eu_8 decorated SWNTs towards UV light and O_2 gas is completely unlike that of bare SWNTs, allowing us to explore the mechanisms of device behavior without the controversy concerning the direct interaction between SWNTs and O_2.[60a,140,151] Ultimately, the incorporation of the Eu_8-SWNT system into low power, micro-electronic devices may find a broad range of applications in civilian and military arenas as personal safety devices for workers in confined spaces or for ambient level O_2 sensors for enclosed working environments where space, weight, and energy consumption are at a premium, such as mines, aircraft, submarines or spacecraft.

Acknowledgements

The authors thank Prof. D. H. Waldeck for his many insightful comments, and acknowledge the facilities, scientific and technical assistance of the Materials Micro-Characterization Laboratory of the Department of Mechanical Engineering and Materials Science, Swanson School of Engineering, University of Pittsburgh. This work was performed in support of ongoing research in sensor systems and diagnostics at the National Energy Technology Laboratory under RDS contract DE-AC26-04NT41817.

8.0 CONCLUDING REMARKS

The increasing interest in SWNT-based platforms for chemical sensors and energy production necessitates a fundamental understanding of the chemical and electronic processes that occur in the system. The two major avenues for studying such interactions are optical spectroscopy and electrical transport measurements. The chapters contained in this document outline the work that I have completed while pursuing a Ph. D. in Alexander Star's research group. In general, the complexity of the work has increased with each new chapter. For example, the initial work involved a purely electrical investigation of gas adsorption on metal decorated SWNTs. From there, an approach was introduced that utilized a simultaneous combination of optical spectroscopy and electrical transport measurements to study the electronic structure of SWNT networks during gas adsorption. With this new approach in hand, the problem of gas adsorption on metal decorated SWNTs was re-visited, and a more thorough description of the charge transfer mechanism was provided. Lastly, the most complex system involved SWNTs decorated with a photoactive, and O_2 sensitive Eu^{3+}-containing dendrimer. This work produced an elegant description of the system's O_2 sensitivity, and it was the first reported SWNT-based sensor for room temperature and ambient temperature O_2 gas.

My hope is that this work may serve as a stepping-stone for future researchers striving to further develop an understanding of chemical interactions and charge transfer with SWNT-based systems. In my opinion, fundamental studies that aim towards elucidating the mechanistic aspects of CNT-based systems, such as the ones outlined in this document, will undoubtedly lead to novel discoveries and help develop useful applications.

BIBLIOGRAPHY

(1) H. W. Kroto, J. R. Heath, S. C. O'Brien, R. F. Curl, R. E. Smalley *Nature* **1985**, *318*, 162.

(2) S. Iijima *Nature* **1991**, *354*, 56.

(3) S. Iijima, T. Ichihashi *Nature* **1993**, *363*, 603.

(4) (a) T. W. Odom, J. –L. Huang, P. Kim, C. M. Lieber *J. Phys. Chem. B* **2000**, *104*, 2794. (b) K. Balasubramanian, M. Burghard *Small* **2005**, *1*, 180.

(5) M. P. Anatram, F. Leonard *Rep. Prog. Phys.* **2006**, *69*, 507.

(6) (a) H. Katura, Y. Kumazawa, Y. Maniwa, I. Umczu, S. Suzuki, Y. Ohtsuka, Y. Achiba *Synth. Met.* **1999**, *103*, 2555. (b) S. M. Bachilo, M. S. Strano, C. Kittrell, R. H. Hauge, R. E. Smalley, R. Bruce. Weisman *Science* **2002**, *298*, 2361. (c) Y. Lian, Y. Maeda, T. Wakahara, T. Akasaka, S. Kazaoui, N. Minami, N. Choi, H. Tokumoto *J. Phys. Chem. B* **2003**, 107, 12082.

(7) S. V. Rotkin in *Applied Physics of Carbon Nanotubes* (Eds.: S. V. Rotkin and S. Subramoney), Springer, New York, **2005**, pp. 3-39.

(8) (a) I. Božović, N. Božović, M. Damnjanović *Phys. Rev. B.* **2000**, *62*, 6971. (b) I. Milošević, T. Vuković, S. Dmitrović, M. Damnjanović *Physica E* **2002**, *12*, 745.

(9) C. Journet, W. K. Maser, P. Bernier, A. Loiseau, M. Lamy de la Chapelle, S. Lefrant, P. Deniard, R. Lee, J. E. Fisher *Nature,* **1997**, *388*, 756.

(10) http://www.carbonsolution.com

(11) A. Javey, J. Guo, Q. Wang, M. Lundstrom, H. Dai *Nature* **2003**, *424*, 654.

(12) (a) S. Suzuki, C. Bower, Y. Watanabe, O. Zhou *Appl. Phys. Lett.* **2000**, *76*, 4007. (b) J. Zhao, J. Han, J. P. Lu, *Phys. Rev. B* **2002**, *65*, 194304. (c) M. Shiraishi, M. Ata *Carbon* **2001**, *39*, 1913.

(13) (a) Y. Zhang, N. W. Franklin, R. J. Chen, H. Dai *Chem. Phys. Lett.* **2000**, *331*, 35. (b) Y. Zhang, H. Dai *Appl. Phys. Lett.* **2000**, *77*, 3015.

(14) (a) S. J. Tans, A. R. M. Verschueren, C. Dekker *Nature* **1998**, *393*, 49. (b) R. Martel, T. Schmidt, H. R. Shea, T. Hertel, P. Avouris *Appl. Phys. Lett.* **1998**, *73*, 2447.

(15) B. L. Allen, P. D. Kichambare, A. Star *Adv. Mater.* **2007**, *19*, 1439.

(16) E. S. Snow, J. P. Novak, P. M. Campbell, D. Park *Appl. Phys. Lett.* **2003**, *82*, 2145.

(17) S. Heinze, J. Tersoff, R. Martel, V. Derycke, J. Appenzeller, P. Avouris *Phys. Rev. Lett.* **2002**, *89*, 106801.

(18) Z. Chen, J. Appenzeller, J. Knoch, Y. –M. Lin, P. Avouris *Nano Lett.* **2005**, *5*, 1497.

(19) J. Appenzeller, J. Knoch, V. Derycke, R. Martel, S. Wind, P. Avouris *Phys. Rev. B* **2002**, *89*, 126801.

(20) K. Bradley, J. Cumings, A. Star, J. –C. P. Gabriel, G. Grüner *Nano Lett.* **2003**, *3*, 639-641.

(21) (a) K. Bradley, J.-C. P. Gabriel, M. Briman, A. Star, G. Grüner *Phys. Rev. Lett*. **2003**, *91*, 218301. (b) J. Kong, N. R. Franklin, C. Zhou, M. G. Chapline, S. Peng, K. Cho, H. Dai *Science* **2000**, 287, 622.

(22) D. R. Kauffman, A. Star *Nano Lett.* **2007**, 7, 1863.

(23) (a) G. G. Wildgoose, C. E. Banks, R. G. Compton *Small* **2006**, 2, 182. (b) X. R. Ye, L. H. Chen, C. Wang, J. F. Aubuchon, I. C. Chen, A. I. Gapin, J. B. Talbot, S. Jin *J. Phys. Chem. B* **2006**, 110, 12938. (c) L. Qu, L. Dai, E. Osawa *J. Am. Chem. Soc.* **2006**, 128, 5523.

(24) (a) B. Shan, K. Cho *Phys. Rev. B* **2004**, *70*, 233405. (b) F. Léonard, J. Tersoff *Phys. Rev. Lett.* **2000**, *84*, 4693.

(25) J. Kong, M. G. Chapline, H. Dai *Adv. Mater.* **2001**, *13*, 1384.

(26) I. Lundström, S. Shivaraman, C. Svensson, L. Lundkvist *Appl. Phys. Lett.* **1975**, *26*, 55.

(27) A. Star, V. Joshi, S. Skarupo, D. Thomas, J. –C. P. Gabriel *J. Phys. Chem. B* **2006**, *110*, 21014.

(28) W. A. Brown, D. A. King *J. Phys. Chem. B* **2000**, *104*, 2578.

(29) J. Zhang, A. Boyd, A. Tselev, M. Paranjape, P. Barbara *Appl. Phys. Lett*. **2006**, *88*, 123112.

(30) (a) P. A. Anderson *Phys. Rev.* **1959**, *115*, 553. (b) H. B. Michaelson *J. Appl. Phys.* **1950**, *21*, 536. (c) D. E. Eastman *Phys. Rev. B* **1970**, *2*, 1. (d) H. B. Michaelson *J. Appl. Phys.* **1977**, *48*, 4729.

(31) A. Zangwill *Physics at Surface*, Cambridge University Press, Cambridge, U. K., **1998**.

(32) (a) A. Kolmakov, D. O. Klenov, Y. Lilach, S. Stemmer, M. Moskovits *Nano Lett.* **2005**, *5*, 667. (b) B. –K. Kim, N. Park, P. S. Na, H. –M. So, J. –J. Kim, H. Kim, K. J. Kong, H. Chang, B. –H. Ryu, Y. Choi, O. –J. Lee *Nanotech.* **2006**, *17*, 496.

(33) F. Ruffino, M. G. Grimaldi, F. Giannazzo, F. Roccaforte, V. Raineri *Appl. Phys. Lett.* **2006**, *89*, 243113.

(34) D. S. Hecht, R. J. A. Ramirez, M. Briman, E. Artukovic, K. S. Chichak, J. F. Stoddart, G. Grüner *Nano Lett*. **2006**, *6*, 2031.

(35) T. Ioannides, X. E. Verykios *J. Catal.* **1996**, *161*, 560.

(36) Y. Nosho, Y. Ohno, S. Kishimoto, T. Mizutani *Nanotech.* **2006**, *17*, 3412

(37) D. R. Kauffman, A. Star *Small* **2007**, *3*, 1324.

(38) (a) S. Niyogi, M. A. Hamon, H. Hu., B. Zhao, P. Bhowmik, R. Sen, M. E. Itkis, R. C. Haddon *Acc. Chem. Res.* **2002**, 35, 1105. (b) D. A. Britz, A. N. Khlobystov, *Chem. Soc. Rev*. **2006**, *35*, 637. (c) M. P. Anantram, F. Léonard *Rep. Prog. Phys*. **2006**, *69*, 507.

(39) P. Avouris *Acc. Chem. Res.* 2002, 35, 1026.

(40) (a) N. Hamada, S. Sawada, A. Oshiyama *Phys. Rev. Lett*. **1992**, *68*, 1579. (b) R. Saito, M. Fujita, G. Dresselhaus, M. S. Dresselhaus *Appl. Phys. Lett*. **1992**, 2204.

(41) (a) E. Joselevich *Chem. Phys. Chem.* **2004**, *5*, 619. (b) S. Kazaoui, N. Minami, R. Jacquemin *Phys. Rev. B* **1999**, *60*, 13339. (c) Y. Maeda, S. Kimura, M. Kanda, Y. Hirashima, T. Hasegawa, T. Wakahara, Y. Lian, T. Nakahodo, T. Tsuchiya, T. Akasaka, J. Lu, X. Zhang, Z. Gao, Y. Yu, S. Nagase, S. Kazaoui, N. Minami, T. Shimizu, H. Tokumoto, R. Saito *J. Am. Chem. Soc.* **2005**, *127*, 10287. (d) K. An, J. S. Park, C. M. Yang, S. Y. Jeong, S. C. Lim, C. Kang, J. H. Son, M. S. Jeong, Y. H. Lee *J. Am. Chem. Soc.* **2005**, *127*, 5196. (e) P. Leyton, J. S. Gómez-Jeria, S. Sanchez-Cortes, C. Domingo, M. Campos-Vallette *J. Phys. Chem. B* **2006**, *110*, 6470. (f) J. Lu, S. Nagase, X. Zhang, D. Wang, M. Ni, Y. Maeda, T. Wakahara, T. Nakahodo, T. Tsuchiya, T. Akasaka, Z. Gao, D. Yu, H. Ye, M. N. Mei, Y. Zhou *J. Am. Chem. Soc.* **2006**, *128*, 5114. (g) D. Chattopadhyay, I. Galeska, F. Papadimitrakopoulos *J. Am. Chem. Soc.* **2003**, *125*, 3370. (h) C. Ménard-Moyon, N. Izard, E. Doris, C. Mioskowski *J. Am. Chem. Soc.* **2006**, *128*, 6552.

(42) M. S. Strano, C. A. Dyke, M. L. Usrey, P. W. Barone, M. J. Allen, H. Shan, C. Kittrell, R. H. Hauge, J. M. Tour, R. E. Smalley *Science* **2003**, *301*, 1519.

(43) C. -M. Yang, K. H. An, J. S. Park, K. A. Park, S. C. Lim, S. -E. Cho, Y. S. Lee, W. Park, C. Y. Park, Y. H. Lee *Phys. Rev. B* **2006**, *73*, 075419.

(44) M. Zheng, B. A. Diner *J. Am. Chem. Soc.* **2004**, *126*, 15490.

(45) M. S. Strano, C. B. Huffman, V. C. Moore, M. J. O'Connell, E. H. Haroz, J. Hubbard, M. Miller, K. Rialon, C. Kittrell, S. Ramesh, R. H. Hauge, R. E. Smalley *J. Phys. Chem. B* **2003**, *107*, 6979.

(46) A. Star, T.-R. Han, J.-C. P. Gabriel, K. Bradley, G. Grüner *Nano Lett.* **2003**, *3*, 1421.

(47) (a) X. Tang, S. Bansaruntip, N. Nakayama, E. Yenilmez, Y. -I. Chang, Q. Wang *Nano Lett*. **2006**, *6*, 1632. (b) T. Yamada *Appl. Phys. Lett*. **2006**, *88*, 083106.

(48) M. E. Itkis, S. Niyogi, M. E. Meng, M. A. Hamon, H. Hu, R. C. Haddon *Nano Lett.* **2002**, 2 155.

(49) J. L. Bahr, J. M. Tour *J. Mater. Chem*. **2002**, 12, 1952.

(50) Z. Wu, Z. Chen, X. Du, J. M. Logan, J. Sippel, M. Nikolou, K. Kamaras, J. R. Reynolds, D. B. Tanner, A. F. Hebard, A. G. Rinzler, *Science.* **2004**, 305, 1273.

(51) (a) D. M. Guldi, G. M. A. Rahman, N. Jux, D. Balbinot, U. Hartnagel, N. Tagmatarchis, M. Prato, *J. Am. Chem. Soc.* **2005**, *127*, 9830. (b) C. Ehli, G. M. A. Rahman, N. Jux, D. Balbinot, D. M. Guldi, F. Paolucci, M. Maraccio, D. Paolucci, M. Melle-Franco, F. Zerbetto, S. Campidelli, M. Prato, *J. Am. Chem. Soc.* **2006**, *128*, 11222-12231; c) H. Murakami, T. Nomura, N. Nakashima, *Chem. Phys. Lett.* **2003**, *378*, 481-485; d) G. M. A. Rahman, D. M. Guldi, S. Campidelli, M. Prato, *J. Mater. Chem.* **2006**, *16*, 62-65; e) J.Chen, C. P. Collier *J. Phys. Chem. B* **2005**, *109*, 7605-7609.

(52) D. R. Kauffman, O. Kuzmych, A. Star *J. Phys. Chem. C* **2007**, *111*, 3539.

(53) (a) K. M. Kadish, K. M. Smith, R. Guilard. (Eds.) *Porphyrin Handbook* Academic Press, New York, **2000**. (b) D. Dophin *The Porphyrins: Volume VII: Biochemistry, Part B* Academic Press, New York, **1979**.

(54) (a) N. A. Rakow, K. S. Suslick *Nature* **2000**, 406, 710. (b) A. Morales-Bahnik, R. Czolk, H. J. Ache *Sens. Act. B* **1994**, 18-19, 493. (c) R. Czolk *Sens. Ac. B* **1996**, 30, 61. (d) K. R. Rodgers *Curr. Op. Chem. Bio.* **1999**, 3, 158.

(55) (a) M. S. M. Quintino, H. Winnischofer, M. Nakamura, K. Araki, H. E. Toma, L. Angnes *Anal. Chim. Acta* **2005**, 539, 215. (b) K. I. Ozoemena, Z. Zhao, T. Nyokong *Electrochem. Commun.* **2005**, 7, 679.

(56) A. D. Schwab, D. E. Smith, B. Bond-Watts, D. E. Johnston, J. Hone, A. T. Johnson, J. C. de Paula, W. F. Smith *Nano Lett*. **2004**, 4, 1261.

(57) (a) A. Merkoçi, M. Pumera, X. Llopis, B. Pérez, M. del Valle, S. Alegret *Trends Anal. Chem.* **2005**, 24, 826. (b) J. J. Davis, K. S. Coleman, B. R. Azamian, C. B. Bagshaw, M. L. H. Green *Chem. Eur. J.* **2003**, 9, 3732.

(58) P. Serp, M. Corrias, P. Kalck *Appl. Catal., A* **2003**, 253, 337.

(59) (a) T. Belin, F. Epron *Mater. Sci Eng., B* **2005**, 119, 105. (b) R. Jacquemin, S. Kazaoui, D. Yu, A. Hassanien, N. Minami, H. Kataura, Y. Achiba *Synth. Met.* **2000**, 115, 283.

(60) (a) P. Collins, K. Bradley, M. Ishigami, A. Zettl *Science* **2000**, 287, 1801. (c) C. Y. Lee, M. S. Strano *Langmuir* **2005**, 21, 5192. (d) E. S. Snow, F. K. Perkins, J. A. Robinson *Chem. Soc. Rev.* **2006**, 35, 790.

(61) (a) T. Hasobe, S. Fukuzumi, P. V. Kamat *J. Am. Chem. Soc.* **2005**, *127*, 11884. (b) F. Cheng, A. Adronov *Chem. Eur. J.* **2006**, **12**, 5053. (c) K. S. Chichak, A. Star, M. V. P. Altoé, F. J. Stoddart, J. F. *Small* **2005**, *1*, 452.

(62) (a) D. M. Guldi, G. M. A. Rahman, M. Prato, N. Jux, S. Qin, W. Ford *Angew. Chem. Int. Ed.* **2005**, 44, 2015. (b) N. Tagmatarchis, M. Prato, D. M. Guldi *Physica E* **2005**, 29, 546.

(63) (a) A. Star, E. Tu, J. Niemann, J. C. P. Gabriel, C. S. Joiner, C. Valcke *Proc. Natl. Acad. Sci. USA* **2006**, 103, 921. (b) E. S. Jeng, A. E. Moll, A. C. Roy, J. B. Gastala, M. S. Strano *Nano Lett.* **2006**, 6, 371.

(64) D. A. Heller, E. S. Jeng, T. K. Yeung, B. M. Martinez, A. E. Moll, J. B. Gastala, M. S. Strano *Science* **2006**, 311, 508.

(65) L. J. Boucher *J. Am. Chem. Soc.* **1970**, *92*, 2725.

(66) (a) B. B. Wayland, L. W. Olson *Inorg. Chim. Acta.* **1974**, *11*, L23. (b) B. B. Wayland, L. W. Olson, Z. U. Siddiqui *J. Am. Chem. Soc.* **1978**, *98*, 94. (c) B. B. Wayland, J. V. Minkiewicz, M. E. Abd-Elmageed *J. Am. Chem. Soc.* **1974**, *96*, 2795.

(67) (a) J. D. Hobbs, S. A. Majumder, L. Lou, G. A. Sickelsmith, J. M. E. Quirke, C. J. Medforth, K. M. Smith, J. A. Shelnutt *J. Am. Chem. Soc.* **1994**, *116*, 3261. (b) R. Schwietzer-Stenner, C. Lemke, R. Haddad, Y. Qiu, J. A. Shelnutt, J. M. E. Quirke, W. Dreybrodt *J. Phys. Chem. A* **2001**, *105*, 6680.

(68) (a) J. C. Pinkert, R. W. Clark, J. N. Burstyn *J. Biol. Inorg. Chem.* **2006**, 11, 642. (b) M. Shimizu, F. Basolo, M. N. Vallejo, J. E. Baldwin *Inorg. Chim. Acta.* **1984**, 91, 247.

(69) (a) D. M. Guldi, G. M. A Rahman, N. Jux, N. Tagmatarchis, M. Prato *Angew. Chem. Int. Ed.* **2004**, 43, 5526. (b) Z. Guo, F. Du, D. Ren, Y. Chen, J. Zheng, Z. Liu, J. Tian *J. Mater. Chem.* **2006**, 16, 3021.

(70) (a) V. C. Moore, M. S. Strano, E. H. Haroz, R. H. Hauge, R. E. Smalley, J. Schmidt, Y. Talmon, *Nano Lett.* **2003**, *3*, 1379. (b) M. S. Strano, V. C. Moore, M. K. Miller, M. J.

Allen, E. H. Haroz, C. Kittrell, R. H. Hauge, R. E. Smalley *J. Nanosci. Nanotechnol.* **2003**, *3*, 81. (c) J. H. Choi, M. S. Strano *Appl. Phys. Lett.* **2007**, *90*, 223114.

(71) M. J. O'Connell, E. E. Eibergen, S. K. Doorn *Nat. Mater* **2005**, *4*, 412.

(72) H. Li, B. Zhou, Y. Lin, L. Gu, W. Wang, K. A. S. Fernando, S. Kumar, L. F. Allard, Y. –P. Sun *J. Am. Chem. Soc.* **2004**, *126*, 1014.

(73) J. Y. Lee, S. J. Lee, H. J. Kim, H. J. Kim *J. Phys. Chem. B* **2006,** 110, 5337.

(74) (a) K. Okazaki, Y. Nakato, K. Murakoshi *Phys. Rev. B* **2003**, 68, 035434.

(75) (a) N. J. Tao *Phys. Rev. Lett.* **1996**, 76, 4066. (b) T. Sagara, M. Fukuda, N. Nakashima *J. Phys. Chem. B* **1998**, 102, 521.

(76) (a) S. B. Lei, J. Wang, Y. H. Dong, C. Wang, L. J. Wan, C. L. Bai *Surf. Interface Anal.* **2002**, 34, 767. (b) N. J. Tao, G. Cardenas, F. Cunha, Z. Shi *Langmuir* **1995**, 11, 4445.

(77) D. R. Kauffman, A. Star *J. Phys. Chem. C* **2008**, *112*, 4430.

(78) D. R. Kauffman, A. Star *Angew. Chem. Int. Ed.* **2008**, *47*, 6550.

(79) (a) S. Peng, K. Cho, P. Qi, H. Dai *Chem. Phys. Lett*. **2004**, *387*, 271. (b) H. Chang, J. D. Lee, S. M. Lee, Y. H. Lee *Appl. Phys. Lett*. **2001**, *79*, 3863. (c) J. Zhao, A. Buldum, J. Han, J. P. Lu *Nanotech.* **2002**, *13*, 195. (d) L. M. Woods, Ş. C. Bădescu, T. L. Reinecke *Phys. Rev. B* **2007**, *75*, 155415. (e) R. Larciprete, L. Petaccia, S. Lizzit, A. Goldoni *J. Phys. Chem. C* **2007**, *111*, 12169.

(80) M. D. Ellison, M. J. Crotty, D. Koh, L. Spray, K. E. Tate *J. Phys. Chem. B* **2004**, *108*, 7938.

(81) A. Goldoni, R. Larciprete, L. Petaccia, S. Lizzit *J. Am. Chem. Soc.* **2003**, *125*, 11329.

(82) (a) Y. Zhang, C. Suc, Z. Liu, J. Li *J. Phys. Chem. B* **2006**, *110*, 22462. (b) F. Mercuri, A. Sgamellotti, L. Valentini, I. Armentano, J. M. Kenny *J. Phys. Chem. B* **2005**, *109*, 13175. (c) W. –L. Yim, X. G. Gong, Z. –F. Liu *J. Phys. Chem. B* **2003**, *107*, 9363.

(83) K. Seo, K. A. Park, C. Kim, S. Han, B. Kim, Y. H. Lee. *J. Am. Chem. Soc.* **2005**, *127*, 15724.

(84) E. Bekyarova, I. Kalinina, M. E. Itkis, L. Beer, C. Nelson, R. C. Haddon *J. Am. Chem. Soc.* **2007**, *129*, 10700.

(85) (a) http://.www.2spi.com. (b) Conductive Ag paint contains ~20 μm Ag particles (depending on the manufacturer it may also contain ~1 μm Au and/or Cu particles), glass

frit, and zinc oxide in a binding medium of polyesters with a butyl carbitol acetate solvent.

(86) A. Kongkanand, P. V. Kamat *ACS Nano* **2007**, *1*, 13.

(87) C. Y. Lee, S. Baik, J. Zhang, R. I. Masel, M. S. Strano *J. Phys. Chem. B* **2006**, *110*, 11055.

(88) (a) M. S. Fuhrer, J. Nygård, L. Shih, M. Forero, Y. –G. Yoon, M. S. C. Mazzoni, H. J. Choi, J. Ihm, S. G. Louie, A. Zettl, P. L. McEuen *Science* **2000**, *288*, 494. (b) L. Hu, D. S. Hecht, G. Grüner *Nano Lett.* **2004**, *4*, 2513.

(89) W. Kim, A. Javey, O. Vermesh, Q. Wang, Y. Li, H. Dai *Nano Lett.* **2003**, *3*, 193.

(90) (a) X. Feng, S. Irle, H. Witek, K. Morokuma, R. Vidic, E. Borguet *J. Am. Chem. Soc.* **2005**, *127*, 10533. (b) J. A. Robinson, E. S. Snow, Ş. C. Bădescu, T. L. Reinecke, F. K. Perkins *Nano Lett.* **2006**, *6*, 1747.

(91) D. R. Kauffman, D. C. Sorescu, D. P. Schofield, B. L. Allen, K. D. Jordan, A. Star *Nano Lett.* **2010**, *10*, 958.

(92) (a) A. Bianco, K. Kostarelos, M. Prato *Curr. Opin. Chem. Bio.* **2005**, *9*, 674. (b) F. Lu, L. Gu, M. J. Meziani, X. Wang, P. G. Luo, L. M. Veca, L. Cao, Y. –P. Sun *Adv. Mater.* **2009**, *21*, 139. (c) Z. Liu, S. M. Tabakman, Z. Chen, H. Dai *Nature Protoc.* **2009**, *4*, 1372.

(93) (a) G. Che, B. B. Lakshmi, E. R. Fisher, C. R. Martin *Nature* **1998**, *393*, 346. (b) P. Ramesh, M. E. Itkis, J. M. Tang, R. C. Haddon *J. Phys. Chem. C* **2008**, *112*, 9089. (c) G. Girishkumar, T. D. Hall, K. Vinodgopal, P. V. Kamat *J. Phys. Chem. B* **2006**, *110*, 107. (d) W. Li, C. Liang, W. Zhou, J. Qiu, Z. Zhou, G. Sun, Q. Xin *J. Phys. Chem. B* **2003**, *107*, 6292.

(94) (a) D. R. Kauffman, A. Star *Chem. Soc. Rev.* **2008**, *37*, 1197. (b) G. Grüner *Anal. Bioanal. Chem.* **2006**, *384*, 322. (c) D. A. Heller, S. Baik, T. E. Eurell, M. S. Strano *Adv. Mater*. **2005**, *17*, 2793.

(95) (a) Y. Fan, B. R. Goldsmith, P. G. Collins *Nature Mater.* **2005**, *4*, 906. (b) V. Georgakilas, D. Gournis, V. Tzitzios, L. Pasquato, D. M. Guldi, M. Prato *J. Mater. Chem.* **2007**, *17*, 2679. (c) D. S. Kim, T. Lee, K. E. Geckeler *Angew. Chem. Int. Ed.* **2006**, *45*, 104. (d) H. M. Duong, K. Ishikawa, J. Okawa, K. Ogura, E. Einarsson, J. Shiomi, S. Maruyama *J. Phys. Chem. C* **2009**, *113*, 14230. (e) Y. –S. Loh, K. –J. Lee, H. –M. So, H. Chang, J. –J. Kim, J. –O. Lee *Phys. Status Solidi B* **2009**, *246*, 2824.

(96) (a) M. Penza, R. Rossi, M. Alvisi, G. Cassano, E. Serra *Sens. Act. B* **2009**, *140*, 176. (b) Y. Lin, K. A. Watson, M. J. Fallbach, S. Ghose, J. G. Smith Jr., D. M. Delozier, W. Cao,

R. E. Crooks, J. W. Connell *ACS NANO* **2009**, *3*, 871. (e) J. –P. Tessonnier, O. Ersen, G. Weinberg, C. Pham-Huu, D. S. Su, R. Schlög *ACS NANO* **2009**, *3*, 2081. (f) B. –S. Kong, D. -H Jung, S. –K. Oh, C. –S. Han, H. –T. Jung *J. Phys. Chem. C* **2007**, *111*, 8377.

(97) Y. Lu. J. Li, J. Han, H. –T. Ng, C. Binder, C. Partridge, M. Meyyappan *Chem. Phys. Lett.* **2004**, *391*, 344.

(98) C. Bittencourt, A. Felten, E. H. Espinosa, R. Ionescu, E. Llobet, X. Correig, J. –J. Pireaux *Sens. Act. B* **2006**, *115*, 33.

(99) M. Penza, R. Rossi, M. Alvisi, G. Cassano, M. Signore, E. Serra, R. Giorgi *J. Sens.* **2008**, Article ID 107057.

(100) (a) Q. Zhao, M. B. Nardelli, W. Lu, J. Bernholc *Nano Lett.* **2005**, *5*, 847. (b) P. Pannopard, P. Khongpracha, M. Probst, J. Limtrakul *J. Molec. Graphics Model.* **2009**, *28*, 62. (c) R. Wang, D. Zhang, W. Sun, Z. Han, C. Liu *THEOCHEM* **2007**, *806*, 93.

(101) (a) T. Engel, G. Ertl *Adv. Catal.* **1979**, *28*, 1. (b) E. R. Savinova, F. Hahn, N. Alonso-Vante *J. Phys. Chem. C* **2008**, *112*, 18521. (c) H. Hartshorn, C. J. Pursell, B. D. Chandler *J. Phys. Chem. C* **2009**, *113*, 10718.

(102) (a) H. C. Choi, J. Shim, S. Bangsaruntip, H. Dai *J. Am. Chem. Soc.* **2002**, *124*, 9058. (b) B. M. Quinn, C. Dekker, S. G. Lemay *J. Am. Chem. Soc.* **2005**, *127*, 6146. (c) D. Wang, Z. –C. Li, L. Chen *J. Am. Chem. Soc.* **2006**, *128*, 15078.

(103) (a) T. M. Day, P. R. Unwin, N. R. Wilson, J. V. Macpherson *J. Am. Chem. Soc.* **2005**, *127*, 10639. (b) P. Qiang, Z. Wu, P. Diao, G. Zhang, J. Zhang, Z. Liu *J. Phys. Chem. C* **2008**, *112*, 13346.

(104) D. C. Wagner, W. M. Riggs, L. E. Davis, J. F. Moulder, G. E. Muilenber, G. E. (Eds.) *Handbook of X-Ray Photoelectron Spectroscopy*; Perkin-Elmer Corp., Physical Electronics Div.: Eden Prairie, MN, USA, **1979**.

(105) (a) G. Kresse, J. Hafner *Phys. Rev*. B **1993**, *48*, 13115. (b) G. Kresse, J. Furthmüller *Comput. Mat. Sci.* **1996**, *6*, 15. (c) G. Kresse, J. Furthmüller *Phys. Rev.* B **1996**, *54,* 11169.

(106) P. E. Blöchl *Phys. Rev. B* **1994**, *50*, 17953.

(107) G. Kresse, D. Joubert *Phys. Rev*. B **1999**, *59*, 1758.

(108) J. P. Perdew, K. Burke, M. Ernzerhof *Phys. Rev. Lett.* **1996, *77***, 3865.

(109) R. Bader *Atoms in Molecules: A Quantum Theory*; Oxford University Press: New York, USA, 1990.

(110) (a) A. Henkelman, A. Arnaldsson, H. Jónsson *Comp. Mat. Sci.* **2006**, 36, 354. (b) E. Sanville, S. D. Kenny, R. Smith, G. Henkelman *J. Comp. Chem.* **2007**, 28, 899.

(111) M. Brandbyge, J. –L. Mozos, P. Ordejon, J. Taylor, K. Stokbro *Phys. Rev. B.*, **2002**, 65, 165401.

(112) Quantum Wise home page: http://www.quantumwise.com

(113) (a) B. R. Cuenya, S. –H. Baeck, T. F. Jaramillo, E. W. McFarland *J. Am. Chem. Soc.* **2003**, *125*, 12928.

(114) K. l. Kelly, E. Coronado, L. L. Zhao, G. C. Schatz *J. Phys. Chem. B* **2003**, *107*, 668.

(115) (a) N. Nair, W. –J. Kim, M. L. Usrey, M. S. Strano *J. Am. Chem. Soc.* **2007**, *129*, 3946.

(116) (a) A. M. Rao, E. Richter, S. Bandow, B. Chase, P. C. Eklund, K. A. Williams, S. Fang, K. R. Subbaswamy, M. Menon, A. Thess, R. E. Smalley, G. Dresselhaus, M. S. Dresselhaus *Science* **1997**, *275*, 187. (b) J. Chen, A. M. Rao, S. Lyuksyutov, M. E. Itkis, M. A. Hamon, H. Hu, R. W. Cohn, P. C. Eklund, D. T. Colbert, R. E. Smalley, R. C. Haddon *J. Phys. Chem. B* **2001**, *105*, 2525.

(117) (a) H. –Y. Shin, S. M. Kim, S. –M. Yoon, A. Benayad, K. K. Kim, S. J. Kim, H. K. Park, J. –Y. Choi, Y. H. Lee *J. Am. Chem. Soc.* **2008**, *130*, 2062. (b) R. Voggu, C. S. Rout, A. D. Franklin, T. S. Fisher, C. N. R. Rao *J. Phys. Chem. C* **2008**, *112*, 13053.

(118) N. Park, D. Sung, S. Lim, S. Moon, S. Hong *Appl. Phys. Lett.* **2009**, *94*, 73105.

(119) (a) H. Lou, Z. Shi, N. Li, Z. Gu, Q. Zhuang *Anal. Chem.* **2001**, *73*, 915. (b) J. Li, A. Cassell, L. Delzeit, J. Han, M. Meyyappan *J. Phys. Chem. B* **2002**, *106*, 9299.

(120) A. C. Templeton, J. J. Pietron, R. W. Murray, P. Mulvaney *J. Phys. Chem. B* **2000**, *104*, 564.

(121) B. B. Blizanac, M. Arenz, P. N. Ross, J. Marković *J. Am. Chem. Soc.* **2004**, *126*, 10130.

(122) (a) P. –A. Buffat, M. Flüeli, R. Spycher, P. Stadelmann, J. –P. Borel *Faraday Discuss.* **1991**, *92*, 173. (b) L. D. Marks *Rep. Prog. Phys.* **1994**, *57*, 603. (c) M. A. El-Sayed *Acc. Chem. Res.* **2001**, *34*, 257. (d) V. Petkov, Y. Peng, G. Williams, B. Huang, D. Tomalia, Y. Ren *Phys. Rev. B* **2005**, *72*, 195402. (e) Y. Q. Wang, W. S. Liang, C. Y. Geng *J. Nanopart. Res.* **2010**, *12*, 655.

(123) G. A. Samorjai *Introduction to Surface Chemistry and Catalysis*; John Wiley & Sons: New York, USA, **1994**.

(124) S. Link, C. Burda, Z. L. Wang, M. A. El-Sayed *J. Chem. Phys.* **1999**, *111*, 1255.

(125) (a) A. Arbouet, C. Voisin, D. Christofilos, P. Langot, N. Del Fatti, F. Valée, J. Leremé, G. Celep, E. Cottancin, M. Gaudry, M. Pellarin, M. Broyer, M. Maillard, M. P. Pileni, M. Treguer *Phys. Rev. Lett.* **2003**, *90*, 177401. (b) P. E. Hopkins, J. L. Kasselbaum, M. P. Norris *J. Appl. Phys.* **2009**, *105*, 23710.

(126) D. R. Kauffman, C. M. Shade, H. Uh, S. Petoud, A. Star *Nature Chem.* **2009**, *1*, 500.

(127) (a) Z. Rosenzweig, R. Kopelman *Anal. Chem.* **1995**, *67*, 2650. (b) O. S. Wolfbeis *Anal. Chem.* **2008**, *80*, 4269.

(128) (a) J. Janata, M. Jasowicz, P. Vanysek, D. M. DeVaney *Anal. Chem.* **1998**, *70*, 179R. (b) J. J. Madou, S. R. Morrison *Chemical Sensing with Solid State Devices*, Academic Press, New York, **1989**.

(129) R. Ramamoorthy, P. D. Dutta, S. A. Akbar *J. Mater. Sci.* **2003**, *38*, 4271.

(130) (a) G. Neri, A. Bonavita, G. Micali, G. Rizzo, S. Galvagno, M. Niederberger, N. Pinna *Chem. Comm.* **2005**, 6032. (b) D. Wang, C. Hao, W. Zheng, Q. Peng, T. Wang, Z. Liao, D. Yu, Y. Li *Adv. Mater.* **2008**, *20*, 2628.

(131) P. Avouris, Z. Chen, V. Perebeinos *Nature Nanotech.* **2007**, *2*, 605.

(132) L. Valentini, I. Armentano, J. M. Kenny, S. Bidali, A. Mariani *Thin Solid Films* **2005**, *476*, 162.

(133) (a) C. McDonagh, C. S. Burke, B. D. MacCraith *Chem. Rev.* **2008**, *108*, 400. (b) M. de Sousa, M. Kluciar, S. Abad, M. A. Miranda, B. de Castro, U. Pischel *Photochem. Photobiol. Sci.* **2004**, *3*, 639.

(134) D. R. Lide CRC handbook of chemistry and physics, 85th ed., CRC Press, New York, **2005.**

(135) J. P. Cross, M. Lauz, P. D. Badger, S. Petoud *J. Am. Chem. Soc.* **2004**, *126*, 16278.

(136) V. Savvate'ev, Z. Chen-Esterlit, J. W. Aylott *Appl. Phys. Lett.* **2002**, ***81***, 4652.

(137) I. Heller, A. M. Janssens, J. Männik, E. D. Minot, S. G. Lemay, C. Dekker *Nano Lett.* **2008**, *8*, 591.

(138) A. Star, J. –C. P. Gabriel, K. Bradley, G. Grüner *Nano Lett.* **2003**, *3*, 459.

(139) (a) R. J. Chen, N. R. Franklin, J. Kong, J. Cao, T. W. Tombler, Y. Zhang, H. Dai *Appl. Phys. Lett.* **2001**, *79*, 2258. (b) M. Shim, J. H. Back, T. Ozel, K. –W. Kwon *Phys. Rev. B* **2005**, *71*, 205411.

(140) V. Derycke, R. Martel, J. Appenzeller, P. Avouris *Appl. Phys. Lett.* **2002**, *80*, 2773.

(141) (a) A. Star, Y. Lu, K. Bradley, G. Grüner *Nano Lett.* **2004**, *4*, 1587. (b) J. Borghetti, V. Derycke, S. Lenfant, P. Chenevier, A. Filoramo, M. Goffman, D. Vuilluame, J. –P. Bourgoin *Adv. Mater.* **2006**, *18*, 2535.

(142) L. –L. Chua, J. Zaumseil, J. –F. Chang, E. C. –W. Ou, P. K. –H. Ho, H. Sirringhaus, R. H. Friend *Nature* **2005**, *434*, 194.

(143) A. Hartstein, D. Young *Appl. Phys. Lett.* **1981**, *38*, 631.

(144) (a) S. T. Pantelides *Thin Solid Films* **1982**, *89*, 103. (b) L. Giordano, P. V. Sushko, G. Pacchioni, A. L. Shluger *Phys. Rev. Lett.* **2007**, *99*, 136801.

(145) C. Anghel, V. Derycke, A. Filoramo, S. Lenfant, B. Giffard, D. Vuillaume, J. –P. Bourgoin *Nano Lett.* **2008**, *8***,** 3619.

(146) H. J. Queisser *Phys. Rev. Lett.* **1985**, *54*, 234.

(147) J. –C. G. Bünzli, C. Piguet *Chem. Soc. Rev.* **2005**, *34*, 1048.

(148) A. Hangleiter *Phys. Rev. B* **1993**, *48*, 9146.

(149) K. Kajihara, H. Kamioka, M. Hirano, T. Miura *J. Appl. Phys.* **2005**, *98*, 013528.

(150) V. Aroutiounian *Int. J. Hydrogen Energy* **2007**, *32*, 1145.

(151) D. C. Sorescu, K. D. Jordan, P. Avouris *J. Phys. Chem. B* **2001**, *105*, 11227.